THE ALEY CARBONATITE COMPLEX

by

URS KARL MÄDER

Dipl. Natw. ETH, Zürich, Switzerland

A THESIS SUBMITTED IN PARTIAL FULFILMENT OF

THE REQUIREMENTS FOR THE DEGREE OF

MASTER OF SCIENCE

in

THE FACULTY OF GRADUATE STUDIES

Department of Geological Sciencies

We accept this thesis as conforming

to the required standard

THE UNIVERSITY OF BRITISH COLUMBIA

October 1986

In presenting this thesis in partial fulfilment of the requirements for an advanced degree at the University of British Columbia, I agree that the Library shall make it freely available for reference and study. I further agree that permission for extensive copying of this thesis for scholarly purposes may be granted by the head of my department or by his or her representatives. It is understood that copying or publication of this thesis for financial gain shall not be allowed without my written permission.

Department of GEOLOGICAL SCIENCIES

The University of British Columbia
1956 Main Mall
Vancouver, Canada
V6T 1Y3

Date OCTOBER 15, 1986

Abstract

The Aley carbonatite complex, a property belonging to Cominco Ltd., is 140 km north-northeast of Mackenzie, British Columbia at latitude 56°27′ N, longitude 123°45′ W. The complex intruded Cambrian rocks 345 ma ago near the shelf / off-shelf boundary of ancient North America and is now contained in an imbricate thrust sheet of the Northern Rocky Mountains. The circular complex is 3 km in diameter, cylindrical with respect to the third dimension and little affected by structures of the Rocky Mountains. The relationship of nearby lamprophyric dikes and the lamproitic Ospika diatreme, closely related in time, is unclear.

The Aley carbonatite complex consists of an older, outer "syenite" ring (33% of the area) and a younger dolomite carbonatite core with minor calcite carbonatite "sweats". Rare-earth rich ferro-carbonatite dikes intruded the contact aureole. The contact aureole is composed of recrystallized rocks characterized by brownish weathering, but is little affected by metasomatism and shows no indication of high temperature contact metamorphism.

The mineralogy and mineral chemistry were studied in detail. Over forty mineral species are described, including rare-earth carbonates (burbankite, ancylite, cordylite, huanghoite etc.), niobium oxides (pyrochlore, fersmite, columbite) and alkali-rich silicates (arfvedsonite, aegirine, richterite). Dolomite carbonatite contains apatite, pyrite and fersmite pseudomorphs after pyrochlore. Calcite carbonatite is composed of apatite, magnetite, biotite, pyrochlore, pyrite, ±richterite.

The inner part of the contact aureole forms an annular, cylindrical ductile shearzone suggesting that doming was the major mechanism of emplacement. This is consistent with the circular structural trends in the carbonatite core. Temperatures deduced from field observations and mineralogy (250°C-400°C) disagree with temperatures calculated for a cooling igneous body based on a simple heat conduction model (500°C-600°C) further supporting the view that the complex was

emplaced at subsolidus temperatures.

Oxygen and carbon isotope ratios ($\delta^{18}O$ = 7.7-15.4, $\delta^{13}C$ = -4.7 - -6.1) and some initial Sr isotope ratios ($^{87}Sr/^{86}Sr$ = 0.7034-0.7036) are indicative of a mantle source of carbonatite and syenite.

Geochemically, the carbonatites are enriched in the incompatible elements LREE, Th, U, Nb, Ta, Zr. The rare-earth carbonatite dikes represent a residual liquid extremely enriched in Fe, S, LREE, Sr and Ba. The "syenite" is not a typical alkali-syenite, bearing quartz instead of felspathoids. A strong metasomatic overprint is marked by secondary aegirine and metamorphic textures.

Processes by which the rocks of the Aley may be related genetically are discussed in the light of petrography, geochemistry and experimental studies.

Table of Contents

Abstract ii

Table of Contents iv

List of Tables vii

List of Figures ix

Acknowledgements xi

Introduction xii

1. Geology, Age and Stratigraphy 1

1.1 Location and Access 1

1.2 Regional Geology 1

1.3 Age 2

1.4 Stratigraphy 4

1.4.1 Kechika Formation (Cambrian) 4

1.4.2 Skoki Formation (Ordovician) 6

1.4.3 Road River Group (Ordocician - Silurian) 9

1.5 Local Geology 10

2. Structure 12

2.1 Ductile Versus Brittle Deformation 12

2.2 Ductile Shearing Related to Doming 12

2.3 Stress Field around a Doming Intrusion - Dike Emplacement 18

2.4 Structures within the Intrusive Complex 19

2.5 Structures and Shear Zones Related to the Fold and Thrust Belt 23

2.6 Cross Sections 28

2.7 Regional Tectonic Setting 28

2.8 A Possible Sequence of Tectonic Events 30

3. Mineralogy and Mineral Chemistry 33

3.1 Introduction 33

3.2 Carbonates 35

3.3 Phosphates 41
3.4 Oxides 42
3.5 Silicates 48
3.6 Sulfates 55
3.7 Sulfides 55
4. Petrography 57
4.1 Dolomite Carbonatite 57
4.2 Calcite Carbonatite 60
4.3 Rare - Earth Carbonatite Dikes 61
4.3.1 Rare-Earth Carbonatite Dikes of the North Ridge 62
4.3.2 Rare-Earth Carbonatite Dikes of the Northwest Ridge 63
4.4 "Syenite" 64
4.5 Contact Aureole 67
5. Geochemistry 69
5.1 Rocks of the Carbonatite Complex 69
5.1.1 Dolomite Carbonatite 69
5.1.2 Calcite Carbonatite 69
5.1.3 Rare-Earth Carbonatite Dikes 71
5.1.4 "Syenite" 71
5.2 Rocks of the Contact Aureole 71
5.3 Isotope Geochemistry 76
5.3.1 Strontium and Rubidium 76
5.3.2 Oxygen and Carbon Isotope Ratios 77
6. Aspects of Petrogenesis 80
6.1 Evidence on Sequence of Emplacement 80
6.2 Temperature Distribution around the Carbonatite Complex 81
6.3 Sequence of Crystallization in Carbonatite Magmas 88

6.4 Genetic Relationships 91

6.5 Physical Properties of Carbonatite Magmas 93

6.6 Hypothetical Processes in Carbonatite Magma Chambers 94

7. Conclusions 96

BIBLIOGRAPHY 98

APPENDIX A: MINERALOGY AND MINERAL CHEMISTRY 105

APPENDIX B: X-RAY FLUORESCENCE ANALYSES 146

APPENDIX C: TRANSIENT TEMPERATURE DISTRIBUTIONS CALCULATED FOR THE MARGIN OF A COOLING IGNEOUS BODY 160

LIST OF TABLES

Table Page

1 : List of minerals identified in the Aley carbonatite complex 33

2 : Geochemistry of calcite and dolomite carbonatite 70

3 : Geochemistry of REE-carbonatite dikes 72

4 : Geochemistry of syenite 73

5 : Trace element geochemistry of the contact aureole 75

6 : Locations of samples used in tab 5 75

7 : Rubidium and strontium isotope data 76

8 : $\delta^{13}C$ and $\delta^{18}O$ ratios for carbonatite 78

9 : Composition of calcite used for geothrmometry 82

10: References on experimental topics related to carbonatites 90

11: Standard sets used for EMS-analysis 106

12: Composition of standards for EMS-analyses 107

13: EMS analyses of dolomite 108

14: EMS-analyses of ankerite 109

15: EMS-analyses of calcite 110

16: EMS-analyses of albite 111

17: EMS-analyses of arfvedsonite 112

18: EMS analyses of arfvedsonite 113

19: EMS-analyses of aegirine 114

20: List of possible XRF peak overlaps 148

21: List of samples processed for XRF analyses 150

22: Machine settings for XRF analyses 150

23: Mass attenuation coefficiants 151

24: Major element concentrations of standards 152

25: Mass attenuation coefficients for standards 153

26: Mass attenuation coefficients for standards 154

27: Mass attenuation coefficients of unknowns 155

28: Mass attenuation coefficients of unknowns 156
29: Major element concentrations of unknowns 157
30: Normalized major element concentrations of unknowns 158
31: Trace element concentrations of unknowns 159

LIST OF FIGURES

Figure Page

1 : Regional map 1

2 : Geological map 3

3 : Stratigraphic column 5

4 : Gastropods from the Skoki Dolomite 6

5 : Stratigraphy of the Skoki Volcanic Unit 7

6 : "Chocolate-tablet" boudinage 14

7 : Shear folds 15

8 : Strained limestone 16

9 : Sheath folds 17

10: Stressfield around an updoming intrusion 19

11: Relaxation stress field 19

12: Magnetite layering 21

13: Structural map of mineral layering 21

14: Ruptured syenite with carbonatite veins 24

15: Anticline along the west-side of the complex 25

16: Detail of anticline in figure 15 26

17: Deformed limestone 27

18: Geological cross sections 29

19: Possible sequence of tectonic events 31

20: Xenoliths in "syenite" 66

21: Age versus $^{87}Sr/^{86}Sr$ diagram 77

22: $\delta^{13}C$ versus $\delta^{18}O$ diagram 79

23: P-T diagram of the system $CaO\text{-}MgO\text{-}SiO_2\text{-}CO_2$ 83

24: T-X_{CO_2} diagram of the system $CaO\text{-}MgO\text{-}SiO_2\text{-}H_2O\text{-}CO_2$ 84

25: t-T-x diagram for a syenite intrusion 87

26: Back-scattered electron image - REE carbonates 115

27: Back-scattered electron image - REE carbonates 116

28: Back-scattered electron image - REE carbonates 117
29: Back-scattered electron image - REE carbonates 118
30: Photomicrograph of REE-carbonates 119
31: Photograph of burbankite in rare-earth dike 119
32: Back-scattered electron image of dolomite with rutile lamellae 120
33: Photomicrograph of twinned baddeleyite 120
34: Habit of pyrochlore 121
35: Back-scattered electron image of pyrochlore 121
36: Photomicrograph of pyrochlore 122
37: Autoradiograph of zoned pyrochlore 122
38: Habit of primary fersmite 123
39: Back-scatterd electron image of fersmite pseudomorph 124
40: Detail of figure 39 124
41: Photomicrograph of syenite xenolith 125
42: Composition space for sodic amphiboles 126
43: Block diagram of arfvedsonite 126
44: Composition space for sodic-calcic amphiboles 127
45: Block diagram for richterite 127
46: Block diagram for aegirine 128
47: Photomicrograph of syenite with aegirine 128
48: Coordinate system during solidification 162
49: Coordinate system after solidification 162
50: Model parameter λ 167
51: Solidification time as a function of λ 168
52: Contact temperature as a function of λ 169
53: t-T-x diagram for a carbonatite dike 170

Acknowledgements

Dr. H.J. Greenwood provided academic, financial and moral support whenever needed. Cominco Ltd. made this project possible with generous financial and logistic support. Valuable discussions and guidance in the field by K.R. Pride, P.C. LeCouteur and B.H. Mower (all of Cominco Ltd.) formed a sound basis for mapping and petrographic analysis. J.M. Hamilton of Cominco Ltd. greatly improved the manuscript by critical reciews. Drs. J.K. Russell, E.P.Meagher, J. Pell and D.C. Murphy devoted time and interest for critical discussions. Skillfull technical assistance was provided by Stanya Horsky, Krista Scott, Ed Montgomery, Rob Berman, John Knight, Yvonne Douma and by Dr. E.D. Ghent and John Machacek (both at the University of Calgary). Ursula, with a lot of care and understanding, supported me through the hardships of life. The Geology Grad Group contributed much to my extra curricular education and Canadianization by dragging me out to the hockey rink and by patiently trying to explain the rules of baseball (although I still think Swiss non-sparkling cider, fondue with Kirsch and Swiss chocolate have yet to be surpassed by other cultures).

Introduction

The brown-weathering carbonatite rocks and the dark coloured amphibole-syenite were first mapped by Thompson (1978) on a reconnaissance scale as part of the Ordovician volcanic section. During an exploration campaign in 1980 by Cominco Ltd. "strange looking rocks" were collected by K.R. Pride, leading subsequently to the recognition of the largest known alkaline-carbonatite complex in British Columbia. The Aley turned out to be one of the best exposed and preserved carbonatite complexes in the world. Staking of the claims was completed in October 1982 (Pride, 1983) followed by mapping, trenching and soil sampling during the field seasons thereafter. The first diamond-drilling project started in 1985 and was continued in 1986.

Economic interest focuses on the niobium-bearing mineral assamblages within the carbonatite rocks with an academic interest in some rare-earth concentrations.

The exotic mineralogy, the unusual chemistry of these igneous carbonate rocks and the lack of understanding of many of the processes leading to alkaline-carbonatite magmatism has been a challenging project and the combination of academia and industry has been most productive.

1. GEOLOGY, AGE AND STRATIGRAPHY

1.1 LOCATION AND ACCESS

The Aley property (Pride, 1983) is located approximately 140 kilometers north-northwest of Mackenzie and east of Williston Lake at latitude 56°27′ N, longitude 123°45′ W on NTS map sheet 94B/5 (figure 1).

The property may be reached by fixed wing aircraft to Davis airstrip on the east side of Williston Lake and then about 50 kilometers east by helicopter.

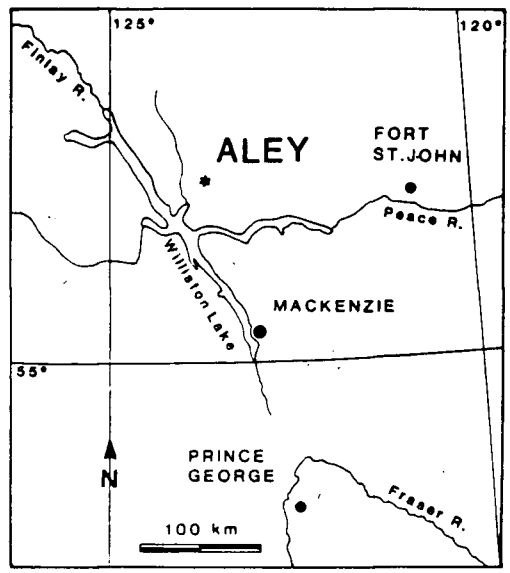

Figure 1: Regional map of the Williston Lake area

1.2 REGIONAL GEOLOGY

The Aley carbonatite complex crops out within an imbricate thrust sheet of the Northern Rocky Mountains fold and thrust belt (Rocky Mountains structural subprovince of Thompson 1978, 1985) in the southwest corner of the Halfway River map area (94B). The complex is nearly circular, about three kilometers in diameter, mid-Paleozoic in age (see section 1.3) and little affected by the Rocky Mountains structures (figure 2). The stratigraphy, structure and tectonic evolution of the map

area is presented by Thompson (1978, 1979, 1982, 1985) based on field work (1975, 1976) and on previous studies (Irish, 1970; Taylor & Stott, 1973, 1979; Taylor, 1979, 1983).

The Rocky Mountains structural subprovince consists of eastward-transported imbricate thrust sheets comprising Hadrinian to Devonian sedimentary rocks of the continental margin of ancient North America (Thompson 1978). In contrast to the Southern Rocky Mountains, folding contributes significantly to the overall shortening of the fold and thrust belt in the Northern Rocky Mountains (Thompson, 1979). Paleogeographically, the alkaline-carbonatite complex intruded the miogeoclinal sedimentary wedge near the carbonate - shale boundary of early to mid-Paleozoic time. This boundary corresponds to the shelf off-shelf boundary of the continental margin (Thompson, 1978). The simple shape of this boundary further to the north is obscured in the area of interest by the Ospika Embayment (eastward closing) and its southern border the Peace River Arch (Thompson, 1985).

In a larger context, the Aley complex is part of widespread alkaline activity along the ancient continental margin represented along both sides of the Rocky Mountain Trench (Pell, 1985, 1986; Currie, 1976). The Aley is similar in size and structural setting to the Ice River alkaline complex (Currie, 1975).

1.3 AGE

At present, three K-Ar ages on biotite are available: 339±12 ma and 349±12 ma from carbonatite samples (LeCouteur, pers. com., 1986) and 334 ma (Armstrong, pers. com., 1986) on the nearby Ospika diatreme (figure 2). A first attempt to date zircons failed because of the very low lead content of the sample (Parrish, pers. com., 1986). Further studies on U-Pb systematics of pyrochlore and possibly monazite and badelleyite are in progress (Parrish, pers. com., 1986).

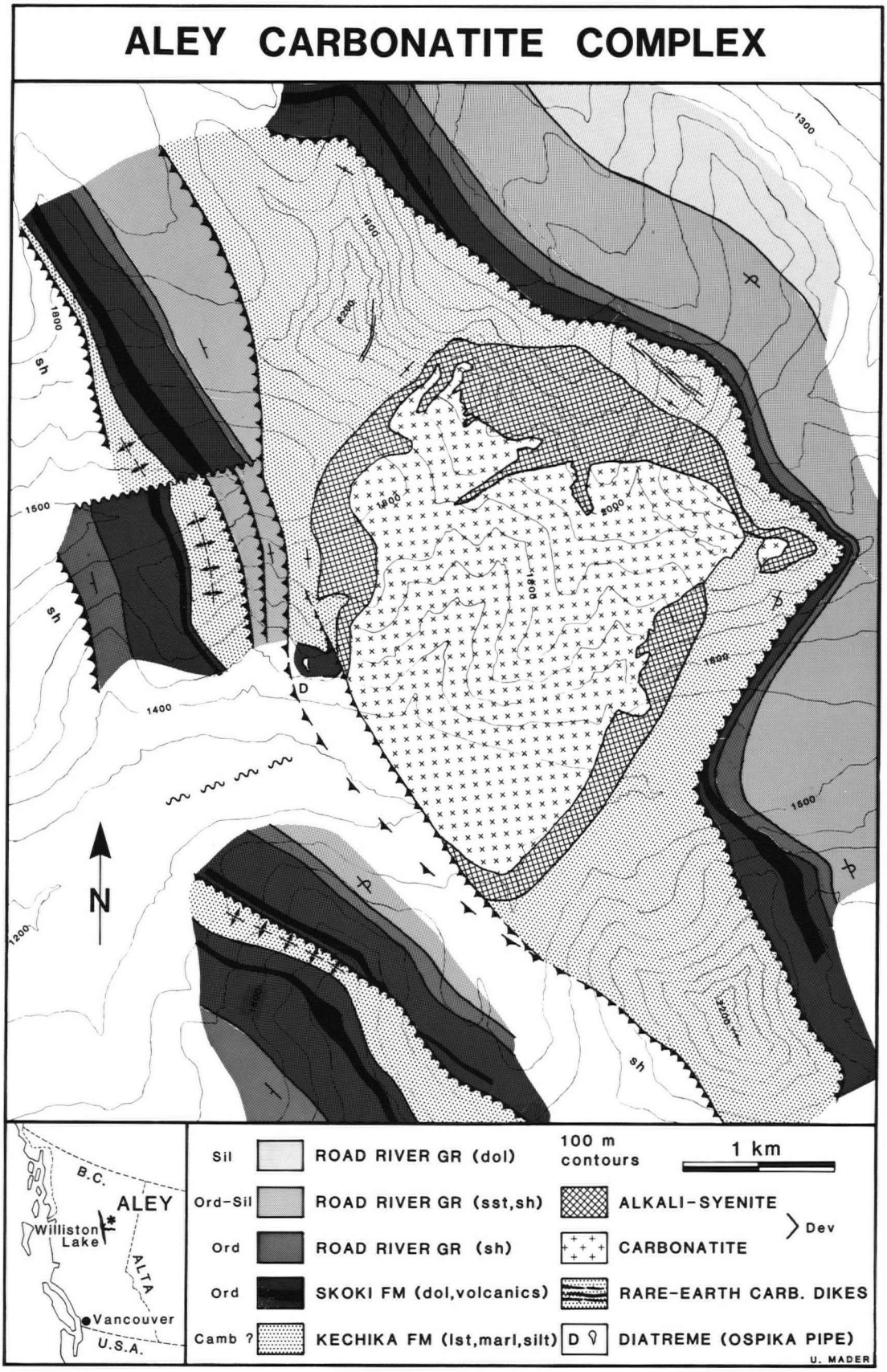

Figure 2: Geological map

1.4 STRATIGRAPHY

The stratigraphy of the Halfway River map area has been established with enough detail by Thompson (1985) to correlate mappable lithological units with established formation names.

Ages of the sedimentary rocks in the Aley area are not well constrained paleontologically. Only a few locations have provided graptolites. A Cambrian limestone unit, the Ordovician Skoki (dolomite) Formation with its volcanic succession and an upper Ordovician graded sandstone sequence provide excellent marker horizons for field mapping.

Figure 3 is a stratigraphic column for the area mapped, with subdivisions based on lithologies. Due to faulting and folding there is no complete reference cross section available in the area. Locations of type localities for individual lithologies are referred to in their respective paragraphs. The thicknesses of the units in figure 3 represent the maximum sections of a particular unit within the area mapped. The thicknesses of shaley units must be considered as minimum values due to tectonic thinning. The stratigraphic column before the Columbian orogeny might therefore have been considerably thicker than presented below.

1.4.1 KECHIKA FORMATION (CAMBRIAN)

The reference cross section is located within the contact aureole extending from the intrusive contact (12750N, 10200E) along the ridge northwestwards. The upper part of the Cambrian Kechika Formation present in the area may be subdivided into four lithologies, starting with the oldest unit:

Cream Dolomite Unit (>80 m): This unit occurs only within the contact aureole of the carbonatite complex and is recrystallized to a cream weathering, bedded (5-40 cm), clean dolomite marble with minor units of calcite marble. Characteristic are 1 to 10 mm thick interbedded marly horizons. The base is not

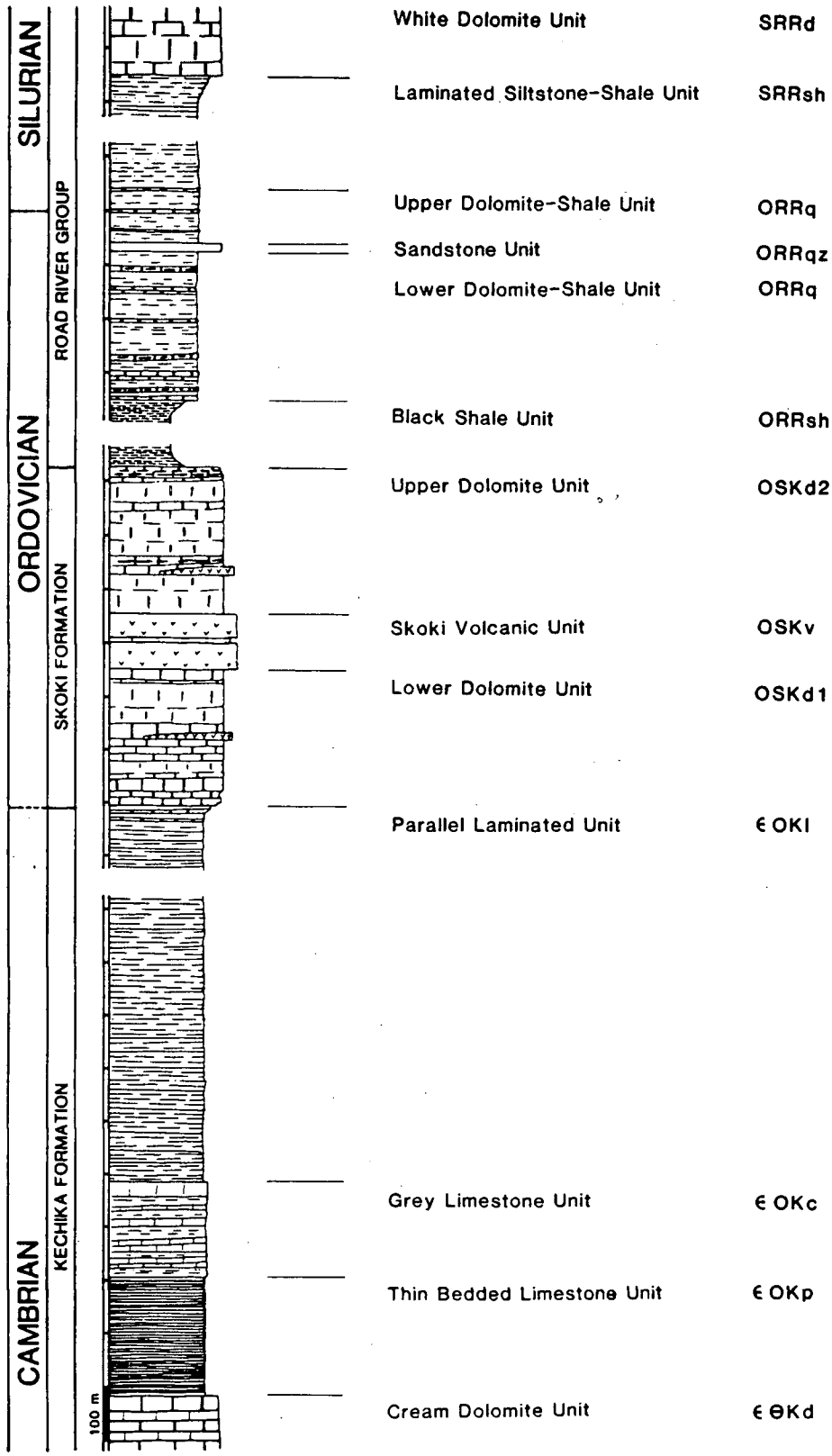

Figure 3: Stratigraphic column for the area mapped

exposed in the map-area. The top is marked by a sharp lithologic change.

Thin Bedded Limestone Unit (100 - 200 m): This unit consists of evenly alternating beds of grey, impure calcareous limstone (2-5 cm) and dark marls (1-3 cm). Characteristic is the abundance of minor folds. Within the contact aureole of the complex, the limestone beds (marbles) weather recessively with respect to the recrystallized marly layers. The upper contact is gradational over a few meters.

Grey Limestone Unit (100 - 150 m): Laminated grey limestones and bedded limestones (10-50 cm) are interbedded with orange-brown siltstones and shales. Some sections resemble the unit below. The top is marked by the absence (or scarcity) of thicker limestone beds.

Parallel Laminated Unit (>700 m): This unit consists of buff-brown and grey weathering thinly laminated limestones and minor nodular limestones interbedded with silty and shaley laminated layers. The uppermost part of the unit is marked by the occurrance of massive (5-50 cm) grey dolomite beds typical of the Skoki Formation. The top is defined by the onset of bedded to massive dolomite. The Kechika Formation is generally in fault contact with the Skoki Formation.

1.4.2 SKOKI FORMATION (ORDOVICIAN)

This cliff-forming dolomite formation is divided by a volcanic sequence into a lower and an upper dolomite unit. Up to two additional volcanic horizons may be present in the northwestern pert of the map-area in the lower and the upper dolomite units. Locations of reference sections are shown in figure 5.

Lower Dolomite Unit (200 - 300 m): This unit is medium to thick bedded, massive, dark grey weathering dolomite with rare large (5 cm) gastropods (*Maclurites*, identification by Cominco Ltd.) , crinoids and minor chert lenses. At point 13070N, 8070E, 10 meters below the main volcanic sequence, two beds contain abundant well preserved gastropods (figure 4). Near 14350N, 9700E a 10 to

20 meter thick volcanic layer is present consisting of ash mixed with dolomite. The top of the unit is a sharp or gradational (1-5 m) contact with fine-grained volcaniclastic rocks.

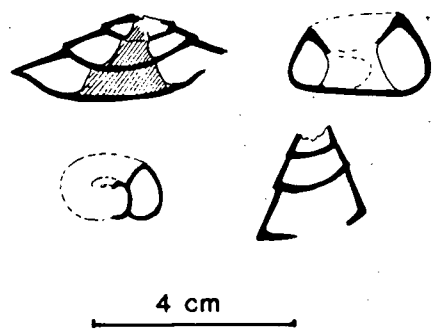

Figure 4: Gastropods from the Lower Dolomite Unit (13070N, 8070E)

Skoki Volcanic Unit (50 - 100 m): (Figure 4) The lower part of the unit consists dominantly of cream, buff-brown, brown-green and purple laminated to bedded very fine-grained marine tuffs and crystal tuffs. In the middle and upper part amygdaloidal basalt flows (10-100 cm) may be present. Near the middle part one or several breaks in volcaniclastic supply occurred marked by normal Skoki dolomite sedimentation (1 - 5 m). A curled nautiloide was found at point 8400N, 9730E. A shaley, brown-green weathering sheared sequence may be present in the middle part of the section. Near the top thick (1-5 m) conglomerate beds occur containing angular to subangular unsorted fragments of amygdaloidal flows and tuffaceous material ranging in size from mm to 1 m. The top is marked by a sharp or gradational change from fine volcaniclastic to normal dolomite sedimentation. Texturally well preserved pillow basalts occur in a subcrop in a creek at point 11870N, 8480E but have not been observed in outcrop.

Upper Dolomite Unit (250 - 400 m): This unit typically is thick bedded to very massive with minor black chert. Black chert lenses become more abundant towards the top. A fine tuffaceous 20 m thick section is present in the western part of the map-area (13340N, 8120E). The top is marked by the first appearance of black shale.

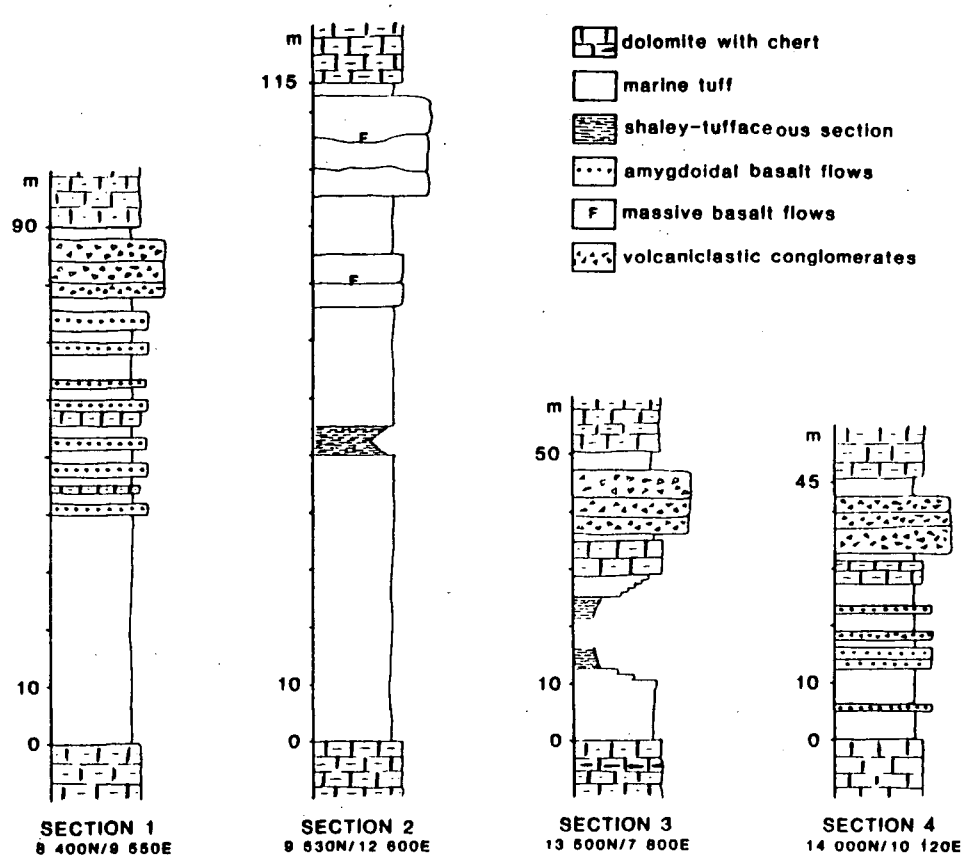

Figure 5: Stratigraphy of the Skoki Volcanic Unit

1.4.3 ROAD RIVER GROUP (ORDOCICIAN - SILURIAN)

Reference sections are exposed along the ridges from points 12430N, 8600E and 12400N, 12250E as well as 11630N, 13070E. The lower part of the Road River Group present in the area mapped is divided into six units:

Black Shale Unit (>100 m): The unit consists of dark grey, calcareous, planar laminated, fissile, graptolitic (*Glossograptus*, identification by Cominco Ltd) shale. The contact with the underlying Skoki Formation is locally unconformable. The top is marked by the first appearance of grey dolomite beds.

Lower Dolomite - Shale Unit (250 - 300 m): The unit is characterized by abundant, well bedded dolomite horizons (5 cm - 3 m) between laminated, calcareous and dolomitic shale. Slump textures and intrabed breccias are common. In the upper part the dolomite beds are fossiliferous (rugosa corals, crinoids) and chert layers (2 - 10 cm, generally fossiliferous) are abundant. The top of the unit is defined by the appearance of graded sandstone.

Sandstone Unit (5 - 15 m): This marker unit consists of well bedded (5-80 cm), medium grained, mature, graded sandstones with minor laminated calcareous layers. The top and bottom of the unit are sharply defined.

Upper Dolomite - Shale Unit (100 - 200 m): The upper unit is similar to the lower dolomite-shale unit but with far less abundant dolomite and additional siltstones. *Dicellograptus Morrosi* (mid-Ordovician, identification by Cominco Ltd.) may occur in this part of the section. The top of the unit is not well defined, gradually becoming more silty and dolomite banks becoming scarce.

Laminated Siltstone Unit (>200 m): This unit consists of laminated to fine-bedded siltstones, silty shale and minor light-grey weathering dolomite beds (cm - dm). *Monograptus Spiralus* (identification by Cominco Ltd.) occurs occasionally in the shaley lower part of this section indicating a Silurian age. The top is sharply defined by the first appearance of massive, white dolomite.

White Dolomite Unit (>100 m): This massive dolomite weathers a distinctive light grey colour. The top of the unit was not examined.

1.5 LOCAL GEOLOGY

Two brief references about the Aley give an introduction to the geology (Pride, 1983; Pell, 1986b). The nearby Ospika diatreme is mentionend in Pell, 1986a.

The alkaline-carbonatite complex is ovoid in outline, 3 to 3.5 km in diameter and occupies an area of about seven square km (figure 2). Outcrop is scarce near the bottom of the major valley (1300-1350 m altitude), abundant above tree line (around 1600 m) and continous along the high ridges (1800-2200 m). The body is cylindrical with respect to the third dimension with a westward plunging, nearly vertical axis and has probably been but little tilted compared to its original orientation.

The two major rock types of the intrusion form a ring complex with a "syenite" rim and a carbonatite core. Two rare-earth element rich ferrocarbonatite dike swarms intruded rocks of the Kechika formation parallel to the northwest side and the northeast side of the intrusion.

The carbonatite complex and its contact aureole are part of an imbricate thrust sheet bounded to the west by a high angle thrust fault juxtaposing Cambrian rocks against Silurian. The Silurian rocks form part of a tectonically thinned eastern limb of a tight anticline with a Cambrian core to the west. This structural element is disected by faults striking at high angles to the Rocky Mountain trend (NNW-SSE). Along the eastern side of the complex a tectonically thinned reversed stratigraphic section with a set of subparallel lower-angle thrust faults is thrusted onto an imbricate sheet containing Silurian rocks (to the east of the area mapped; Thompson, 1978). Tectonic movements within the reversed section occurred along the Kechika-Skoki and the Skoki-Road River unconformable contacts.

Lamprophyres occur within the Kechika Formation and the Road River Group. A small lamproitic diatreme (Ospika pipe; Pell, 1986a) intruded dolomite of the Skoki Formation 250 meters west of the complex (10850N, 9450E).

2. STRUCTURE

The Aley carbonatite complex provides an excellent opportunity to study relationships between intrusion and tectonics. Its convenient size, lack of disruption and good exposure make it particularly suitable for study, and its setting in an unmetamorphosed fold and thrust belt allows to distinguish between deformation related to the emplacement of the body and that related to the formation of the fold and thrust belt.

2.1 DUCTILE VERSUS BRITTLE DEFORMATION

The deformation related to the intrusion of the complex affected contact metamorphic rocks (marbles, recrystallized marls and shales) at elevated temperatures (cf. section 6.2) and will therefore be under a ductile regime. Note also that marls are structurally incompetent with respect to limestone when unmetamorphosed but competent when metamorphosed. Minor folds, for example, can thus be related by their geometry unequivocally to deformation under contact metamorphic conditions versus deformation under unmetamorphic conditions (Brack, 1981).

The deformation related to the formation of the fold and thrust belt affected unmetamorphosed sedimentary rocks (and cooled rocks of the complex and its aureole) and these may have behaved as brittle materials. Structures close to the outer margin of the contact aureole may not be related easily to one of the two distinct events.

2.2 DUCTILE SHEARING RELATED TO DOMING

The complex intrudes into a similar stratigraphic level all the way around the intrusion. The Cambrian Cream Dolomite marble, for example, borders the intrusive contact for nearly half of the circumference of the complex in the northern part.

Bedding of the host rocks near the intrusion is subvertical and parallels the syenite (carbonatite) - host rock contact.

Radial shortening within the first few hundred meters adjacent to the igneous contact is extreme. Extension took place within a vertical curved surface parallel to the contact and subparallel to bedding. Horizontal and vertical components resulted in "chocolate-tablet" boudinage of recrystallized marly layers within the Cream Dolomite Unit (figure 6). Measurements of extension (Δl / l_0) in both directions give minimum values for extension between 200 and 400 %. An average value of 300 % applied uniformly within the plane of extension will result in shortening perpendicular to the plane by a factor of 16 assuming constant volume.

In the Thin Bedded Limestone Unit abundant shear folds, shear bands and some sheath folds are indicative of high strain (figures 7, 8, 9). The trends of the sheath axes of folds (at point 12130N, 9570E, adjacent to the syenite contact, figure 9) are nearly vertical and suggest a strong vertical shear component. A horizontal shear component resulted in en échelon boudinage of competent beds and early veins (figure 8).

The inner part of the contact aureole is therefore interpreted to be an annular, cylindrical ductile shear zone developed during emplacement of the complex. Doming must have played an important role as an intrusion mechanism at the exposed structural level. Extreme radial shortening can account for a major part of the lateral room problem created by the emplacement of the igneous body. Evidence for sidestoping and overhead stoping is lacking, strongly suggesting an intrusion mechanism different from many granitoid plutons.

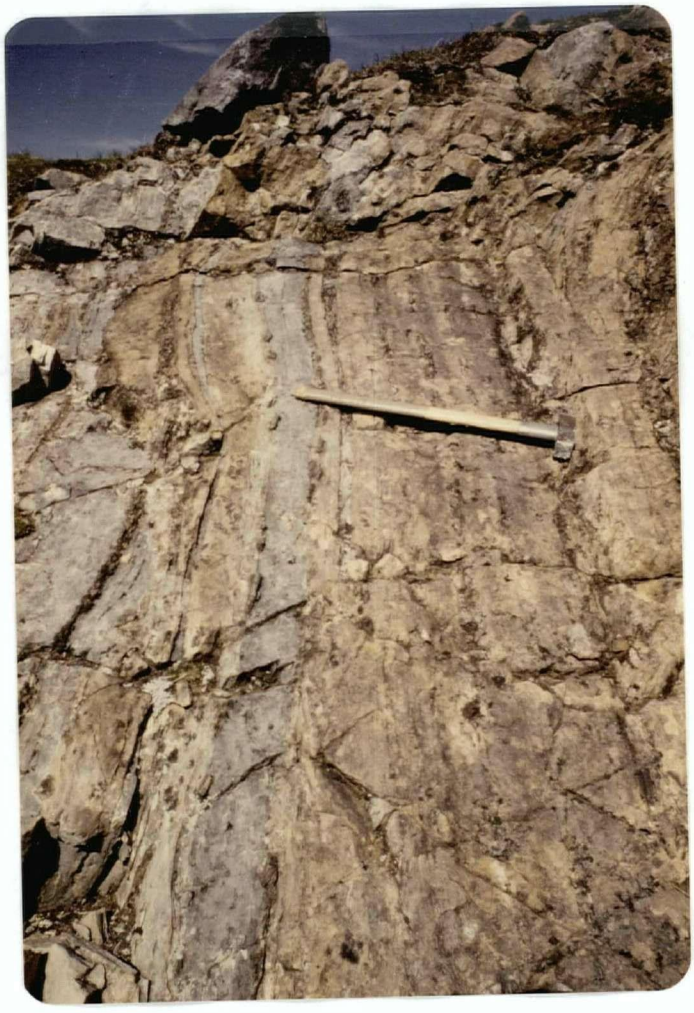

Figure 6: "Chocolate-tablet" boudinage in the Cream Dolomite Unit (Kechika Formation). (12500N, 11780E)

Figure 7: Shear folds, Kechika Formation. (11550N, 12250E)

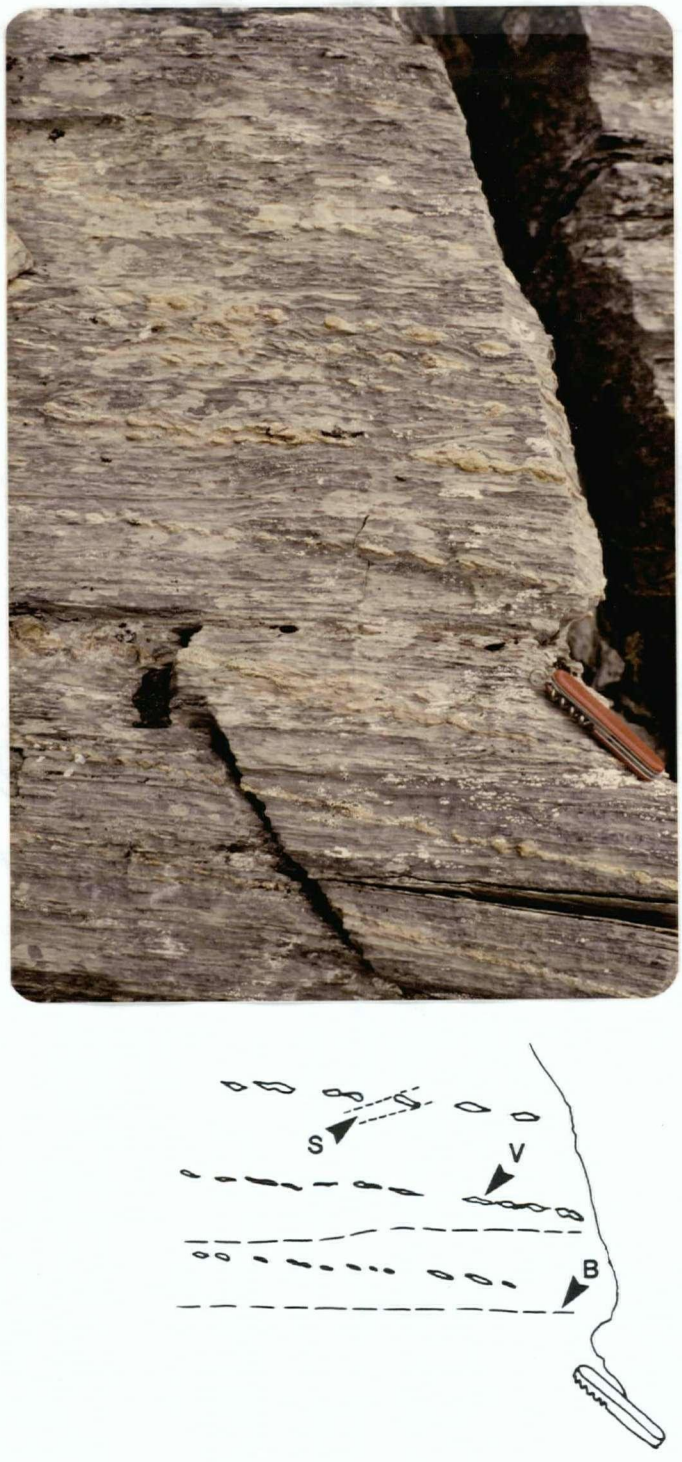

Figure 8: Highly strained Thin Bedded Limestone Unit, Kechika Formation. B = bedding, V = en échelon boudinaged carbonate vein, S = shear band. (12780N, 10100E)

Figure 9: Sheath folds, Thin Bedded Limestone Unit, Kechika Formation. (12130N, 9570E)

2.3 STRESS FIELD AROUND A DOMING INTRUSION - DIKE EMPLACEMENT

Physical models to explain stress distributions around intrusions have been derived successfully by analysis of dike patterns surounding plutons (Anderson, 1936; Billings, 1945; Currie, 1956; v. Eckermann, 1958; Gussow, 1968; Kresten, 1980).

Intrusion of a major mass of igneous or salt material will cause updoming of the overlying country rock. Radial dikes may form, following directions perpendicular to maximum stress. The stress field created by the upward movement may give rise to two sets of joints: tension joints and shear joints (figure 10). The former are believed to be responsible for the intrusion of cone sheets (Anderson, 1936).

Upon cooling and degassing of the magma chamber (and injection of dikes) the pressure is expected to decrease. If the pressure becomes lower than that exerted by the overlying rocks, a new stress distribution will cause subsidence of the wallrock. Subvertical shear joints may result in the formation of ring dikes (Anderson, 1936; Reynolds, 1956; figure 11).

Following this line of reasoning, the nearly vertical rare-earth carbonatite dikes that parallel the intrusion contact could not have been emplaced synchronously with the intrusion (cf. figure 10). The dikes must have intruded either as sills before intrusion of the complex took place or as late stage ring dikes during a relaxation stress field. If the dikes were pre-intrusive they should be as intensly deformed as the "chocolate-tablet" marls. The minor boudinage observed at the dike swarm along the northeastern margin, however, might be due to the brittle Rocky Mountain deformation related to the thrust zone along the east side of the complex, but generally, evidence for such strain is lacking. For petrologic reasons (cf. section 6.4) it is regarded as most reasonable to classify the carbonatite dikes as late stage ring dikes rather than pre-intrusive sills, although the field observations are somewhat ambiguous.

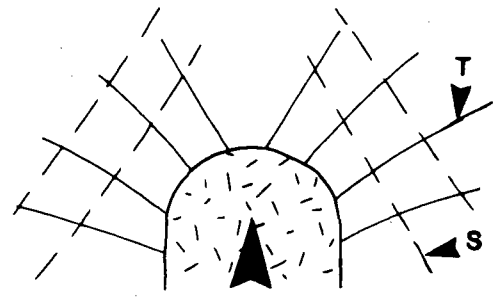

Figure 10: Updoming intrusion with distribution of shear joints (S) and tension joints (T)

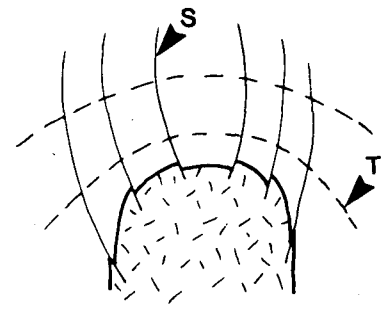

Figure 11: Distribution of shear joints (S) and tension joints (T) in a relaxation stress field

2.4 STRUCTURES WITHIN THE INTRUSIVE COMPLEX

The carbonatite complex with its immediate aureole must have behaved as a rigid body during the formation of the Rocky Mountains in order to be as well preserved as indicated by the exposure in the northern part of the body. No major fault zones are exposed which dissect the complex, perhaps with the exception of the southwest corner, which may have been sliced off by a poorly exposed high angle fault or shear zone. This fortunate tectonic setting together with the very low grade of regional metamorphism offers the opportunity to find primary magmatic textures preserved.

Mineral layering:

Mineral banding or layering, often emphasized by a well developed parallel cleavage or foliation, is very common throughout the complex, particularly towards its margins. In dolomite carbonatite the parallel texture is commonly formed by disk-shaped flattened apatite aggregates up to 1.5 cm in diameter paralleled by a weakly or strongly developed cleavage. In mineralized zones magnetite, pyrochlore, fersmite, biotite and amphibole enhance this parallel texture to various degrees by mineral banding and compositional zoning (figure 12). The oxides are mostly euhedral to subhedral with magnetite grains commonly broken apart whereas amphiboles form very fine bluegreen needles aligned parallel to the fabric.

Field measurements show the planar texture to dip steeply with the strike directions roughly parallel to the margin of the complex (figure 13). There is a slight tendency towards steep western dips along the west side as well as along the east side. Near the center of the body attitudes vary more at random. Cross-sections based on drill core to a depth of 200 m show that the plunge of the fabric does not vary much with depth.

The mineral layering is interpreted to be vertical flow banding, and thus to be a primary magmatic texture. Approximately circular stressfields, possibly late magmatic and subsolidus, enhanced the flowbanding by the overprint of a planar fabric. This regime of compressional and shear stress might well relate to the doming of the intrusion. More intensly developed fabrics towards the margin and especially close to the syenite-carbonatite contact may be explained in the same way.

Near vertical orientation of mineral zoning is observed in many other alkaline - carbonatite complexes: Oka (Gold, 1967), Magnet Cove (Erickson & Blade, 1963).

Figure 12: Magnetite layering in calcite carbonatite (MR-301H; float; 12800N, 10200E)

Breccia zones and fracture zones:

Drill cores near the margin of the carbonatite body display a variety of narrow (5-50 cm) shear zones, fracture zones and brecciated zones marked by intense weathering and abundant oxidized pyrite. Displacement along these trends, which often parallel the fabric outlined by mineral layering, appears to be minor and is more likely associated with a more recent event, possibly with the formation of the Rocky Mountains fold and thrust belt.

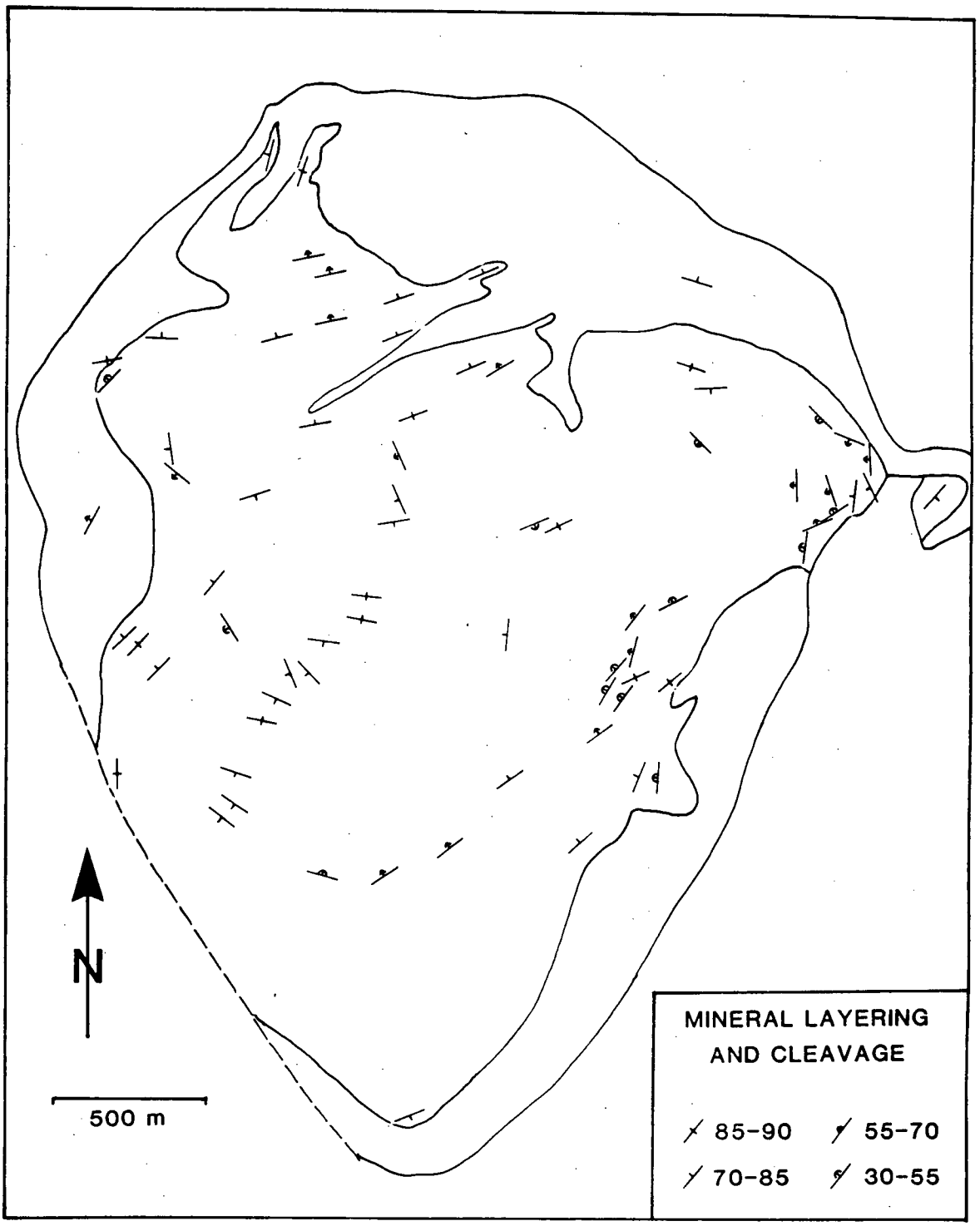

Figure 13: Structural map of cleavage and mineral layering outlined by apatite, magnetite, pyrochlore, amphibole (structural data by K.R. Pride, P.C. LeCouteur (Cominco Ltd.) and U.K. Mäder)

Along the southeastern margin breccia zones and shear zones are quite abundant. One type of shear zone is characterized by abundant chlorite, pyrochlore, magnetite, zircon and relatively high radioactivity. The proximity of the brittle shear zone along the east side may be partly responsible for the more intense deformation in this part of the complex. The mineralization of some of the breccia and fracture zones, however, required hydrothermal activity which could have occurred during a late stage magmatic activity.

Breccia zones at the syenite - carbonatite contact are quite spectacular due to their size and the contrasting colours of the two igneous rocks (figure 14). In detail most of the mega-breccias can be recognized as having formed by rupture of the syenite with carbonatite veins filling the gaps. Major vertical or horizontal relative displacements could not be confirmed. Small scale compositional layering in the veining carbonatite (commonly calcite carbonatite) resembles magmatic flowbanding and would thus suggest that these breccias formed synchronously with the intrusion with injected liquids cementing the vugs.

2.5 STRUCTURES AND SHEAR ZONES RELATED TO THE FOLD AND THRUST BELT

The key outcrop to interpreting the structure along the western side of the carbonatite complex is a north facing cliff striking perpendicular to the structural trends which exposes Cambrian rocks in the core of a tight anticline (figure 15). A penetrative axial planar shistosity is developed (figure 16). Within the steeply dipping limbs to the west and east shearing resulted in greatly reduced stratigraphic thicknesses and produced schistosities parallel to bedding. The Skoki Dolomite is missing in the eastern limb in this section due to the presence of a high angle forelimb thrust which juxtaposes the Cambrian core against rocks of the Road River Formation (upper Lower Dolomite Shale Unit ?). This entire anticlinal package was moved along a high angle thrust fault onto Cambrian rocks of the contact metamorphic aureole (figures 18, 19). Small and large scale boudinage indicate shortening perpendicular to the structural trends (figure 17). Extension joints are

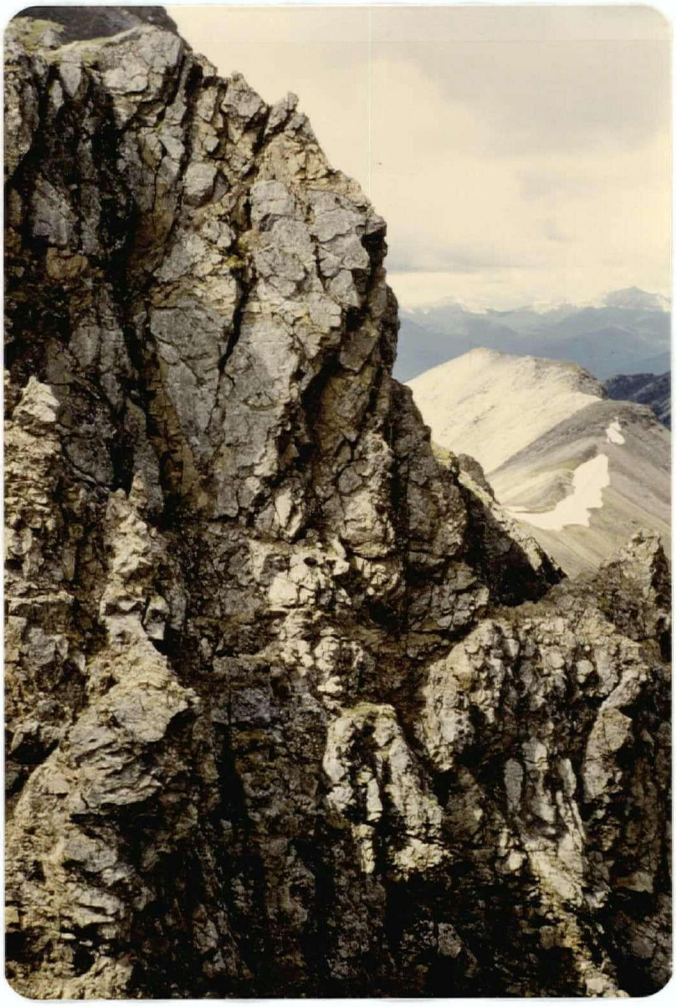

Figure 14: Ruptured syenite with carbonatite veins forming a mega-breccia (11680N, 9730E)

frequently developed in the competent layers within a plane subperpendicular to the fold axis (figure 16). Similar structures can be identified along ridges to the north and to the south, but stratigraphic sections, however, may vary considerably in detail. Along the ridge immediately to the north, for example, the eastern limb of the anticline is stratigraphically complete whereas the western limb is cut off by a thrust fault. The anticlinal structure must therefore be segmented by faults. These faults strike at high angles to the Rocky Mountain trend and may be interpreted as wrench faults due to differential thrusting resulting in the lateral disection of the hanging wall.

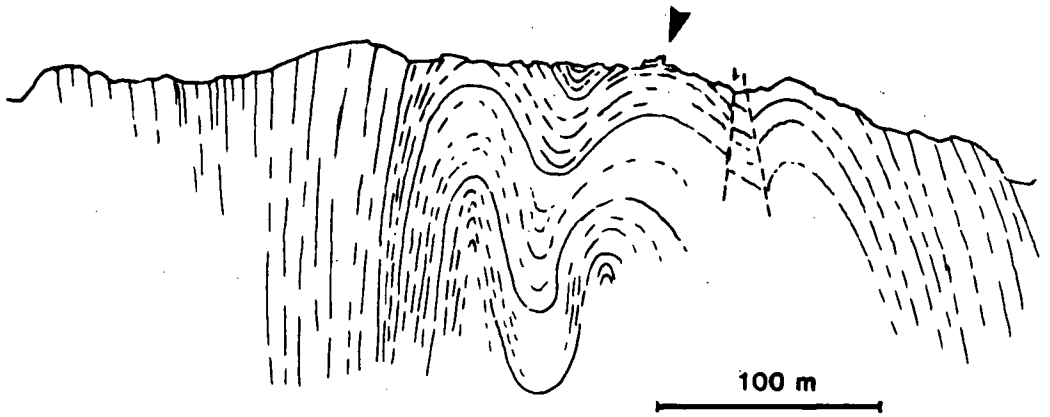

Figure 15: Cambrian core (Kechika Formation) of the anticline along the west-side of the complex. Arrow indicates location of figure 16 (11500N, 8800E)

Along the eastern margin of the complex numerous subparallel thrust faults form an extensive brittle shear zone within a reduced, westward dipping, reversed stratigraphic section. Large scale boudinage of competent rock packages is common. Shaly and marly sections have a strong schistosity developed parallel to bedding. Extension joints are common in competent layers with some large quartz-filled

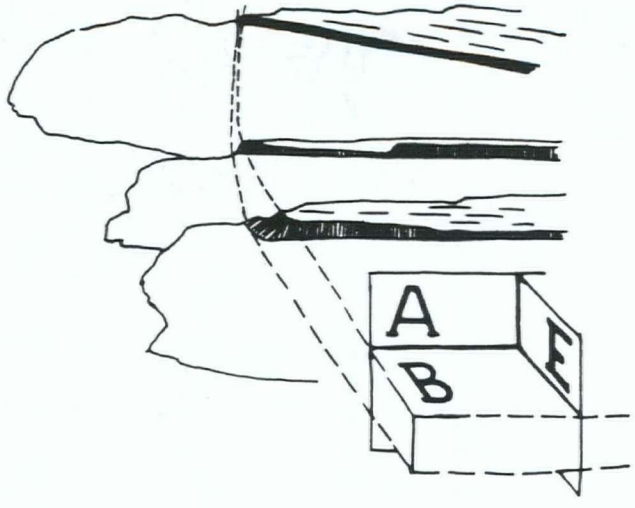

Figure 16: Core of anticline (figure 15) showing axial planar schistosity (A), bedding (B) and extension joints (E). (11450N, 8750E)

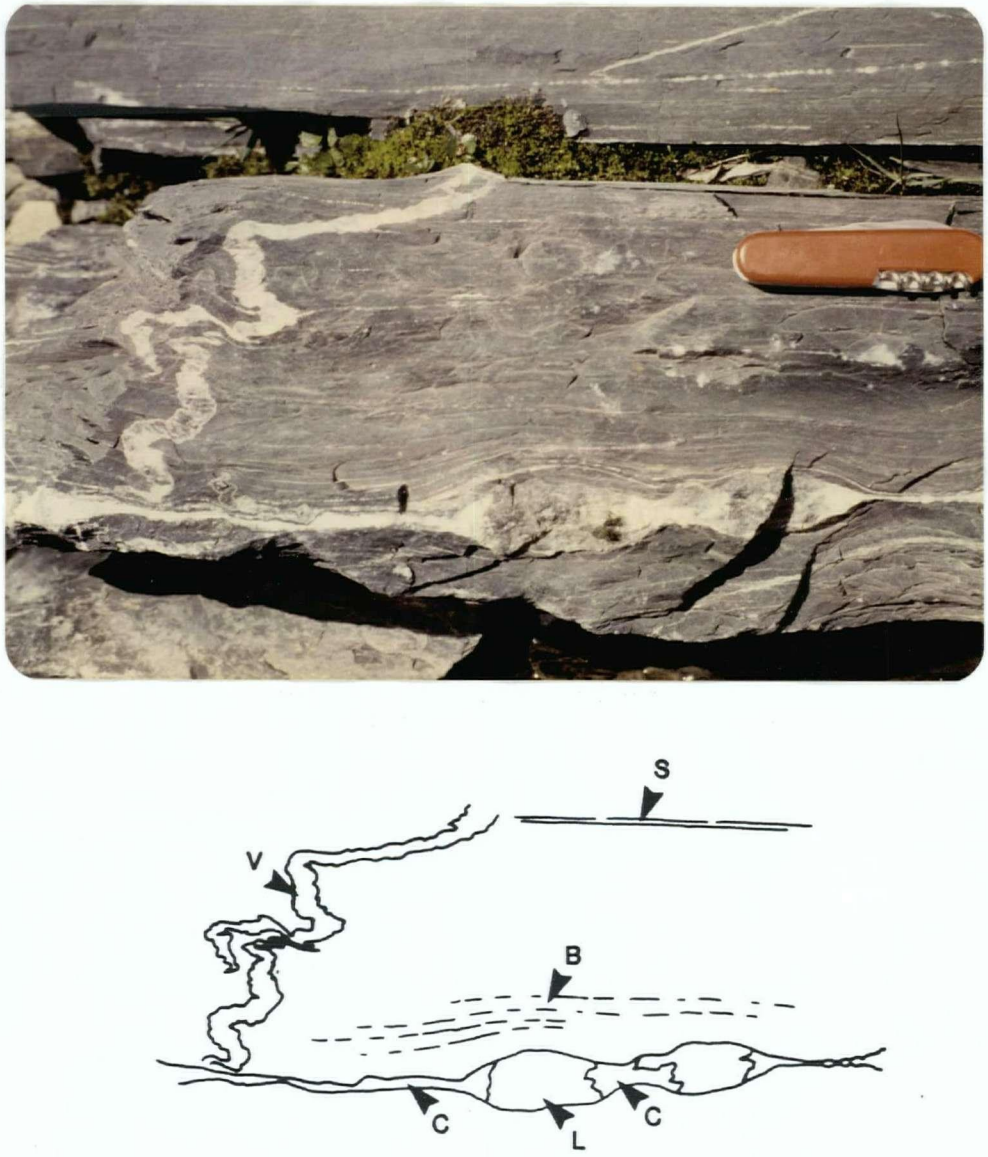

Figure 17: Thinned limestone (Lower Dolomite Shale Unit, Road River Group) showing bedding (B), schistosity (S), boudinaged limestone bed (L) with calcite filled necks (C) and a deformed carbonate vein (V). (1200N, 8900E)

sigmoid shaped extension joints developed in the Sandstone Unit of the Road River Formation. A major fault contact must be located between the contact-metamorphosed Cambrian Kechika rocks and a very reduced package of Skoki Dolomite. Some parts of the Skoki Dolomite however were affected by the intrusion resulting in locally elevated radioactivity. Furthermore an isolated slab of basalt from the Skoki Volcanic Unit (13080N, 11600E) was clearly part of the contact aureole. The stratigraphic section from the carbonatite contact to the Road River Group was therefore fairly continuous at the time of intrusion with significant but not large scale displacements during the Columbian Orogeny. The major displacements within the shear zone took place within the Kechika Formation, at the boundary to the Skoki Formation and within the overlaying shales of the Road River Group. The width of the reversed section towards the east is not known but may well exceed one kilometer.

2.6 CROSS SECTIONS

Two geological cross sections are shown in figure 18. Both are drawn across the carbonatite complex and the sourrounding structures at high angles to the Rocky Mountain structural trends and are located as shown on the geological map.

An important consequence of attempting to extrapolate the structure to depth is the likelihood that the complex may be cut by the eastern shear zone at relatively shallow depths. The two sections project the fault contact underneath the center of the complex to elevations between 800 meters (A - A') and 200 meters (B - B'). The shear zone may however steepen with depth or deflect at the host rock - carbonatite discontinuity.

2.7 REGIONAL TECTONIC SETTING

Thompson's (1978) regional mapping shows the area of the Aley complex as a large anticlinal structure between two branches of the Burden Thrust. The carbonatite itself is shown as part of the Skoki Dolomite Unit and the syenite ring

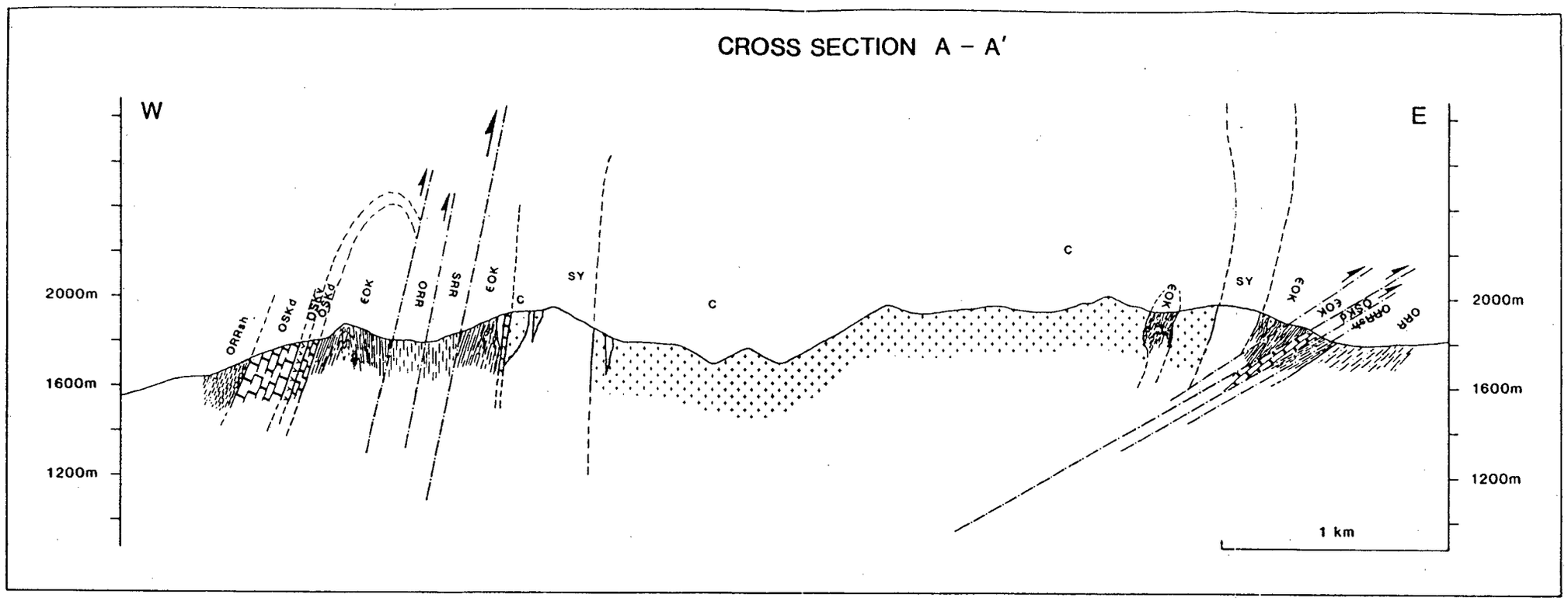

Figure 18: Geological cross sections through the Aley carbonatite complex (for abbreviations cf. figure 3)

as thickened parts of the Skoki Volcanic section.

The general nature of the structure presented in this study is similar to that reported by Thompson (1978), essentially consisting of a steep westward dipping normal stratigraphic section along the western side of the complex and a westward dipping reversed section along the eastern side of the complex with the complication of a tight anticline along the western side of the complex. The "core" of the large scale anticline shown by Thompson is formed by the carbonatite complex. The thrust sheet hosting the Aley complex may be part of a duplex structure encompassed by the Burden Thrust.

2.8 A POSSIBLE SEQUENCE OF TECTONIC EVENTS

Combining the material presented in this chapter a tentative simplified sequence of events is suggested and depicted diagrammatically in figure 19.

a) The emplacment and updoming of the intrusion into a layer-cake stratigraphy created a ring-shaped ductile shear zone.

b) Traces of future thrust faults related to the formation of the Rocky Mountains outline a duplex structure.

c) A blind thrust (1), locked at point L, gave rise to the anticline along the western margin of the complex.

d) Thrusting continued along faults 2 and 3 causing uplift of the western anticlinal package and a footwall shear zone along the eastern margin of the complex.

An interesting consequence of the inferred duplex structure is the likelihood that considerable parts of the complex were cut above and below the presently exposed level. The cut off parts of the complex have been transported as members of different thrust packages further east or left behind to the west along the trajectory of overall eastward thrusting. A detailed knowledge of the regional structural pattern as well as relative amounts of displacement along individual faults may prove to be a valuable exploration tool in the search for other parts of the

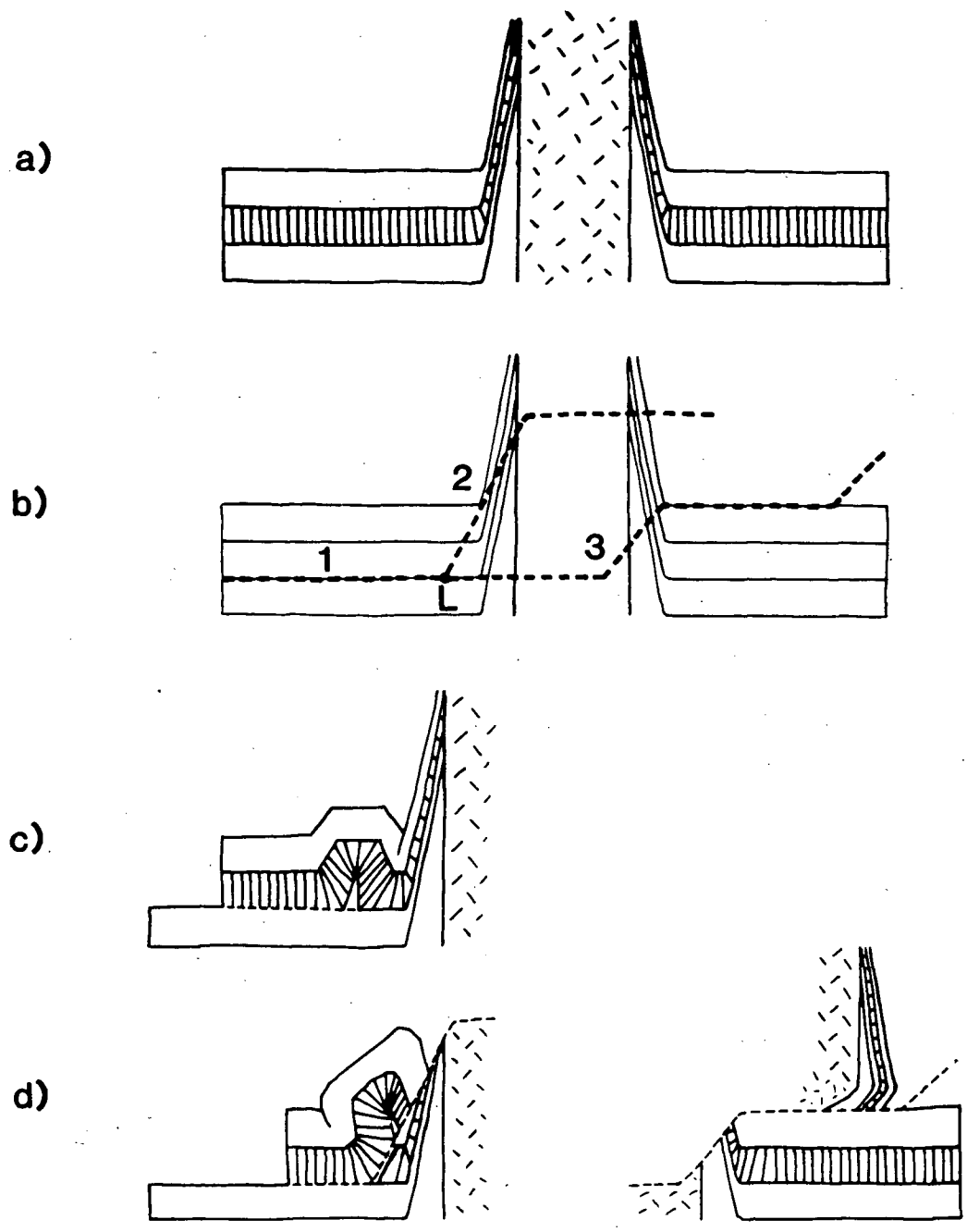

Figure 19: Possible sequence of events. For explanation see text.

complex. Amounts of shortening and displacement may be reconstructed from balanced cross sections with techniques already applied successfully in various parts of the Rocky Mountains (Thompson, 1979, 1986; Brown et al, 1986; Murphy, in press).

3. MINERALOGY AND MINERAL CHEMISTRY

3.1 INTRODUCTION

Carbonatites and related alkaline rocks are well known for their complex mineralogy (Heinrich, 1966; Vlasov, 1966; Tuttle & Gittins, 1966; Kapustin, 1980) and are still a source of new mineral discoveries. The number of rock-forming minerals in carbonatites is small, but the list of rare minerals is endless. A knowledge of the mineralogy and mineral chemistry and their variations is one of the keys towards understanding the geochemistry of these rocks.

Typically, the mineralogy varies spatially within the same rock type and often the chemistry of a mineral species displays a large compositional range. In the rocks of the Aley complex nearly fifty mineral species were identified or characterized within only four major rock types (table 1). The list of minerals is by no means complete with the number of new discoveries being largely a function of patience and magnification.

The minerals are grouped below into mineral classes with no particular ordering scheme. Analysis, energy dispersive spectra, microphotographs, back scattered electron images and crystal optical schemes are arranged in appendix A.

Mineral	Mineral Class	Occurrence
dolomite - ankerite	carbonate	cd,re1,re2,au
calcite	carbonate	cc,au,sy
strontianite (?)	carbonate	re1,cd
alstonite (barytocalcite) (?) $BaCa(CO_3)_2$	carbonate	re1
aragonite - strontianite ss (?)	carbonate	re1,sy
Sr-Ca-Ba carbonate (?)	carbonate	re1
burbankite $(Na,Ca,Sr,Ba,LREE)_6(CO_3)_5$	carbonate	re1
ancylite $LREE(Ca,Sr)(CO_3)_2(OH)\cdot H_2O$	carbonate	re1,sy
cordylite $Ba(LREE,Ca,Sr)_2(CO_3)_3F_2$	carbonate	re1,cd
huanghoite $BaLREE(CO_3)_2F_2$	carbonate	re,cd
Ce-Ba-La-Ca carbonate (?)	carbonate	re1
Ca-La-Nd carbonate (parisite) (?)	carbonate	re2

LREE carbonate (calkinsite, lanthanite) (?)	carbonate	au
Ca-Sr-Ba-Ce carbonate (?)	carbonate	re1,cc
apatite	phosphate	cd,cc,re1,sy
monazite (LREE,Th,Ca)PO_4	phosphate	cd
cheralite (Th,Ca,LREE)PO_4	phosphate	cd
rutile	oxide	cd
hematite	oxide	cd,cc,au
magnetite	oxide	cc
baddeleyite ZrO_2	oxide	cc
thorianite ThO_2	oxide	cd
pyrochlore $(Na,Ca)_2Nb_2O_6(OH,F)$	oxide	cc
fersmite $(Ca,Na)(Nb,Ta,Ti)_2(O,OH,F)_6$	oxide	cd,(cc)
columbite $Fe(Nb,Ta)_2O_6$	oxide	cd
zirkelite (?) $(Ca,Th)Zr(Ti,Nb)_2O_7$	oxide	cc
Ta-Ca zirconate-niobate	oxide	cd
quartz	silicate	sy,cc,cd,re2
albite	silicate	sy,cd
potassium feldspar	silicate	sy,re1
chlorite	silicate	cd,cc,di,la
biotite	silicate	cc,di,la
muscovite	silicate	au
magnesio-arfvedsonite $Na_3(Mg,Fe)_4Fe^{3+}Si_8O_{22}(OH,F)_2$	silicate	sy
richterite $Na_2Ca(Mg,Fe^{2+},Fe^{3+})_5Si_8O_{22}(OH,F)_2$	silicate	cc
aegirine $(Na,Ca)(Fe^{3+},Mg,Fe^{2+},Ti)Si_2O_6$	silicate	sy
lorenzenite $Na_2Ti_2Si_2O_9$	silicate	sy
zircon	silicate	cd
thorite (huttonite)	silicate	cd
cerite (?)	silicate	au
diopside	silicate	di
augite	silicate	di
Mg silicate	silicate	cc
barite	sulfate	re1,re2
pyrite	sulfide	cd,re1,re2,cc
galena	sulfide	re1

Table 1 : List of minerals identified in the Aley carbonatite complex. LREE = light rare-earth element (La,Ce,Nd,Pr); ss = solid solution; cd = dolomite carbonatite; cc = calcite carbonatite; re1 = rare-earth element carbonatite dikes (north ridge); re2 = barite rich rare-earth element carbonatite dikes (northwest ridge); sy = syenite; au = metamorphic rocks of the contact aureole; di = diatreme; la = lamprophyric dikes

3.2 CARBONATES

Dolomite $Ca(Mg,Fe,Mn)[CO_3]_2$ trigonal

Properties: light brown to chocolate-brown weathering; mostly untwinned; lamellar twinning abundant in marbles of the cantact aureole

Chemistry: dolomite - ankerite - kutnahorite solid solution ranging from 4.6 mol% $CaFe(CO_3)_2$ 0.5 mol% $CaMn(CO_3)_2$ (in dolomite carbonatite) to Mn-ankerite compositions (10.7 mol% $CaFe(CO_3)_2$, 5.1 mol% $CaMn(CO_3)_2$) in REE carbonatite dikes $SrCO_3$ values range from 0.02 mol% (dolomite carbonatite) to 0.25 mol% (REE carbonatite dikes)

Occurrence: major constituent of dolomite carbonatite, often as euhedral to subhedral phenocrysts (mm - 2 cm) in a finer-grained dolomite matrix; as rhombohedral crystals (mm) in fine-grained calcite matrix near calcite carbonatite - dolomite carbonatite contacts; ankerite is the major constituent in REE dikes; also forms dolomite marbles of the contact aureole

Alteration: minute grains of Fe-oxide/hydroxide (often hematite) cause a dusty appearance; Fe-oxide/hydroxide may concentrate along the rhombohedral cleavage and along grain boundaries; in various samples rutile forms thin (2 - 10 μ) sagenite figures along the rhombohedral cleavage leading to soft, fine, granular, metallic-looking aggregates (mm - cm); chlorite may also replace dolomite forming irregular or rhombohedral aggregates of fine, greenish black flakey aggregates (mm - cm) often mixed with sagenitic rutile, phosphates and Nb - oxides

Appendix A: tab 13, tab 14, figure 32, EDS-271, EDS-100

Calcite $(Ca,Mg,Fe,Mn)[CO_3]$ trigonal

Properties: grey to grey-brown weathering; mostly fine-grained, anhedral

Chemistry: Ca-Mg-Fe-Mn-Sr solid solution with composition near calcite $Ca(0.973)\ Mg(0.014)\ Fe(0.002)\ Mn(0.003)\ Sr(0.008)\ CO_3$ in calcite carbonatite;

manganese calcite in some syenite samples

Occurrence: major constituent of calcite carbonatite, either uniformly fine-grained (<1 mm) or forming ovoid phenocrysts (1 - 7 mm) in a fine-grained calcite matrix; often intense parallel twinning; manganese calcite associated with aegirine and albite in syenite; forms calcite marbles of the contact aureole

Alteration: calcite carbonatite appears to be more resistant towards weathering forming fresh, hard outcrops and clean drillcore

Appendix A: tab 15, EDS-228

Strontianite (Sr,Ba,Ca)[CO_3] orthorhombic

Properties: distinguishable only under the SEM-EDS

Chemistry: always with significant Ba and Ca substitution

Occurrence: in REE-carbonatite dikes (north ridge) and REE-rich dolomite carbonatite "sweats" associated with REE-carbonates; forms small, irregular grains (20 - 50 μ); it may be a (hydrothermal) alteration product

References: Kapustin, 1980; Heinrich, 1967; Tuttle & Gittins, 1967

Appendix A: figure 26, EDS-24

Alstonite (or Barytocalcite) (?) $BaCa[(CO_3)_2]$ triclinic (monoclinic)

Properties: distinguishable only under the SEM-EDS

Chemistry: always with minor Sr substitution

Occurrence: as irregular grains (<100 μ) associated with the REE-carbonates in REE-carbonatite dikes (north ridge); alstonite and barytocalcite are reported to be low-temperature hyddrothermal alteration pruducts (Kapustin, 1980)

Appendix A: figure 27, figure 28, EDS-136

Aragonite - Strontianite Solid Solution (?) $Ca(Sr,Ba)[CO_3]_2$ orthorhombic

Properties: distinguishable only under the SEM-EDS; sometimes forming fibrous aggregates

Chemistry: composition close to $CaSr(CO_3)_2$ with minor Ba substitution; such a phase is not known to occurr naturally, but was synthesized (Guichard & Wyast, 1943; Faivre, 1944)

Occurrence: forms irregular patches up to 0.2 mm in size associated with REE-carbonates in REE-carbonatite dikes (north ridge); in carbonate rich syenite as fibrous, irregular aggregates

Appendix A: figure 27, EDS-131

Sr-Ca-Ba Carbonate (?)

Properties: distinguishable only under the SEM-EDS

Chemistry: about similar amounts of Sr, Ca and Ba; it might be a solid solution of the isomorphous minerals aragonite - strontianite - witherite

Occurrence: as a minor phase in the REE-carbonate assemblage of REE-carbonatite dikes (north ridge); it may be an alteration product (cf. textures) although the aragonite-group minerals have high dissociation temperatures (800 - 900°C)

Appendix A: figure 28, EDS-112

Burbankite $(LREE,Sr,Ca,Ba,Na)_6[CO_3]_2$ hexagonal

Properties: colour, orange; transparent with a vitreous lustre under the binocular; no good cleavage (prismatic); uniaxial negative; low birefringence: $\Delta = 0.012$; high relief; no euhedral crystals observed; heating curve shows first endothermic inflection around 670°C (Vlasov, 1966)

Chemistry: an anhydrous Ca-Ba-Sr-Na-LREE carbonate; Ce is more abundant

than La; minor Pr, Nd

Occurrence: burbankite forms with ancylite the bulk of the REE-carbonate assemblage in the REE-carbonatite dikes (north ridge); forms irregular grains up to 0.5 mm but always with inclusions of other carbonates, phosphates and barite; it is thought to be the major primary magmatic phase of the REE-carbonate assemblage

References: Pecora & Kerr, 1953; Vlasov, 1966; Kapustin, 1980

Appendix A: figure 26, figure 27, EDS-21, figure 29

Ancylite $LREE(Ca,Sr)[(OH)/(CO_3)_2]\cdot H_2O$ orthorhombic

Properties: colour, greenish - ochre; transparent with vitreous lustre under the binocular; imperfect cleavage; optical properties are carbonate - like; decomposes at 480°C (Vlasov, 1966)

Chemistry: a Sr-LREE carbonate with various amounts of Ca (cf. calcioancylite, Fleischer, 1980); the chemical formula as written above (Vlasov, 1966; Fleischer, 1980) is also written as $(LREE)_4(Ca,Sr)_3[(OH)_4/(CO)_3)_7]\cdot 3H_2O$ (Rösler, 1980); Ce is the dominant LREE followed by La;

Occurrence: it is a major constituent of the REE-carbonate assemblage in the REE-carbonatite dikes (north ridge) forming irregular grains and aggregates (<400 μ); it is a (hydrothermal) alteration product, possibly replacing burbankite and other anhydrous carbonates or fluorcarbonates

References: Kapustin, 1980; Vlasov, 1966; Heinrich, 1967

Appendix A: figure 26, figure 27, figure 28, EDS-139

Cordylite $Ba(LREE,Ca,Sr)_2[F_2/(CO_3)_3]$ hexagonal

Properties: colour, ochre to wax-yellow

Chemistry: a Ba fluorcarbonate with minor Ca and Sr; Ce is the major REE,

followed by La

Occurrence: a minor phase in the REE-carbonate assemblage of the REE-carbonatite dikes (north ridge) forming irregular patches (<100 μ) showing alteration (or exsolution) patterns (slight differences in Ca - Sr ratios); also associated with huanghoite as small grains in REE-rich dolomite carbonatite sweats; cordylite may be a primary magmatic fluorcarbonate

References: Vlasov, 1966; Kapustin, 1980

Appendix A: figure 28, EDS-115

Huanghoite Ba(LREE)[F/$(CO_3)_2$] hexagonal (?)

Properties: colour, greenish yellow; clear with vitreous lustre under the binocular; distinct lamellar cleavage; lamellar, fan-shaped twinning common; always slightly biaxial negative due to deformation; relief and birefringence similar to dolomite; the heating curve shows a small endothermic inflection around 500°C, decarbonatisation occurs around 680°C (Vlasov, 1966)

Chemistry: a Ba-LREE fluorcarbonate with apparently strong selective Ce incorporation; the mineral discribed as Ce-Ba-La-Ca carbonate might be related to huanghoite

Occurrence: forms irregular interstitial aggregates up to cm-size in REE-rich dolomite carbonatite sweats; associated with minor cordylite, barite and phosphates; this is probably the first occurrence of huanghoite in North America

References: Semenov & P'ei - Shan, 1963; Vlasov, 1966; Kapustin, 1980

note: huanghoite was originally named huanchite (cf. Vlasov, 1966)

Appendix A: EDS-312

Ce-Ba-La-Ca Carbonate (?)

Properties: distinguishable only under the SEM-EDS

Chemistry: Ce > Ba > LA > Ca, LREE; similar to huanghoite, but with a higher LREE / Ba ratio and minor Ca substitution

Occurrence: as a minor phase within the REE-carbonate assemblage of the REE-carbonatite dikes of the north ridge

Appendix A; EDS-123

Ca-La-Nd Carbonate (?) (Parisite ?)

Properties: distinguishable only under the SEM-EDS

Chemistry; Ca, Ce > Nd > La > Pr; probably parisite $CaLREE_2[F_2/(CO_3)_3]$ (hexagonal) or synchysite $CaLREE[F/(CO_3)_2]$ (hexagonal)

Occurrence: forming interstitial aggregates (up to 0.5 mm) with barite in the barite-rich REE-carbonatite dikes (northwest ridge)

References: Makasimocic & Panto, 1979; Vlasov, 1966; Kapustin, 1980

Appendix A: EDS-212

LREE Carbonate (?)

Properties: distinguishable only under the SEM-EDS

Chemistry: Ce > La, Nd > Pr > Ca; it is probably one of the hydrous LREE carbonates calkinsite $LREE_2[(CO_3)_3]\cdot 4H_2O$ (orthorhombic) or lanthanite $LREE_2[(CO_3)_3]\cdot 8H_2O$ (orthorhombic)

Occurrence: as prismatic crystals (10 μ) replacing parisite (?) in the Ba-rich REE-carbonatite dikes (northwest ridge); reported to be a weathering product of burbankite (Kapustin, 1980)

References: Pecora & Kerr, 1953; Vlasov, 1966; Kapustin, 1980

Appendix A: EDS-242

Ca-Sr-Ba-Ce Carbonate (?)

Properties: distinguishable only under the SEM-EDS

Chemistry: Ca >> Sr > Ba, Ce > La; may be similar to carbocernite (Ca,LREE,Na,Sr)[CO_3] (orthorhombic) in composition

Occurrence: minor phase in the REE-carbonate assemblage of the REE-carbonatite dikes (north ridge); as minute grains (10 μ) in a drillcore sample of calcite carbonatite

Appendix A: figure 26, figure 28, EDS-238

3.3 PHOSPHATES

Apatite $Ca_5[(OH,F)/(PO_4)_3]$ hexagonal

Properties: easily visible on weathered surfaces as white grains against recessive weathering grey or brown carbonatite; hard to identify on fresh rock

Chemistry: usually contains no SEM-EDS-detectable substitution, except Fe in a few samples of calcite carbonatite; in REE-carbonatite dikes minor LREE (Ce > La, Nd) contents are characteristic

Occurrence: abundant in dolomite carbonatite and calcite carbonatite as prismatic crystals, rounded prisms (in calcite carbonatite) or ovoid, radiating aggregates; small, rounded or irregular grains (50 - 100 μ) in REE-carbonatite dikes and syenite; accessory mineral in sedimentary marbles of the contact aureole

Appendix A: EDS-19, EDS-227

Monazite (LREE,Th,Ca)[PO_4] monoclinic

Properties: mostly small anhedral inclusions and distinguishable only under the SEM-EDS; rarely euhedral, long prismatic (parallel c); high relief; birefringence: $\Delta \simeq 0.05$; biaxial positive; small 2Vz; extinction angle $X < c \simeq 16°$

Chemistry: most SEM-EDS patterns show detectable Th and Ca substitution; Ce is always the dominant REE followed by La, Nd and Pr

Occurrence: in dolomite carbonatite where it is frequently associated with fersmite pseudomorphs after pyrochlore, forming euhedral crystals or small inclusions (10 - 50 μ)

Appendix A: EDS-79, EDS-2

Cheralite (?) (Th,Ca,LREE)[PO_4] monoclinic

Properties: distinguishable only under the SEM-EDS

Chemistry: high Th-content (none or minor U), about similar amounts of Ca and total LREE (Nd, Ce >> La, Pr)

Occurrence: was observed only in one dolomite carbonatite sample as minute inclusions in columbite

Appendix A: EDS-15

3.4 OXIDES

Rutile (Ti,Nb,Fe)O_2 tetragonal

Properties: distinguishable only under the SEM - EDS

Chemistry: always with substitution of Nb an Fe for Ti (ilmenorutile is reported to contain up to 32 wt% Nb_2O_5, Palache et al, 1944); rutile from carbonatites are reported with up to 18 wt% Nb_2O_5 (Kapustin, 1980)

Occurrence: as thin (5 - 10 μ) sagenite lamellae (striation, 120° knee-shaped twinning) along the rhombohedral cleavage of dolomite forming dark, metallic, fine granular aggregates (mm - cm) nucleating from columbite-fersmite aggregates (after pyrochlore ?); also in chlorite aggregates (with Nb-oxides) probably replacing dolomite and pyrochlore in dolomite carbonatite; as small (10 - 50 μ) accessory grains in dolomite carbonatite; as irregular inclusions (2 - 15 μ, exsolution ?) in lorenzenite

References: Kapustin, 1980

Appendix A: figure 32, EDS-12

Hematite Fe_2O_3 hexagonal

Occurrence: abundant in weathered dolomite carbonatite forming small inclusions in dolomite, often accumulated along the rhombohedral cleavage and grain boundaries; as small hexagonal platlets or aggregates of plates; as irregular grains and hexagonal plates in some pseudomorph assemblages replacing pyrochlore in dolomite carbonatite

Magnetite Fe_3O_4 cubic

Properties: frequently displaying cubic habit; also subhedral, large (1 - 2 cm) crystals (some with trapezohedral faces); exsolution lamellae of ilmenite are occasionally developed

Chemistry: most analyses (SEM-EDS) show titaniferous magnetite

Occurrence: typical constituent in calcite carbonatite, often forming bands sorted according to crystal size; may accumulate in areas as big as 100 m^2 in calcite carbonatite with 10 - 30 % magnetite; inclusions of apatite, carbonate and biotite are common; larger grains are often fractured or broken apart; not observed in dolomite carbonatite or REE carbonatite dikes

References: Kapustin, 1980; Ramdohr, 1955

Appendix A: EDS-180, EDS-172

Baddeleyite ZrO_2 monoclinic

Properties: forms prismatic or tabular, rarely equant brown crystals with a vitreous lustre; cleavage, {001} good, {010} poor to distinct; very high relief; very high birefringence: $\Delta > 0.1$; biaxial negative; $2Vx \cong 20 - 30°$; $r > v$; pleochroism: light yellow (Z, Y) to brownish yellow (X); absorption: $X > Y > Z$; always twinned: on {110} and polisynthetic on {100}; thermally stable to very high temperatures with two phase transitions reported (Kapustin, 1980)

Chemistry: no SEM-EDS detectable impurities (small amounts of Fe_2O_3 and HfO_2 are reported: Palache et al, 1944; Kapustin, 1980)

Occurrence: was observed only in one sample of fine grained magnetite - apatite calcite carbonatite as abundant, small (0.2 - 0.6 mm) crystals; associated and partially replaced by niobian zirkelite (?)

References: Kapustin, 1980; Palache et al, 1944

Appendix A: figure 33, EDS-165

Thorianite (?) $(Th,U)O_2$ cubic

Properties: distinguishable only under the SEM-EDS

Chemistry: Th with minor U; no clean EDS - signal was obtained due to the grainsize (2 μ)

Occurrence: as minute inclusions (2 μ) in fersmite pseudomorphs after pyrochlore in dolomite carbonatite

References: Vlasov, 1966; d'Arcy, 1949; Kapustin, 1980

Pyrochlore $(Ca,Fe^{2+},Na,Th,U)_{2-m}(Nb,Ti,Ta,Fe^{3+})_2O_6(O,OH,F)_{1-n} \cdot pH_2O$ cubic

Properties: colour: black, dark brown, honey-brown, straw-brown, tan, reddish brown, brownish pink; habit: octahedral, sometimes modified by the dodecahedron {110} and cube {100} (figure 34); 0.1 - 4 mm in size, some calcite carbonatites with irregular crystals up to 2 cm; fracture, conchoidal or splintery; vitreous to sub-metallic lustre; very high relief; isotropic or slightly anisotropic; intense body colour: dark brown, straw-brown, yellow-brown, red-brown; often zonal structures visible; grey, non - pleochroic under reflected light, similar to magnetite but with a slightly lower reflectivity; usually not metamict with a fairly sharp X-ray diffraction pattern

Chemistry: a complex oxide of the $A_2B_2O_6$ - type with a wide range of composition; the samples analyzed (SEM-EDS, EMS) are all close to the Nb-endmember with various amounts of Ca, Ti, Fe, Na, Ta, Th, U; compositional zoning may or may not be present and is mostly simple, rarely multiple; zoned crystals show a rim with a higher average atomic number than the core with Th being one of the elements enriched in the rim (figure 37)

Occurrence: typical mineral in banded calcite carbonatite associated with apatite, magnetite, ±biotite, ±amphibole; may form relict crystals in fersmite-columbite pseudomrphs in altered, chlorite-rich dolomite carbonatite; often substantially concentrated in narrow bands and sweats in calcite carbonatite; often with inclusions of carbonate, apatite and biotite; zoning frequently macroscopically visible

Alteration: pseudomorphs of fersmite after pyrochlore are abundant in dolomite carbonatite; pyrochlore may show several stages of alteration (ie. secondary growth of fersmite in fersmite pseudomorphs after pyrochlore, columbitization of fersmite pseudomorphs after pyrochlore)

References: Hogarth, 1961; Hogarth, 1977; Palache et al, 1944; Kapustin, 1980

Appendix A: figure 34, figure 35, fig 36, figure 37, EDS-224, 225, 277, 278

Fersmite $(Ca,Na,Th,U)(Nb,Ti,Fe,Ta,Zr)_2(O,OH,F)_6$ orthorhombic

Properties: habit: pseodomorph after octahedral pyrochlore, secondary growth of small prismatic crystals; primary equant crystals (several mm) with prism {110}, pinacoid {010} and orthorhombic dipyramid {111} developed (figure 38); colour, honey-brown to black-brown; resinous lustre if well crystallized (weathered crystal surfaces often dull); zonation often macroscopically visible; no good cleavage, concoidal fracture; very high relief; very high birefringence; colour, brown to grey-brown; often metamict (broad X-ray reflections)

Chemistry: an oxide of the type $AB_2(O,OH,F)_6$ with a complex chemistry (Nb, Ca, Na, Fe, Ti, Ta, Th, U, Zr) similar to pyrochlore, but with a higher Nb content

Occurrence: most common Nb-phase in dolomite carbonatite, almost always pseudomorph after pyrochlore; rarely as a primary phase in dolomite carbonatite; may replace pyrochlore in altered, chlorite-rich calcite carbonatite; associated with other Nb-oxides, phosphates, carbonate and hematite in pseudomorphs after pyrochlore (cf. pyrochlore: alteration)

Alteration: often partially metamict as fine grained aggregates replacing pyrochlore; sometimes partially replaced by columbite

References: Bohnstedt - Kupletskaya & Burova, 1947; Vlasov, 1966; Kapustin, 1980

Appendix A: figure 38, figure 39, figure 40, EDS-267, 70

Columbite $(Fe,Mg)(Nb,Ti,Ta)_2O_6$ orthorhombic

Properties: colour, black; lustre, sub-metallic; irregular grains (aggregates); high relief; opaque; grey under reflected light, reflectivity distinctive lower than pyrochlore (and magnetite); may show reddish brown internal reflections

Chemistry: reported as a complex oxide near $(Fe,Mn,Mg)(Nb,Ta)_2O_6$, isostructural with brookite; the samples examined (SEM-EDS) show considerable

Ti substitution (Ti has been ascribed to impurities [Palache et al, 1944] which was not observed in the samples studied); Mg, Mn and Ta are above the SEM-EDS detection limit

Occurrence: forms irregular, granular aggregates in a dolomite carbonatite sample with chlorite-rutile aggregates, carbonate-rutile aggregates and fersmite pseudomorphs after pyrochlore; some vaguely preserved octahedral forms suggest that columbite forms after pyrochlore; also as acicular, radiating aggregates forming in fersmite pseudomorphs after pyrochlore

References: Palache et al, 1944; Vlasov, 1966; Kapustin, 1980

Appendix A: EDS-7

Zirkelite (?) $(Ca,Th)Zr(Ti,Nb)_2O_7$ monoclinic

Properties: colour, black to dark brown; prismatic crystals (without distinct terminal faces) growing parallel or at 45° angels (0.05 - 0.2 mm); very high relief; isotropic or anisotropic; very strong dark reddish brown body colour;

Chemistry: an $A_2B_2O_7$ oxide consisting of Ti, Zr, Ca, Fe, Th, Nb, and possibly U; Ti / Zr ratio appears to be variable

Occurrence: always intimately associated with baddeleyite and partially replacing it by forming an (epitaxial ?) overgrowth

References: Borodin et al, 1957; Palache et al, 1944; Vlasov, 1966; Kapustin, 1980

note: the old names zirconolite and niobozirconolite are replaced by zirkelite (Hogarth, 1977)

Appendix A: EDS-151

Ta-Ca Zirconate - Niobate

Properties: probably a metamict, granular mass

Chemistry: Ta-rich Nb-phase with Ca, Th, U, Ti and minor Fe (may not be a pure SEM-EDS signal)

Occurrence: together with fersmite replacing pyrochlore in a dolomite carbonatite sample

Appenddix A: EDS-72

3.5 SILICATES

Quartz SiO_2 trigonal

Occurrence: accessory mineral in barite-rich REE-carbonatite dikes (northwest ridge) where it forms irregular aggregates with slightly undulous extinction; rare in altered dolomite carbonatite and calcite carbonatite; as coarse, irregular crystals of milky quartz (2 - 15 mm) accumulated in a dolomite carbonatite sample (float); constituent in syenite in variable abundancies

Albite $Na[AlSi_3O_8]$ triclinic

Properties: as irregular grains, often untwinned; subhedral to euhedral crystals with frequent carlsbad and albite twinning

Chemistry: almost pure $NaAlSi_3O_8$ with minor K_2O (< 0.2 wt%) and FeO (0.4 wt%)

Occurrence: major constituent in syenite-xenoliths in alkali syenite as subhedral to euhedral grains (0.1-2 mm); irregular grains in syenite; accessory mineral in some impure marbles; accessory mineral in a few samples of dolomite carbonatite

Appendix A: table 16, figure 41, EDS-50

Potassic Feldspar $K[AlSi_3O_8]$ monoclinic, triclinic

Chemistry: almost pure potassium feldspar with 0.7 wt% Na_2O and traces of Fe

Occurrence: small, irregular grains as accessory mineral in REE-carbonatite dikes (north ridge); minor constituent in syenite; in marbles of the contact aureole; not observed in calcite carbonatite or dolomite carbonatite

Appendix A: EDS-259

Chlorite $(Mg,Al,Fe)_{12}[(OH)_{16}/(Si,Al)_8O_{20}]$ monoclinic

Properties: colour, dark green; colourless in thin section, brownish if weathered; uniaxial positive; negative elongation; occasionally with anomalous violet interference colours (and positive elongation)

Chemistry: variable Mg / Fe ratio, but always substantial Fe; ranging from grochauite to aphrosiderite in composition

Occurrence: common as a secondary mineral in dolomite carbonatite; subordinate in altered calcite carbonatite; in some chloritized zones it may form up to 50 % of the rock as ovoid crystals (0.5 - 5 mm); it may form fine grained aggregates with minor rutile in dolomite carbonatite

Appendix A: EDS-81

Muscovite - Phengite $K_2Al_2(AL,Mg,Fe)_2[(OH,F)_4/(Al,Si)_2Si_6O_{20}]$ monoclinic

Occurrence: as metamorphic mineral in impure marbles and metamorphic marls of the contact aureole

Biotite - Phlogopite $K_2(Mg,Fe)_{6-4}(Fe,Al,Ti)_{0-2}[(OH,F)_4/Si_{6-5}Al_{2-3}O_{20}]$ monoclinic

Properties: colour, light brown to dark brown or reddish brown; often forming hexagonal prismatic crystals or large flakes; variable pleochroism with reversed pleochroic scheme in calcite carbonatite: X > Y ≃ Z (cf. tetraferriphlogopite of Rimskaya - Korsakova & Sokolova, 1964; mentioned in Kapustin, 1980), X = brown, Y = Z = very pale brown; X = brown, Y = Z = pale greenish brown; X = pale brown, Y = Z = pale green, absorption X ≃ Y ≃ Z; X = deep bordeaux-red, Y = Z = pale brown; sometimes zoned with core (X = pale brown, Y = Z = pale green) and rim (X = green, Y = Z = green, absorption X < Y = Z); also with normal pleochroic scheme in lamproites: X = pale brown to colourless, Y = Z = dark red-brown to brown, absorption X << Y = Z

Chemistry: Mg-rich; some varieties (often the rim in zoned crystals) have SEM-EDS detectable Ti; biotite from the diatreme is Ti-rich and contains minor Cr.

Occurrence: constituent in most calcite carbonatites (reversed pleochroic scheme), where it forms equant crystals (up to 5 mm); often enhancing banding together with pyrochlore, apatite and magnetite; constituent in the diatreme and lamprophyric dikes (groundmass and flakes up to 5 cm, with normal pleochroic scheme); as inclusions in magnetite (with apatite) forms also biotite rich zones at some syenite-calcite carbonatite contacts (very fine grained or coarse, with reversed pleochroic scheme)

References: Kapustin,1980

Appendix A: EDS-77, 222, 223

Magnesio - Arfvedsonite $(Na,Ca,K)_3(Mg,Fe^{2+},Mn)_4(Fe^{3+},Ti)[(OH,F)_2/Si_8O_{22}]$ monoclinic

Properties: colour, greenish black; vitreous lustre; perfect prismatic cleavage {110}; subhedral prismatic crystals (<0.5 mm) with {110} and subordinate {010}; often somewhat poikiloblastic; biaxial negative; 2Vx ≃ 70-80°; v > r very strong; extinction angle Z < c ≃ 30°; birefringence: Δ ≃ 0.015; pleochroism: X = light greyish yellow-green, Y = light greenish grey, Z = pale greenish grey, absorption X ≃ Y ≃ Z; optic axial plane parallel (010); twinning uncommon, parallel (100); anomalous extinction: anomalous brown-violet to anomalous blue

Chemistry: average composition: SiO_2(54.7 wt%), TiO_2(0.2 %), Al_2O_3(0.1 %), FeO(11.0 %), MnO(0.9 %), MgO(16.3 %), CaO(2.5 %), Na_2O(8.3 %), K_2O(1.8 %), F(2.5 %); near magnesio-arfvedsonite with solid solution towards richterite and magnesio-riebeckite and K substitution; Ca values vary coupled with Fe and Mg

Occurrence: abundant in syenite and micro-syenite xenoliths in syenite

References: Kapustin, 1980; Tröger, 1979; Veblen, 1981

Appendix A: table 17, table 18, figure 42, figure 43, EDS54, 95

Richterite $(Na,K)_2Ca(Mg,Fe,Mn)_5[(OH,F)_2/Si_8O_{22}]$ monoclinic

Properties: green to black-green; prismatic to acicular with {110}, {100} and {010}; perfect prismatic cleavage {110}; twinning common parallel (100); biaxial (negative ?); large 2V ≃ 75-105°; birefringence: Δ ≃ 0.02; extinction angle Z < c ≃ 20°; elongation positive; colourless or weak pleochroic: X = Y = pale greenish, Y = pale brown-orange; optic axial plane parallel (010)

Chemistry: Al-poor sodic Mg-Ca pyroxene with variable Fe and Ca contents and always minor K

Occurrence: rare to abundant in calcite carbonatite near syenite; oriented

parralel to planar fabric; sometimes forming almost monomineralic bands with comb-layering texture

Appendix A: fig 44, fig 45, EDS-11

Aegirine $(Na,Ca)(Fe^{3+},Mg,Fe^{2+},Ti)[Si_2O_6]$

Properties: colour, dark green; vitreous lustre; poor prismatic cleavage {110}; acicular, small crystals (< 0.4 mm); square cross sections common; birefringence: $\Delta \simeq 0.04$; $2V \simeq 40\text{-}70^\circ$; stright extinction; pleochroism: X = Y = light yellow-green, Z = green, absorption Z > X ≃ Y

Chemistry: average composition: SiO_2(52.7 wt%), TiO_2(5.8 %), Al_2O_3(0.5 %), Fe_2O_3(23.2 %), MnO(0.4 %), MgO(2.6 %), CaO(1.3 %), Na_2O(13.5 %), K_2O(0.1 %); near 70 mol% acmite, but with additional Na (1.0 Na sites per 6 oxygens), minor Ca and substantial Ti substitution

Occurrence: abundant in syenite as acicular or prismatic crystals; forming inwardly-pointing acicular crystals in small spherulites with albite and manganese calcite in syenite; less abundant in micro-syenite xenoliths in syenite

References: Kapustin, 1980; Tröger, 1979; Reviews in Mineralogy, vol. 7

Appendix A: table 19, figure 46, figure 47, EDS-68, 88

Zircon $Zr[SiO_4]$ tetragonal

Properties: colour, light honey-brown; diamond lustre; pale yellow-brown in thin section

Chemistry: no other elements detectable under the SEM-EDS; apperently very low U-Pb contents (Parrish, pers. com., 1986)

Occurrence: accessory mineral in dolomite carbonatite, usually rare, but enriched in some zones with abundant short prismatic dipyramidal crystals (1 - 5 mm); as small grains (10 μ) associated with fersmite in fersmite

pseudomorphs after pyrochlore in dolomite carbonatite

Lorenzenite $Na_2Ti_2[O_3/Si_2O_6]$ orthorhombic

Properties: dark brown; vitreous lustre on broken surface; striated, long-prismatic crystals; pale lilac-brown in thin section; non-pleochroic; very high relief; very high birefringence: $\Delta > 0.1$; good cleavage parallel c {001}, {110} poor; twinning parallel c frequent; often slightly undulous extinction; biaxial positive with a small 2V

Chemistry: always shows some Nb substitution and rarely SEM-EDS detectable Fe

Occurrence: as an accessory mineral in syenite as prismatic or irregular crystals; forms monomineralic veinlets in syenite

References: Sakama, 1947; Kapustin, 1980

Appendix A: EDS-255

Thorite (Huttonite) (Th,U)[SiO_4] tetragonal (monoclinic)

Properties: distinguishable only under the SEM-EDS

Chemistry: close to Th(SiO_4) with minor U substitution

Occurrence: small, irregular inclusions (5 - 20 μ) in fersmite pseudomorphs after pyrochlore and in columbite replacing pyrochlore in dolomite carbonatite

References: d'Arcy, 1949; Kapustin, 1980

Appendix A: EDS-78

Cerite (?) $(LREE,Ca)_9(Mg,Fe)[Si_7(O,OH,F)_{28}]$ trigonal

properties: distinguishable only under the SEM-EDS

Chemistry: similar amounts of Si, Ca and LREE; Ce more abundant than La,

Nd, Pr; considerable confusion about the chemical formula: $Ca_2(LREE)_8[SiO_4]_7 \cdot 3H_2O$ (Rösler, 1980), $(LREE,Ca)_2[Si(O,OH)_5]$ (Dana, 1896)

Occurrence: small grains in a dolomite marble of the contact aureole

References: Rösler, 1980; Fleischer, 1980; Dana, 1896; Glass et al, 1958; Kapustin, 1980; Vlasov, 1966

Appendix A: EDS-201

Diopside $(Ca,Mg,Fe^{2+},Fe^{3+},Cr)_2[(Si,Al)_2O_6]$ monoclinic

Properties: pistacio green crystals; vitreous lustre; excellent prismatic cleavage

Chemistry: Ca-Si-Mg-Fe pyroxene with minor Al and Cr

Occurrence: very rare as small, ovoid xenocrysts (mm) in the lamproitic diatreme

Appendix A: EDS-3

Augite $(Ca,Mg,Fe^{2+},Fe^{3+},Al,Ti)_2[(Si,Al)_2O_6]$ monoclinic

Properties: black crystals; vitreous lustre; good prismatic cleavage

Occurrence: fairly abundant ovoid xenocrysts in the lamproitic diatreme

Appendix A: EDS-4

Mg - Silicate

Properties: weathering resistent dirty olive-green, roundish crystals (0.5 - 7 mm) with ochre encrustations; dark grey-green on fresh surfaces; vitreous lustre when fresh; clear X-ray diffraction pattern

Chemistry: Mg-silicate with minor Ca

Occurrence: in one sample (float) of calcite carbonatite associated with magnetite and minor pyrite and biotite

3.6 SULFATES

Barite $Ba[SO_4]$ orthorhombic

Properties: visible often only under the SEM-EDS; larger crystals are colourless, show undulous extinction and two good cleavages {100}, {010}

Chemistry: no other elements above SEM-EDS detection limit

Occurrence: accessory mineral in REE-carbonatite dikes of the north ridge forming small grains (10 μ) associated with the REE-carbonate assemblage; abunant in the REE-carbonatite dikes of the West ridge forming interstitial crystals (1 - 5 mm) within euhedral ankeritic dolomite; accessory mineral in alkali - syenite forming small irregular grains (10 - 50 μ)

References: Kapustin, 1980

Appendix A: figure 27, figure 26, EDS-211

3.7 SULFIDES

Pyrite FeS_2 cubic

Occurrence: typical accessory mineral of dolomite carbonatite and calcite carbonatite; mostly idiomorphic (cube), sometimes irregular; often replaced by Fe-oxides/hydroxides; may be locally concentrated; typical in REE-carbonatite dikes (north ridge) as cubes (0.5 - 5 mm)

Pyrrhotite $Fe_{1-X}S$ monoclinic or hexagonal

Occurrence: only observed in a drillcore sample of calcite carbonatite where it forms schlieren with euhedral magnetite, biotite and minor pyrite (exsolution in pyrrhotite ?)

Galena PbS cubic

Occurrence: observed in one sample of a REE-carbonatite dike as a tiny grain (5 μ); appears to be absent in all rock types of the complex

4. PETROGRAPHY

The igneous rocks of the Aley carbonatite complex may be divided into four major types: dolomite carbonatite, calcite carbonatite, rare-earth carbonatite dikes and "syenite". In spite of this apparent simplicity the variety of textures, fabrics and mineral modes is puzzling. Thus, the reader should keep in mind, that "representative" sampling and petrographic analysis is likely to be biased. The following petrographic characterization of the major rock types is an attempt to synthesize the relevant observations and is thus a simplification.

4.1 DOLOMITE CARBONATITE

Petrographic name:

Fersmite- and pyrite-bearing dolomite-apatite-carbonatite

Physical Properties:

Dolomite carbonatite weathers a distinctive reddish brown colour and is white or brownish on fresh surfaces. Radioactivity is spatially variable, generally low, but distinctly higher than in the "syenite" ring and generally lower than in calcite carbonatite. Magnetic susceptibility is low. Density is close to 3.0×10^3 kg/m^3, calculated from dolomite compositions presented in section 3.2.

Mineral mode:

Modal abundances of constituents in dolomite carbonatite range from almost pure dolomite ($\leq$1 % apatite) to apatite-rich varieties ($\simeq$10%). Accessory fersmite is always present and may be enriched in diffusely defined zones, but probably not exceeding 1 % modal concentration. Pyrite is a common accessory mineral, locally enriched (1-2 %) and commonly concentrated in fracture and shear zones (up to 5 %, almost always oxidized). Other accessory minerals include zircon, albite, quartz, rutile, columbite, monazite and strontianite. Alteration products include chlorite (up to 60 %), rutile, columbite and fersmite pseudomorphs after pyrochlore.

Textures:

Different degrees of deformation and alteration result in a variety of textures. The transition between primary magmatic crystallization and recrystallization is probably diffuse such that primary and secondary carbonate textures are commonly ambiguous. Carbonatite dolomite textures do, however, look quite different from dolomite marbles.

A typical, fresh dolomite carbonatite has a large range of grain sizes (0.1-4 mm) with a granoblastic interlocking texture with straight grain boundaries, abundant reentrant angles, unequal angle triple-joints and is almost idiotropic in some parts. Characteristic are small rhombohedral "inclusions" or subgrains of dolomite with a different crystallographic orientation than the dolomite host grain.

Apatite occurs as prismatic (parallel c-axis), rounded crystals (0.1-2 mm) aligned subparallel to the planar fabric without a clear linear trend. Apatite may also form radiating bunches forming disk-like flattened aggregates up to 2 cm in size oriented parallel to the fabric.

Narrow zones of higher strain are marked by abundant twinning of dolomite with conjugate glide-twin systems developed. Narrow fracture zones show much finer grain sizes and a granoblastic - polygonal texture. In these zones veinlets of secondary quartz might occur replacing dolomite but without forming any calc-silicate phases.

Fersmite forms fibrous to fine-grained aggregates within perfect octahedrons, thus replacing pyrochlore (appendix A: figures 39, 40). Primary fersmite (orthorhombic) is rare (appendix A: figure 36). Columbite might replace fersmite which is observed commonly in chloritized zones. Relict cores of pyrochlore are rarely preserved. Fersmite pseudomorphs normally have inclusions of apatite, monazite and albite. Secondary overgrowth of small, prismatic, pyramidal fersmite crystals is common.

Alteration:

Metallic black, fine granular aggregates (0.5-15 mm) which may be mistaken for columbite or fersmite are of widespread occurrence and consist mainly of thin sagenitic niobian rutile plates grown along the rhombohedral cleavage of dolomite (figure 32). These aggregates form brownish, dirty patches in thin section commonly associated with fine granular magnetite and minor Nb-oxides, apatite, monazite, chlorite and minute grains of Th-phases (thorite, thorianite, cheralite). Dolomite carbonatite rich in these aggregates shows a higher level of radioactivity. In some samples these aggregates seem to nucleate from altered pyrochlore cores, but this is the exception.

A second type of black aggregate (1-15 mm) consists of fine grained chlorite with sagenitic rutile and is probably an alteration of dolomite-rutile aggregates. Rectangular grain shapes are indicative of pseudomorphism, although no relicts of the primary phase were observed.

Heavily chloritized dolomite carbonatite zones (0.5-2 m wide) occur along the southeastern margin of the core - complex. They consist of up to 60 % chlorite, 30-35 % dolomite, 2-3 % apatite, 2-4 % quartz and commonly abundant (2-20 %) fine grained (0.1-0.5 mm) fersmite pseudomorphs after pyrochlore with frequently preserved pyrochlore cores. Equant, flaky chlorite (0.2-5 mm) replaces dolomite and quartz. Quartz commonly shows mosaic substructures similar to growth structures observed in vein quartz and is interpreted to be secondary quartz. Colourless, aluminous chlorite with normal interference colours develops anomalous blue fringes in contact with fersmite due to increased Fe-substitution. It is not clear whether the concentration of fersmite pseudomorphs is of primary magmatic origin or due to hydrothermal activity in fracture and breccia zones. The presence of silicification and chloritisation would favour the latter explanation.

4.2 CALCITE CARBONATITE

Petrographic name:

Magnetite, biotite, pyrochlore, amphibole-bearing calcite-apatite- carbonatite

Physical properties:

Calcite carbonatite weathers a distinctive grey to brownish grey colour, distinguishable easily from dolomite carbonatite. Density is about 2.8 to 3.0×10^3 kg/m^3 depending on the amount of metal oxides present. Magnetic susceptibility is high due to the presence of magnetite. Radioactivity is generally higher than in dolomite carbonatite due to the overall higher pyrochlore concentrations in calcite carbonatite.

Mineral mode:

Typically, calcite carbonatite displays a highly variable mineral content due to mineral layering and differences in the mineral content of individual calcite carbonatite "sweats". Mineral modes vary between: calcite (40-95 %), magnetite (0-40 %), apatite (2-10 %), biotite (0-5 %), pyrochlore (0-2 %), amphibole (0-5 %), pyrite (0-0.5 %) and traces of hematite, baddeleyite, zirkelite, quartz and chlorite.

Textures:

Calcite carbonatite typically has a strong parallel fabric marked by a cleavage and mineral layering (appendix A: figure 12). Calcite forms a granoblastic - polygonal texture and is much finer grained (0.05-0.2 mm) than dolomite carbonatite. Conjugate systems of glide-twins are well developed. Some calcite carbonatites have ovoid calcite "phenocrysts" (1-5 mm) in a fine grained matrix.

Apatite forms prismatic, rounded crystals or disk-like flattened aggregates aligned parallel to the fabric. These aggregates are composed of radially textured, long prismatic crystals. The distribution of apatite is inhomogeneous due to the pronounced layering (cm-dm scale).

Biotite forms hexagonal, prismatic, equant crystals (0.1-5 mm) enriched in bands where it is associated commonly with magnetite and/or pyrochlore.

Pyrochlore displays its octahedral habit with grain sizes ranging from 0.1 to 4 mm (appendix A: figure 34). It is isotropic, rarely slightly anisotropic (metamict ?). Pyrochlore is enriched in narrow bands following apatite-rich zones associated with or without biotite and magnetite. Inclusions of biotite, apatite and calcite are common. Zoned crystals are the rule with a marked break between the core and a narrow rim of higher mean atomic number (appendix A: figures 35, 36, 37).

Amphibole of richterite composition is fibrous to acicular (5-200 μ in width) aligned parallel to the fabric. Fibrous amphibole forms in fine grained zones of high strain, commonly marked by a brownish dirty colour in thin section due to preferential weathering. Amphibole is more abundant in calcite carbonatites immediately adjacent to "syenite" suggesting a metasomatic origin of most of the amphibole with the "syenite" being the source of silica and alkalies.

Accessory minerals include pyrite cubes (0.05-0.3 mm) and baddeleyite associated with zirkelite (only in one sample observed).

Alteration:

Calcite carbonatite appears to be more resistant to weathering than dolomite carbonatite (cf. stable isotope data, section 5.3.2). Small amounts of chlorite amd secondary quartz may form in zones of higher strain and more intense weathering. Hematite as an oxidation product of magnetite occurs as minute grains in minor amounts.

4.3 RARE - EARTH CARBONATITE DIKES

Two dike swarms occur in the contact aureole of the complex (cf. fig. 2): one across the north ridge, characterized by orange, ovoid rare-earth carbonate aggregates and one across the northwest ridge, characterized by abundant barite, quartz and dispersed rare-earth carbonates. Work was focussed on the dikes of the north ridge.

4.3.1 RARE-EARTH CARBONATITE DIKES OF THE NORTH RIDGE

Petrographic name:

Rare-earth carbonate and pyrite-bearing ankerite-carbonatite

Physical properties:

The rare-earth dikes weather a distinctive dark chocolate-brown colour. The dikes are resistant to weathering, off-white coloured on fresh surfaces with orange to greenish, granular, porous, ovoid rare-earth carbonate aggregates (appendix A: figure 31). Typical are black haloes around partially oxidized pyrite cubes. Density is about 3.2×10^3 kg/m^3 due to the ankeritic bulk composition. Magnetic susceptibility and radioactivity are very low.

Mineral mode:

The carbonatite dikes consist of 95 to 97 % manganese ankerite, 3 to 5 % rare-earth carbonates and 0.1 to 0.5 % pyrite. Apatite, barite, potassium feldspar, strontianite and alstonite (?) occur in trace amounts.

Textures:

Coarse-grained ankerite (1-4 mm) forms an irregular granular texture with commonly sutured grain boundaries. Intergranular mortar zones are abundant. Ankerite shows wavy extinction, but no twinning. Subgrains are locally developed.

The rare-earth carbonate assemblages form ovoid or irregular aggregates (2-20 mm) (appendix A: figure 31). Characteristic are replacement textures and porosity due to weathering and defects from polishing. Burbankite is the major primary rare-earth carbonate forming grains up to 2 mm in size. Burbankite shows various stages of alteration: coherent grains with a web of thin veinlets of alteration products (appendix A: figure 30) to fine grained aggregates completely replacing burbankite.

Most secondary rare-earth carbonates and other Ca-Ba-Sr carbonates are not distinguishable in thin section due to the small grain size and similar carbonate-like optical properties. One of the replacement minerals forms fibrous, fan-shaped aggregates, but could not be assigned to one of the many phases identified by

X-ray or SEM-EDS techniques.

4.3.2 RARE-EARTH CARBONATITE DIKES OF THE NORTHWEST RIDGE

Petrographic name:

quartz, barite, rare-earth carbonate-bearing ankerite-carbonatite

Physical properties:

The rare-earth dikes weather a distinctive dark chocolate-brown colour, have a brown tint on fresh surfaces and do not show macroscopically visible rare-earth minerals. Density is approximately 3.2×10^3 kg/m^3. Magnetic susceptibility is low, but the radioactivity is significantly higher than most carbonatite types due to abundant minute Th-rich phases.

Mineral mode;

The dikes consist of 85 to 90 % manganese ankerite, 2 to 3 % barite, 3 to 5 % quartz and dispersed, fine grained rare-earth carbonates (3 to 6 %).

Textures:

Ankerite forms irregular grains, 0.05 to 4 mm in size, with irregular grain boundaries. Mortar zones are common in between larger grains. Abundant parallel twinning is developed.

Rare-earth carbonates can not be recognized in thin section due to the carbonate-like optical properties.

Barite occurs in the interstices of ankerite bounded by straight, rational ankerite grain boundaries. Barite always shows undulatory to wavey extinction.

Quartz with undulatory extinction forms irregular, interstitial aggregates rarely bounded by straight ankerite grain boundaries. Quartz appears to replace ankerite and to a minor extent barite marked by globular carbonate relicts within quartz and sutured grain boundaries.

4.4 "SYENITE"

Petrographic name:

Varies between aegirine- and arfvedsonite-bearing albite-quartz-rock and quartz-bearing albite-aegirine-arfvedsonite-rock. The term "syenite" is used to indicate its magmatic origin and petrographic nature before the metasomatic overprint.

Physical properties:

The "syenite" is greyish green to dark green and is resistant towards weathering, jointed and extremely hard. Density is approximately 2.8×10^3 kg/m^3. Radioactivity and magnetic susceptibility are near background values.

Mineral mode:

The mineral content is extremely variable: 30 to 60 % albite, 5 to 50 % quartz, 1 to 10 % arfvedsonite, 3 to 30 % aegirine and accessory calcite, apatite, lorenzenite and rare-earth carbonates.

Textures:

A great variety of textures is displayed by the different types of "syenite". Although clearly of magmatic origin (cf. section 6.1), igneous textures are not commonly preserved, but are obscured by extensive metasomatism resulting in metamorphic fabrics.

Primary igneous textures:

Some preserved relict fabrics indicate an equigranular - hypidiomorphic micro-syenite texture with interstitial quartz, short-prismatic magnesio-arfvedsonite and accessory apatite. Lenticular albite shows abundant carlsbad and albite twinning. This primary texture is obscured by extensive overgrowth of fine, prismatic aegirine replacing albite, quartz and partially arfvedsonite. Quartz may recrystallize to form larger, granoblastic grains whereas albite breakes down to fine granular aggregates.

Secondary textures:

Strongly altered parts of the original syenite are characteristically enriched in quartz relative to albite and show extensive overgrowth of fine aegirine. Quartz is recrystallized and may form a granoblastic texture with fine, prismatic aegirine,

granular albite and relict arfvedsonite in zones of extreme quartz enrichment. A possible source for quartz may be the assimilation of quartzite xenoliths as indicated further below.

Narrow, monomineralic veinlets of lorenzenite or arfvedsonite may occur crosscutting parts of the "syenite".

Globular texture:

In one sample abundant ovoid, small globules (0.2 mm) occur (figure 47). They consist of a well defined envelope, when fresh, and inwardly pointing acicular aegirine nucleating at the periphery. Albite and manganese calcite fill the interior volume. The globules appear to be compositionally uniform. The matrix consists of granoblastic albite and quartz with patchy arfvedsonite, fine, prismatic aegirine and accessory apatite. Compositionally, the matrix is high in silica and alumina and the globules are low in silica, alumina but high in alkalies, carbonate, iron and manganese.

Approximate mineral modes: matrix (80 % albite, 5 % arfvedsonite, 10 % aegirine, 5 % quartz, 0.5 % apatite); globules (45 % aegirine, 40 % calcite, 15 % albite).

These globules do certainly not represent any type of secondary vesicle-fillings. They might represent a liquid immiscibility texture between an alkali - carbonate rich liquid and a silica - alumina rich liquid. Whether this is a primary texture or a secondary, metasomatically induced texture (anatexis ?) is uncertain.

Xenoliths:

In some parts of the "syenite" abundant rounded xenoliths are characteristic and may form as much as 30 % of the rock (figure 20). Two major types of xenoliths occur: sedimentary xenoliths with quartzite being by far the most abundant type and igneous xenoliths, mostly consisting of micro-syenites and some albitites.

Figure 20: Quartzite and syenite xenoliths in "syenite"

Quartzite Xenoliths:

The well rounded inclusions range from millimeters to about 30 centimeters in size and may accumulate in rather large zones of the "syenite" ring, but without a systematic pattern of occurrence. They consist largely of pure, recrystallized quartzites and some feldspathic varieties which contain secondary aegirine. Reaction rims sourround the xenoliths, commonly consisting of a dense, fine grained aegirine-rich layer. Small inclusions of relict quartzite show all stages of absorption.

Other types of sedimentary xenoliths, some banded, metamorphosed marls and shales are rare. The quartzite xenoliths were part of the massive basal qurtzites (late Proterozoic - early Cambrian ?) that crop out further to the west towards the Rocky Mountain Trench (Thompson, 1978, 1985). The stratigraphic position of the

quartzites is at least 1 km below the Cambrian rocks exposed at the Aley.

Igneous xenoliths:

Micro-syenite xenoliths are more than 50 times less abundant than quartzite xenoliths and of smaller size (1-8 cm). Reaction rims are well developed and consist of relict xenolithic albite grains and patchy arfvedsonite overgrown by a dense, acicular aegirine web. Fine grained calcite may be accumulated in these narrow rims (1-10 mm).

The micro-syenite xenoliths display a well preserved igneous equigranular-hypidiomorphic texture formed by lenticular albite with abundant carlsbad-albite twinning. Interstitial secondary calcite and minor quartz is common. Magnesio - arfvedsonite forms short prismatic, somewhat patchy crystals with frayed edges. Aegirine is rare or absent. Apatite and lorenzenite are common accessory minerals.

4.5 CONTACT AUREOLE

Physical properties:

The physical properties are variable due to strong, bedding-parallel compositional heterogeneities. The sediments weather a distinctive ochre to brown colour. The pure dolomite and calcite marbles adjacent to the contact weather a cream colour (Cream Dolomite Unit). Radioactivity may range from background readings to highly anomalous intensities. A good correlation exists between radioactivity and apparently strongly affected strata of the sediments. Densities range from 2.6 to 2.8×10^3 kg/m^3

Textures:

Sediments within the first 300-600 m are completely recrystallized. Rocks near the intrusion-contact are highly strained, marked by an intense planar fabric and abundant glide-twinning in calcite and dolomite marbles.

Metamorphic mineral assemblage:

White mica and potassic feldspar are the only common metamorphic mineral observed in impure marbles, marls and silts. All the samples examined along the northwest ridge profile (out to a distance of 550 m from the contact) showed miner metamorphic white mica. Talc and calc-silicates were sought but not found.

Alteration:

Immediately adjacent to the contact (10-40 cm) in the Cream Dolomite Unit silicification and growth of (richteritic ?) green amphibole are common. Other signs of mass transfer connected with the intrusion are restricted to the distinct weathering colour of the sediments and minor, narrow carbonate veinlets and the occasional fluorite grain. Carbonate veinlets are restricted to the inner part of the contact aureole (0-100 m).

5. GEOCHEMISTRY

The unusual chemical compositions of carbonatites in comparison with average silicate rocks presents analytical problems that are unique to carbonatite rock analysis. Problems related to XRF-analysis together with some solutions and suggestions are addressed in detail in appendix B.

5.1 ROCKS OF THE CARBONATITE COMPLEX

5.1.1 DOLOMITE CARBONATITE

Dolomite carbonatite covers about two thirds of the area of the carbonatite complex and is thus the major igneous rock type exposed. The major element composition of dolomite carbonatite from the Aley is characterized by essentially no silica, no alumina, low alkali, but abundant phosphorous. The trace element geochemistry (table 2) may be described as follows: enriched in the incompatible elements LREE, Th, U, Nb, Ta, Zr but with low Ti, Rb, K, Pb; concentrations of siderophile metals (Co, Ni, Mo) that are close to the detection limit; low in sulfur and nearly undetectable chalcophile metals (Cu, Ag, Zn, As, Sb, Bi). A peculiarity in comparison with more common rocks is the extremely high carbon dioxide content of carbonatites, 40 to 43 wt% for "average" dolomite carbonatite (pure dolomite contains 47.73 wt% CO_2), but no water except traces in pyrochlore and fersmite.

5.1.2 CALCITE CARBONATITE

Three analyses from drill core composites (data provided by COMINCO Ltd.) were chosen to represent "average" calcite carbonatite. Compared with dolomite carbonatite the calcite carbonatites are higher in silica, iron, phosphorous and sodium (if amphibole is present). The trace geochemistry (table 2) is similar to dolomite carbonatite (LREE, Y, Zr, Sr, Ba, Rb).

	Dolomite Carbonatite				Calcite Carbonatite		
wt%	MR-550	MR-553	MR-552	MR-554	A85-4	A85-5	A85-8
SiO_2	0.50	0.28	0.52	1.08	3.84	2.17	3.53
Al_2O_3	0.26	0.14	0.16	0.72	0.03	0.02	0.51
TiO_2	<0.01	<0.01	0.01	0.12	0.10	0.04	0.08
FeO(tot)	2.95	1.08	1.92	0.76			
Fe_2O_3					2.24	1.32	13.17
FeO					2.10	0.97	0.51
MnO	0.26	0.87	0.77	0.25	nd	nd	nd
MgO	17.34	16.68	14.79	18.02	7.71	5.85	2.92
CaO	32.89	34.82	34.29	33.71	41.47	45.69	41.34
Na_2O	0.63	0.08	bd	bd	0.46	0.48	0.18
K_2O	0.02	0.01	0.02	0.01	0.13	0.05	0.03
P_2O_5	1.74	1.36	8.69	3.15	5.03	4.60	7.73
S	<0.01	0.01	0.01	0.01	0.35	0.21	0.01
LOI	43.52	42.00	40.16	41.96	36.06	38.72	30.20
total	100.0	100.0	100.0	100.0			
(total)	95.70	93.04	100.25	95.87	99.2	99.9	100.3
ppm							
Nb (2.9)	490	168	1796	1384	4610	3290	5030
Zr (2.6)	66	465	499	497	559	604	308
Y (3.0)	41	14	69	122	93	97	122
Sr (2.7)	359	4377	4449	457	4630	5281	686
U (8.9)	bd	223	19	74	<20	<20	26
Rb (2.6)	4	35	5	2	<20	<20	25
Th (7.3)	128	bd	21	184	106	65	464
Ta (7.8)	18	nd	17	166	<20	<20	59
Ba (13.4)	39	1225	85	33	248	314	308
La (9.6)	307	142	322	355	360	314	669
Ce (16.0)	746	224	909	856	823	708	1318
Nd (6.5)	237	59	310	297	nd	nd	nd
Ce/La	2.4	1.6	2.8	2.4	2.3	2.3	2.0
Ce/Nd	3.2	3.8	2.9	2.9			

Table 2: Major element and trace element concentrations of dolomite carbonatite and calcite carbonatite. Analyses of calcite carbonatite by Cominco Ltd. (composites from drill cores, XRF-analyses, major elements on fused disks). Numbers in parentheses are average detection limits for dolomite carbonatite analyses. LOI = loss on ignition, bd = below detection limit, nd = not determined, (total) = measured total including LOI, total = normalized total. For details of analysis see appendix B.

5.1.3 RARE-EARTH CARBONATITE DIKES

Two geochemically different types of ankeritic rare-earth rich dikes exist: the barium-rich, siliceous dikes of the northwest ridge and the low-silica, barium-poor rare-earth dikes of the north ridge. Compared to dolomite carbonatite they have high concentrations of ferrous iron, manganese and sulfur, but low phosphorous values (table 3). Strontium, barium and total light rare-earth elements may reach major element concentrations. They are depleted in the incompatible elements niobium and tantalum. Cerium is the dominant LREE, followed by neodymium (northwest ridge) or lanthanum (north ridge) and praseodymium.

5.1.4 "SYENITE"

Although clearly of igneous origin (cf. section 6.1), the silicate phase of the carbonatite complex displays a variety of textures and its chemistry appears to vary erratically. Four analyses of syenite are presented in table 4. Note that the high alkali content would permit classification of this rock as an alkali-syenite, but the absence of nepheline and presence of modal quartz instead require classifying it as a syenite or quartz-syenite. Its trace element geochemistry is of "diluted" carbonatite character, but with undetectable uranium and thorium contents and higher titanium.

5.2 ROCKS OF THE CONTACT AUREOLE

The trace element geochemistry and measurement of radioactivity are the only quantitative indicators of the metasomatic processes that accompanied the intrusion. There is little visible evidence of metasomatism except the odd fluorite grain or minute particle of metal oxide. Yet the characteristic brown to ochre weathering colours of the aureole rocks leave no doubt that metasomatic fluids affected the rocks.

The trace element abundances are highly variable as might be expected from the bedding-parallel banded weathering pattern of the rocks and primary

wt%	Northwest ridge MR-503	North ridge MR-570	North ridge COM
SiO_2	7.30	0.65	0.56
Al_2O_3	0.67	0.21	0.49
TiO_2	0.04	0.01	0.02
FeO (tot)	10.49	8.41	
Fe_2O_3 (tot)			5.82
MnO	3.30	4.11	1.58
MgO	7.91	11.29	13.48
CaO	24.59	28.14	27.73
Na_2O	0.79	1.13	0.10
K_2O	0.06	0.04	0.02
P_2O_5	0.09	0.14	0.34
S	1.11	0.06	nd
F	nd	nd	0.88
LOI	33.31	42.55	nd
BaO	7.74	0.69	1.37
La_2O_3	0.27	0.31	nd
Ce_2O_3	0.84	0.56	nd
Nd_2O_3	0.42	0.12	nd
total	98.74	98.77	42.39(*)
ppm			
Nb (4.8)	29	bd	10
Zr (4.3)	96	583	nd
Y (5.0)	96	13	nd
Sr (4.5)	699	5546	nd
U (10.3)	bd	21	nd
Rb (3.8)	bd	bd	nd
Th (12.6)	839	28	293
La (15.0)	2291	2668	nd
Ce (22.1)	7213	4757	nd
Nd (9.0)	3584	1020	nd
Ce/La	3.1	1.8	
Ce/Nd	2.0	4.7	

Table 3: Major element and trace element concentrations of rare-earth carbonatite dikes. Analysis of sample COM by Cominco Ltd. (XRF-analysis, major elements on fused disks). LOI = loss on ignition, bd = below detection limit, nd = not determined, (*) = total withot LOI. Numbers in parentheses are detection limits for sample MR-503. For details of analysis see appendix B.

wt%	MR-316	MR-551	COM-a	COM-b
SiO_2	66.36	75.15	53.00	60.17
Al_2O_3	4.28	8.30	1.33	6.39
TiO_2	0.68	0.41	0.35	1.31
FeO (tot)	12.00	3.88		
Fe_2O_3			12.91	10.98
MnO	0.27	0.14	0.35	0.45
MgO	2.55	0.87	16.00	3.61
CaO	4.05	2.28	3.50	3.98
Na_2O	7.79	3.85	7.71	8.72
K_2O	0.24	3.68	1.15	0.20
P_2O_5	0.70	0.20	0.68	0.60
S	0.02	0.01	nd	nd
F	nd	nd	0.90	0.30
LOI	0.84	1.16	nd	nd
total	100.0	100.0		
(total)	98.86	106.20	97.88	96.71
ppm				
Nb (3)	71	72	280	10
Zr (3)	267	887	387	nd
Y (3)	6	18	21	nd
Sr (3)	302	141	671	nd
U (9)	bd	bd	<20	nd
Rb (3)	bd	35	<20	nd
Th (7)	bd	bd	<20	12
Ba (13)	1343	184	537	461
La (10)	63	60	234	nd
Ce (16)	168	143	110	nd
Nd (7)	56	46	nd	nd
Ce/La	2.7	2.4	2.1	
Ce/Nd	3.0	3.1		

Table 4: Major element and minor element concentrations of syenite samples. Analyses COM-a and COM-b by Cominco Ltd. (XRF-analyses, major elements on fused disks). Numbers in parentheses are average detection limits for MR-samples. LOI = loss on ignition, bd = below detection limit, nd = not determined, (total) = measured total including LOI, total = normalized total. For details of alyses see appendix B.

compositional differences. Generally, the amount of material metasomatically introduced appears to decrease with distance from the contact (cf. KR-samples, table 5), but the heterogeneity of the sedimentary rocks causes large heterogeneities in their apparent intensity of alteration (cf. MR-samples, table 5).

Trace elements noticeably enriched in strongly altered parts of the contact aureole (MR-511, MR-523) include Nb, REE, Th and F (chlorine was not determined). The extent of major element mass transfer is difficult to estimate because of the primary heterogeneity of the rocks. The recrystallized carbonate-rich sedimentary rocks do not provide simple replacement textures, except within 0.5 meters of the syenite. Dolomite marbles (Cream Dolomite Unit) adjacent to the syenite show secondary alkali-amphiboles (richterite ?) and are commonly silicified.

The reader may have noticed that the term "fenite" has not been used. Fenite should be reserved for country rock that was affected by alkali-metasomatism (Heinrich, 1966). While there is no doubt that the rocks of the Aley aureole have been affected by metasomatic fluids, the changes are so subtle, and the major element proportions are so little affected, that the name "fenite" may be misleading.

	Northwest Ridge				West Ridge					
ppm	MR-505	MR-506	MR-511	MR-523	KR-18a	KR-19	KR-24a	KR-27b	KR-27c	KR-28e
Nb	144	183	19	24	<20	<20	193	380	126	379
Zr	50	70	115	41	134	94	42	98	48	242
Y	60	59	29	26	nd	nd	nd	nd	nd	nd
Sr	379	257	115	41	nd	nd	nd	nd	nd	nd
U	bd	bd	bd	10	nd	nd	nd	nd	nd	nd
Rb	bd	7	10	8	nd	nd	nd	nd	nd	nd
Th	109	58	bd	9	<20	<20	46	65	39	<20
Ba	41690	2420	503	345	224	299	794	23	74	473
La	13	38	64	36	<20	<20	<20	137	801	317
Ce	73	103	90	bd	<20	<20	45	304	1455	638
Nd	bd	64	34	bd	nd	nd	nd	nd	nd	nd
F	nd	nd	nd	nd	160	120	205	960	310	4300

Table 5: Trace elements of selected sedimentary rocks from the contact aureole. KR-sample data from Cominco Ltd. (XRF-analyses on powder pellets). nd = not determined, bd = below detection limit. See text for sample locations and appendix B for details of XRF-analyses.

Sample No	Unit	Distance from contact [m]	Sample weight [kg]
MR-505	Grey Limestone Unit	367	3.7
MR-506	Grey Limestone Unit	361	4.5
MR-511	Thin Bedded Limestone Unit	215	2.6
MR-523	Cream Dolomite Unit	52	2.4
KR-18a	Grey Limestone Unit	ca 200	
KR-19	Grey Limestone Unit	ca 180	
KR-24a	Thin Bedded Limestone Unit	ca 100	
KR-27b	Thin Bedded Limestone Unit	ca 80	
KR-27c	Thin Bedded Limestone Unit	ca 80	
KR-28e	Cream Dolomite Unit	ca 50	

Table 6: List of samples and sample locations used in table 5.

5.3 ISOTOPE GEOCHEMISTRY

5.3.1 STRONTIUM AND RUBIDIUM

Three samples were examined as a quick reconnaissance project. The analyses were done by Krista Scott using the facilities of R.L. Armstrong at the University of British Columbia. Results are summarized in table 7.

Sample No.	Rock type	Sr (ppm)	Rb (ppm)	Rb/Sr	$^{87}Sr/^{86}Sr$
MR-550	dol. carb.	362	0.6	0.002	0.70344(4)
MR-554	dol. carb.	419	0.9	0.002	0.70482(7)
MR-316	syenite	545	0.0	0.000	0.70364(4)

Table 7: Strontium isotope analyses of carbonatite and syenite samples. No in situ decay corrections are necessary due to the negligible rubidium concentrations. dol. carb. = dolomite carbonatite.

The variation of $^{87}Sr/^{86}Sr$ ratios from 0.7035 (MR-316, MR-550) to 0.7048 (MR-554) is far too large to be accounted for by original variations in the magma and reflects effects of alteration or assimilation. A greater sample density is required to constrain observed trends. The interpretation of strontium isotope data would be more rigorous if stable isotope values (oxygen, carbon) were used as an "alteration filter".

The low $^{87}Sr/^{86}Sr$ ratios (0.7035) compare well with data from other carbonatite complexes (Bell & Powell, 1970; Pineau & Allègre, 1972; Bell et al, 1982; Grünenfelder et al, 1986). These authors interpret such low ratios as being indicative of a mantle source depleted in large ion lithophile (LIL) elements in comparison with the bulk earth. On a graph of age versus $^{87}Sr/^{86}Sr$ two values for

the Aley plot between the bulk earth trend and the three billion year old depleted mantle source trend proposed by Bell et al (1982) for some alkaline rocks of Northern Ontario (figure 21). One dolomite carbonatite sample plots above the bulk earth trend and may represent effects of deuteric alteration or analytical difficulties.

Note, that in contrast with lead isotope systematics, the $^{87}Sr/^{86}Sr$ ratios are not a sensitive measure of minor crustal contamination beacause of high strontium concentrations (Grünenfelder, 1986).

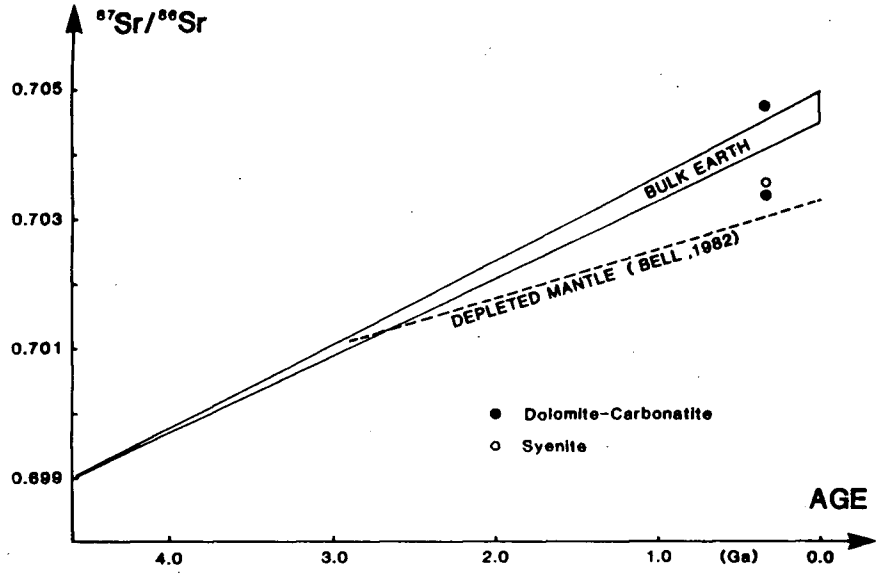

Figure 21: Age versus $^{87}Sr/^{86}Sr$ diagram modified after Bell et al (1982) with data points from the Aley carbonatite complex.

5.3.2 OXYGEN AND CARBON ISOTOPE RATIOS

Eight samples were analysed by Dr. Karlis Muehlenbachs at the University of Alberta. One sample (MR-552) did not yield enough carbon dioxide for analysis. Table 8 and figure 22 summarise the analytical results.

All the $\delta^{13}C$ ratios show values typical of primary igneous carbonatites of mantle origin (Taylor et al, 1967; Pineau et al, 1973). The $\delta^{18}O$ values are variable, a feature commonly observed in carbonate minerals. An elevated $\delta^{18}O$ signature in

Sample No.	Rock type	Mineral analysed	$\delta^{13}C$ (PDB‰)	$\delta^{18}O$ (SMOW‰)
MR-550	dol. carb.	dolomite	-5.0	15.4
MR-553	dol. carb.	dolomite	-5.1	7.7
MR-85-5-I	dol. carb.	dolomite	-4.9	15.1
MR-85-2-J	calc. carb.	calcite	-6.1	8.0
MR-85-5-D	calc. carb.	calcite	-5.9	7.7
MR-570	REE-dike	ankerite	-4.7	12.0
MR-572	REE-dike	ankerite	-4.8	10.9

Table 8: $\delta^{13}C$ and $\delta^{18}O$ ratios for carbonate minerals of some carbonatite samples. PDB = Pee Dee Formation belemnite, SMOW = standard mean ocean water. dol. carb = dolomite carbonatite, calc. carb. = calcite carbonatite, REE-dike = rare-earth carbonatite dike.

comparison with mantle values is usually taken to be indicative of post-magmatic recrystallization and deuteric alteration (Taylor et al, 1967). Both processes preferentially affect carbonate minerals (rather than silicates) and oxygen isotope ratios rather than carbon isotope ratios. The extremely fresh samples of calcite carbonatite from drill-cores are not affected at all by alteration. Dolomite carbonatite, almost always with a brownish tint due to weathering, shows $\delta^{18}O$ values typical of mantle origin and elevated $\delta^{18}O$ values due to recrystallisation and deuteric alteration. Ankerite from carbonatite dikes rich in rare-earths shows somewhat elevated $\delta^{18}O$ signatures, but $\delta^{13}C$ values of mantle character.

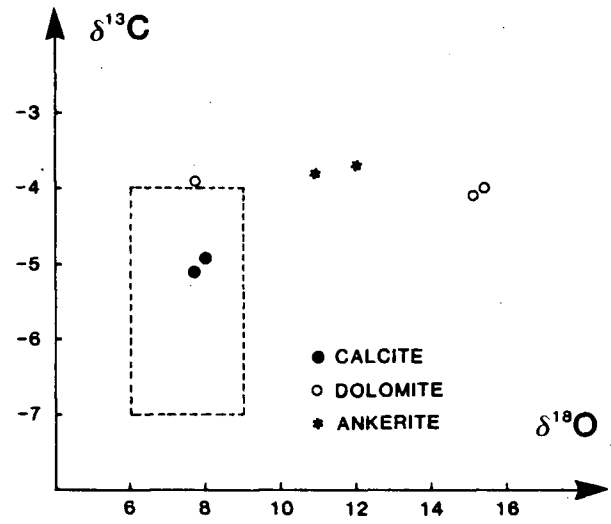

Figure 22: $\delta^{13}C$ versus $\delta^{18}O$ diagram of data listed in table 8. Box outlines the general range of primary igneous carbonatites unaffected by weathering or deuteric and hydrothermal alteration (Taylor et al, 1967).

6. ASPECTS OF PETROGENESIS

An hypothesis for the mode of emplacement should explain the field observations, be consistent with the principles of physics and be the simplest possible solution. Such an hypothesis would describe a possible process but not necessarily the actual sequence of events as they occurred during emplacement of the carbonatite complex.

6.1 EVIDENCE ON SEQUENCE OF EMPLACEMENT

Syenite - carbonatite core: The carbonatite core clearly intruded the syenite ring. Extensive veining on all scales of calcite carbonatite and dolomite carbonatite occurs along the entire inner circumference of the syenite ring.

Calcite carbonatite - dolomite carbonatite: The field relationship between dolomite carbonatite and calcite carbonatite is ambiguous at some outcrops. Most commonly, however, calcite carbonatite veins are observed within dolomite carbonatite. Dolomite carbonatite veins within calcite carbonatite do occur as well as the occasional diffuse contact. The emplacement of calcite carbonatite dikes and "sweats" might thus be related in time very closely to the dolomite carbonatite emplacement and solidification, but appears to postdate dolomite carbonatite generally.

Rare-earth carbonatite dikes: The relative position of the rare-earth carbonatite dikes with respect to syenite and the carbonatite core cannot be deduced from field observations due to the lack of crosscutting relationships. Structural considerations (cf. section 2.3) would be consistent with the dike emplacement either predating or postdating the emplacement of the complex. Petrologic (section 6.4) and geochemical (section 5.1.3) considerations indicate that the dikes are residual differentiates and thus suggest late-stage emplacement of the dikes in a manner similar to mafic dikes associated with many granitoid systems. The relationship of the carbonatite dikes to the timing of wall-rock alteration is not clear: the dikes of the north ridge appear to be unaffected but the dikes of the

northwest ridge show silicification which might or might not be related to the formation of the contact aureole.

Lamprophyric dikes: The lamprophyric dikes within the contact aureole are clearly affected by the fluids that formed the aureole. Crosscutting relationships with the carbonatite complex or the syenite ring were not observed. The youngest sedimentary unit crosscut by lamprophyres is the Lower Dolomite-Shale Unit (Road River Group, late Ordovician ?).

Ospika Pipe: There are no crosscutting relationships between the diatreme and rocks of the carbonatite complex. The Ospika Pipe is similar in age to the carbonatite (cf. section 1.3). It is not clear whether the pipe is affected by the formation of the contact aureole. The massive host unit (Skoki Dolomite) is not very susceptible to fluids and thus betrays commonly no evidence of penetrating fluids.

6.2 TEMPERATURE DISTRIBUTION AROUND THE CARBONATITE COMPLEX

Three different approaches were taken in order to deduce temperature distributions within the contact aureole: calcite-dolomite thermometry, comparison of metamorphic phase assemblages with calculated phase diagrams and calculated temperature distributions around a cooling intrusion based on a simple model. None of the methods by themseleves give satisfactory answers but the three methods combined allow some important conclusions.

Calcite-dolomite thermometry:

Microprobe analyses of coexisting calcite and dolomite in samples at various distances from the contact show very low and variable solid solution of $MgCO_3$ in calcite (table 9). Temperatures calculated with the geothermometer formula of Rice (1977) range from 241°C to 345°C with no apparent dependence on the distance from the intrusion contact.

Sample No	EMS-No	Distance from contact	MgO	FeO	MnO	X_{MgCO_3}	T°C
MR-513	PROF-3	149m	1.15	1.21	1.41	0.0115	345
MR-10	PROF-1	40m	0.88	0.10	0.06	0.0088	320
MR-10	PROF-2	40m	0.32	0.10	0.12	0.0032	241
MR-10	PROF-2	40m	0.59	0.18	0.18	0.0059	286
MR-10	PROF-2	40m	0.89	0.20	0.18	0.0089	321

Table 9: Composition of calcite (mol%) coexisting with dolomite and calculated temperatures based on the formula by Rice (1977):
$\text{Log}_{10} X_{MgCO_3} = -1690 \div T[°K] + 0.795$

The extrapolation towards lower temperatures than experimentally constrained (Harker & Tuttle, 1955; Graf & Goldsmith, 1955, 1858; Goldsmith & Newton, 1969) may result in large errors. The heterogeneity of the $MgCO_3$ content of calcite within the same probe section reflects the difficulty of attaining equilibrium at low temperatures. Corrections that account for $FeCO_3$ and $MnCO_3$ contents compared to the the pure system are expected to be in the order of 20 to 50 °C (Bickle & Powell, 1977).

Metamorphic phase assemblages and calculated phase diagrams:

The contact aureole consists of metamorphic carbonate rocks but lacks talc and calc-silicates such as tremolite, diopside and forsterite. The only metamorphic mineral besides potassium feldspar is phlogopite that occurs in impure marbles, metamorphosed marls and siltstones as an accessory mineral. Phlogopite formed in rocks next to the carbonatite complex as well as in sediments up to a distance of at least 500 meters along the northwest ridge.

A pressure - temperature and a temperature - fluid composition diagram were calculated with the program package "PT-SYSTEM" (UBC). The pressure at the

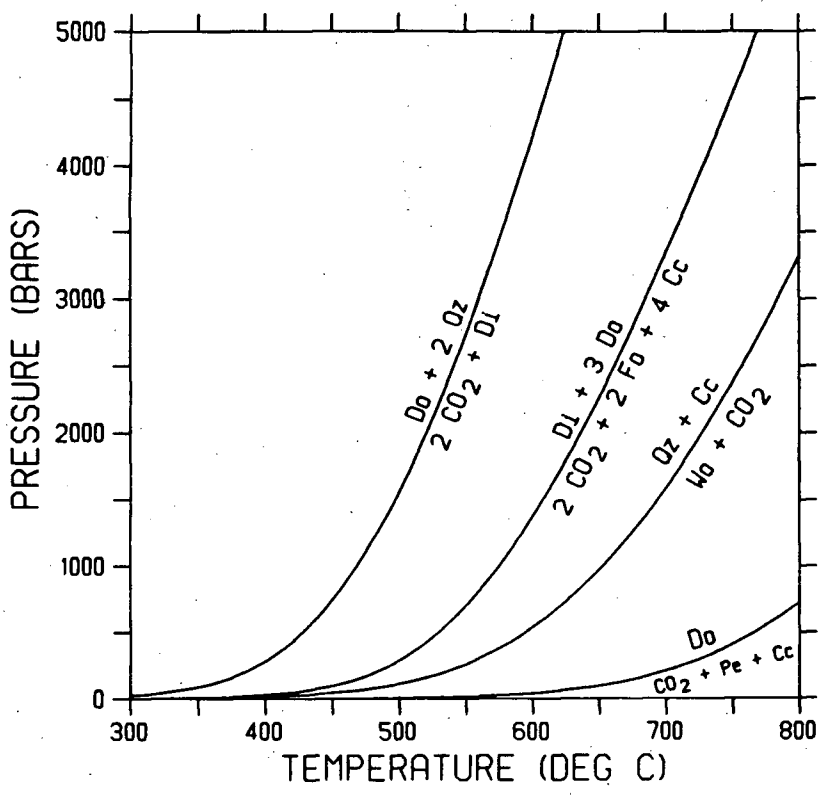

Figure 23: Pressure - temperature diagram of the system CaO - MgO - SiO_2 - CO_2. Do = dolomite, Cc = calcite, Qz = quartz, Di = diopside, Fo = forsterite, Wo = wollastonite, Pe = periclase

time of emplacement may be estimated from the approximate sedimentary overburden. Thompson's (1985) stratigraphic compilation suggests an overlying stratigraphic section of 5 to 8 km which would have produced pressures between 1.5 and 2.5 kbar. The large uncertainty is a result of the position of the Aley complex near the Paleozoic shelf/off-shelf boundary.

Two extreme cases are represented by the calculated phase diagrams: the P-T-diagram represents metamorphism with pure excess CO_2 present, whereas the T-X-diagram assumes the fluid pressure to be equal to the total pressure.

Figure 23 shows the phase relationships in the presence of pure, dry CO_2. Calc-silicates, in this case, are not expected to form below 500°C at a pressure of 2 kbar. Note, however, that the occurrence of phlogopite indicates the presence of at least some steam or a H_2O-CO_2 fluid.

Figure 24 shows the phase relationships as a function of fluid composition (X_{CO_2}). In the presence of CO_2-rich fluids talc and calc-silicates may not form at temperatures below 500°C. At a high H_2O partial pressure, however, talc may form at temperatures below 400°C, if the fluid composition is not buffered along the phlogopite producing reaction boundary towards higher X_{CO_2} compositions. Note that the indifferent crossover of the phlogopite-forming reaction with the tremolite-forming reaction may not be demonstrable in the rocks due to the increased stability of phlogopite of natural compositions. These compositional effects will shift the equilibrium towards lower temperatures.

Deduced temperatures of around 500°C are consistent with the observed phase assemblages only if one assumes unreasonable water-poor fluids. Temperatures around 400°C or below seem most consistent with predicted phase relationships.

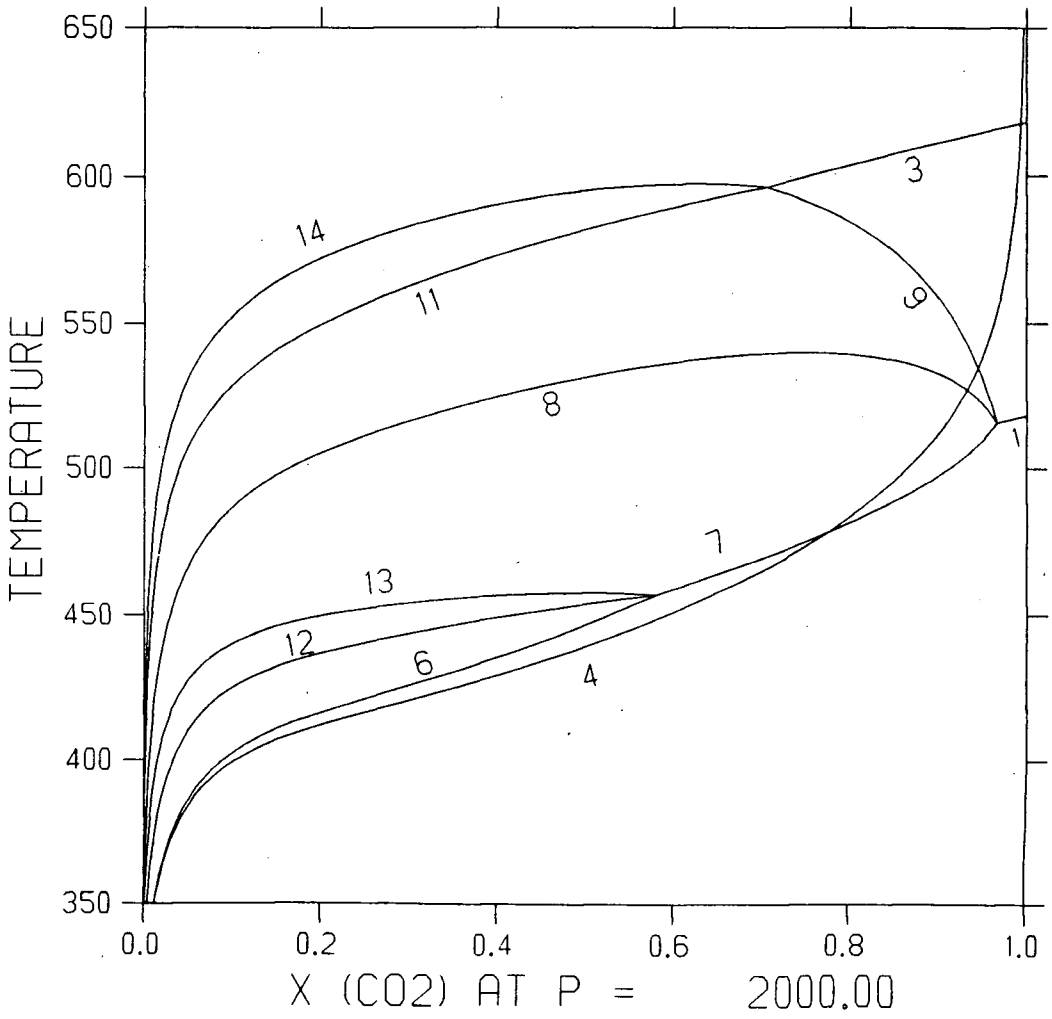

Equilibria calculated:

1 $Do + 2Qz = Di + 2CO_2$
3 $Di + 3Do = 2Fo + 4Cc + 2CO_2$
4 $6Do + 2Ksp + 2H_2O = Phl + 6Cc + 6CO_2$
6 $Do + Qz + H_2O = Tc + 3Cc + 3Co_2$
7 $8Qz + 5Do + H_2O = Tr + 3Cc + 7CO_2$
8 $Tr + 3Cc + 2Qz = 5Di + 3CO_2 + H_2O$
9 $Tr + 3Cc = 4Di + Do + CO_2 + H_2$
11 $Tr + 11Do = Fo + 5Cc + 5CO_2$
12 $5Tc + 6Cc + 4Qz = 3Tr + 6CO_2 + 2H_2O$
13 $2Tc + 3Cc = Tr + Do + CO_2 + H_2$
14 $3Tr + 5Cc = 11Di + 2Fo + 5CO_2 + 3H_2O$

Figure 24: Temperature - fluid composition diagram of the system CaO - MgO - SiO_2 - H_2O - CO_2. Cc = calcite, Do = dolomite, Tr = tremolite, Tc = talc, Qz = quartz, Di = diopside, Fo = forsterite, Phl = phlogopite, Ksp = potassium feldspar

Calculated transient temperature distributions around a cooling igneous body

A simple conductive cooling model of an igneous body (cf. appendix C) allows the calculation of transient temperature distributions for the margins of an igneous body.

Field observations confirm a two-stage intrusive event (cf. section 6.1.1) with an earlier syenite emplacement and a later concentric carbonatite intrusion. The temperature effect of the carbonatite on the contact aureole is thus screened by the syenite ring. The model is therefore applied to a syenite body of the dimensions of the Aley complex.

Figure 25 is a t-T-x section (time - temperature - distance) calculated with physical properties of syenite (Turcotte & Schubert, 1982; Best, 1981) (cf. appendix C for boundary conditions). The calculated maximum temperature at the contact is 524°C.

The same model applied to a carbonatite dike (rock data from Treiman & Schedl, 1983; Le Bas, 1981, Turcotte & Schubert, 1982) predicts a temperature at the contact of about 400°C. This much lower temperature is a combined effect of the lower solidification temperature and the lower heat of fusion compared to silicate melts.

If the model were capable of accounting for convective heat transfer within the magma chamber, the faster cooling rate would result in higher temperatures within the wallrock. Convective heat transfer within the wallrock would result in a higher rate of heating of distal portions of the aureole and thus lower the temperatures at the contact.

Calculated temperature distributions around a syenite intrusion are predicted to be high enough to expect calc-silicate assemblages in impure marbles. The discrepancies in the predicted temperature distributions and the temperatures inferred from field observations must be explained by a different mode of emplacement than one on which the thermal model is based.

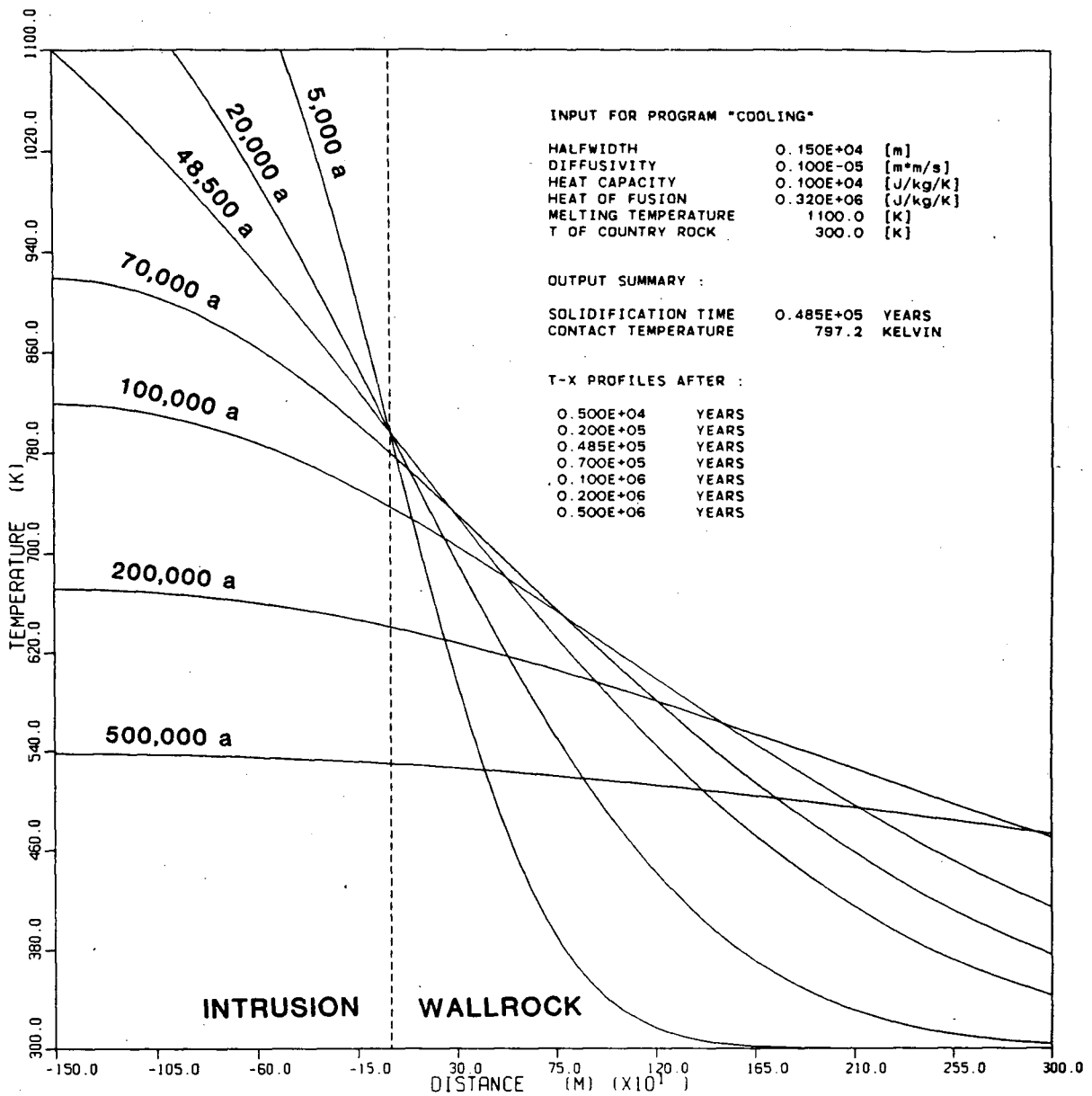

Figure 25: t-T-x diagram for a syenite intrusion

6.3 SEQUENCE OF CRYSTALLIZATION IN CARBONATITE MAGMAS

Textural evidence:

Dolomite carbonatite: Apatite appears to have crystallized early, on the basis of its euhedral habit in undeformed parts of dolomite carbonatite. Pyrochlore that was replaced by fersmite at a later stage is believed to be an early phase on the liquidus, on the basis of flowbanding textures and its idiomorphic habit. Dolomite crystallization is difficult to unravel due to the ease with which carbonates recrystallize. If zonation patterns could be successfully studied by cathode luminescence, Nomarski contrast interferometry or laser interferometry some insight might be gained into phenocryst - matrix relationships.

Calcite carbonatite: Flow banding textures indicate that pyrochlore, apatite, magnetite and biotite appeared relatively early on the liquidus. Some samples that appear to contain calcite-phenocrysts in a fine-grained calcite matrix may indicate a large temperature (time) interval of calcite crystallization. The role of the sodic-calcic amphiboles is unclear. Fibrous amphibole in zones of higher strain appear to have formed metasomatically at a late stage. Fresh, prismatic crystals could represent primary magmatic amphibole.

Rare-earth carbonatite dikes: The interstitial occurrence of rare-earth carbonates and barite indicate that these phases have crystallized late. Quartz in the dikes of the northwest ridge is probably a replacement mineral (cf.section 4.4.2).

Constraints from experimental studies:

Simplified carbonatite systems have been investigated experimentally since the late fifties. Table 10 lists experimental studies in carbonatite systems. References on liquid immiscibility, fluid inclusions, physical properties of carbonatite magmas and some studies on related silicate systems are included.

System / Topic	Author	Year
$CaCO_3$-H_2O	Wyllie & Tuttle	1959
CaO-CO_2-H_2O	Wyllie & Tuttle	1960
	Wyllie & Boettcher	1969
	Koster van Groos	1982
$CaCO_3$-$MgCO_3$	Irving & Wyllie	1975
	Byrnes & Wyllie	1981
$CaCO_3$-$Ca(OH)_2$-CaS	Helz & Wyllie	1979
CaO-MgO-CO_2-H_2O	Wyllie & Biggar	1966
	Wyllie	1985
	Fanelli et al	i.p.
Na_2-K_2-$CaCO_3$	Cooper et al	1975
$Ca(OH)_2$-$CaCO_3$-$Ca_3(PO_4)_2$-H_2O	Biggar	1969
CaO-CaF_2-P_2O_5-CO_2-H_2O	Wyllie & Biggar	1966
$BaSO_4$-$CaCO_3$-CaF_2	Kuellmer et al	1966
CaF_2-$Ca(OH)_2$-$CaCO_3$	Gittins & Tuttle	1964
Rare-earth carbonatite systems	Chai	1978
	Kutty et al	1978
	Jones & Wyllie	1983a
	Jones & Wyllie	1983b
	Jones & Wyllie	1986
Summary papers	Tuttle & Gittins	1966
	Bowen	1945
	Koster van Groos	1975
	Le Bas	1977
	Le Bas	1981
	Wyllie & Jones	1985
SiO_2-H_2O-CO_2	Boettcher	1984
CaO-MgO-SiO_2-CO_2	Wyllie & Huang	1975
	Wyllie & Huang	1976
$NaAlSi_3O_8$-$CaCO_3$-$Ca(OH)_2$-H_2O	Watkinson & Wyllie	1969
$MgSiO_4$-SiO_2-H_2O-CO_2	Eggler	1975
$CaSiO_3$-H_2O	Buckner et al	1960
Na_2O-CaO-Al_2O_3-MgO-SiO_2-CO_2	Eggler	1978
$NaAlSi_3O_8$-$NaAlSiO_4$-$NaFeSi_2O_6$	Nolan	1966
CO_2 in melts	Mysen et al	1976
	Eggler	1978
	Eggler & Rosenhauer	1978
	Boettcher	1984
Physical properties	Treiman & Schedl	1983
Fluid inclusions	Romanchev	1972
	Rankin & Le Bas	1974
	Rankin	1975
	Nesbitt & Kelly	1977

Liquid immiscibility	Greig	1928
	Koster van Groos & Wyllie	1966
	Koster van Groos & Wyllie	1968a
	Philpotts & Hodgson	1968
	Koster van Groos & Wyllie	1973
	Gittins	1973
	Koster van Groos	1975
	Wendlandt & Harrison	1979
	Hamilton et al	1979
	Freestone & Hamilton	1980
	Bogoch & Magaritz	1983

Table 10: List of references on experimental topics related to carbonatites

The studies in simplified carbonatite systems provide insight into the possible sequence of crystallization and approximate solidus and liquidus temperatures of various peritectic and eutectic phase assemblages. Phases that appear early on the liquidus surface in the experimental systems include calcite, dolomite, apatite and periclase. Late crystallizing phases include portlandite, barite and rare-earth carbonates. Earlier experiments indicated the omnipresence of a calcite - portlandite eutectic which has never been corroborated by field observations. More recent experiments (Fanelli et al, in press; Wyllie & Jones, 1985) demonstrate the possibility of precipitation of calcite or dolomite or both over a large range of temperatures without ending in a eutectic with portlandite.

The experiments also indicate the possibility that carbonatite melts may persist to low temperatures compared to silicate systems. These indications include: coprecipitation of calcite, dolomite and periclase from melts at 650°C at 2 kbar (Fanelli et al, in press; Wyllie & Jones, 1985); a eutectic in the system $CaCO_3$ - $Ca(OH)_2$ - CaF_2 - $Ca_3(PO_4)_2$ at 575°C at 1 kbar was reported (Wyllie & Biggar, 1966; Wyllie & Jones, 1985); addition of $La(OH)_3$ to the eutectic composition of the preceding system resulted in a minimum of the solidus at 18% $La(OH)_3$ and

543°C at 1 kbar.

6.4 GENETIC RELATIONSHIPS

Although "true" carbonatites do show geochemical signatures indicative of mantle origin, they are thought by many to be derivative magmas and not primary melts from the mantle (Tuttle & Gittins, 1966; Wyllie & Huang, 1975; Le Bas, 1977; Wyllie & Jones, 1985). Experimental phase equilibrium studies demonstrate possible differentiation paths from high temperature silicate melts to low temperature carbonatite melts (cf. references in table 10 under silicate systems; Le Bas, 1977, 1981; Wyllie & Jones, 1985). Liquid immiscibility might occur in more alkali-rich melts (cf. references in table 10) to produce carbonatite melts.

At the present stage, geochemical data on the Aley complex and thermo-chemical data on carbonatite-alkaline systems do not allow quantitative modeling of systems closely related to carbonatite magma genesis. The following points are made in an attempt to relate the rocks of the Aley complex to each other. This will at the most contribute towards understanding of possible processes towards the end of magma ascent and will not have any bearing on processes occurring in the mantle source region. One of the major problems is the unknown quantity and composition of fluid phases present at various stages of magma diversification.

Dolomite carbonatite - rare-earth carbonatite dikes:

Major element and trace element geochemistry suggest a possible relationship by fractional crystallization of a dolomite carbonatite-like parent magma towards a small amount of residual melt represented by the rare-earth carbonatite dikes. Fractionation of apatite, magnetite, dolomite and pyrochlore is consistent with the expected crystallization of phases appearing early on the liquidus. By this process the residual melt will be depleted in phosphate, magnesium, niobium and tantalum and enriched in iron (ankerite), sulfur and other incompatible elements (Sr, Ba, Mn).

Enrichment of rare-earth elements will occur if the amount of apatite crystallization is not capable of depleting the parent melt. Note, that the mineral-melt partition coefficient for REE in apatite is in favour of apatite only at low concentrations of REE in the melt. Thorium would generally be expected to be removed from the melt with pyrochlore and phosphate fractionation. The high thorium contents of the dikes of the northwest ridge appears to be unusual. The difference in concentration and state of occurrence of sulfur in the two type of dikes might be explained by a difference in oxygen fugacities: the presence of barite (sulfate) in the dikes of the northwest ridge suggest a higher oxygen fugacity than the sulfide-bearing dikes of the north ridge. This might also explain the two different rare-earth assemblages: if barium crystallizes in sulfate-form, bastnaesite-group carbonates (barium-free, northwest ridge) are more likely to form instead of burbankite and other barian rare-earth carbonates (north ridge).

Quantitative testing of the "residual melt" hypothesis would involve mass balance calculation as a first step. The major difficulty would arise in the adequate modelling of the composition of fractionating a dolomite - ankerite - kutnahorite solid solution as a function of composition. Crystal-liquid partition coefficients are not yet known well enough to further constrain the hypothesis. Thermodynamic constraints appear to be even further in the future.

Dolomite carbonatite - calcite carbonatite:

Field evidence indicates that dolomite carbonatite and calcite carbonatite magma must have been physically separate liquids emplaced at different times (cf. section 6.1.1). The exposed relative proportions of dolomite carbonatite and calcite carbonatite (97 % and 2-3 % respectively) generally do not necessarily reflect the relative proportions of the respective magmas.

The apparently later injecting calcite carbonatite sweats do not have the geochemical characteristics of a residual carbonatite melt and thus, are not an equivalent to pegmatites in granitoid systems. The large proportion of dolomite

carbonatite compared to calcite carbonatite is unusual compared to most carbonatite complexes (Heinrich, 1966; Le Bas, 1977): commonly calcite carbonatite forms the bulk of the core carbonatite followed by dolomitic, ankeritic or sideritic and finally rare-earth rich carbonatites. If vertical zonation is assumed (Le Bas, 1977, 1981) the relative proportions of carbonatite types is merely an effect of the level exposed.

It is difficult to relate dolomite carbonatite and calcite carbonatite by fractionation, because calcite carbonatite would have to be produced as an early fractionating phase (Wyllie, 1985; Le Bas, 1981; Fanelli et al, in press). The major reason is that the calcite-magnetite dominated crystallization has to change rather abruptly to dolomite crystallization, while such a path is not supported by experimental data (Wyllie & Jones, 1985; Fanelli et al, in press).

Better knowledge of the liquidus surfaces in the relevant system would greatly improve our ability to interpret field observations. Calcite carbonatite and dolomite carbonatite in the Aley complex cannot easily be related by a parent-daughter relationship. They probably had a common magma source, but followed different paths of diversification.

Carbonatite - Syenite:

Field relationships, trace element geochemistry and initial $^{87}Sr/^{86}Sr$ ratios suggest a genetic relationship between syenite and carbonatite. Geochemical and experimental data are too scarce to delineate a specific differentiation path, possibly from a high temperature silicate melt to a low temperature carbonatite melt or, possibly a relationship by liquid immiscibility (Le Bas, 1977, 1981; Hamilton & Freestone, 1980; Wyllie & Jones, 1985).

6.5 PHYSICAL PROPERTIES OF CARBONATITE MAGMAS

Carbonatite liquids are nearly unpolymerized ionic liquids with physical and thermal properties that are entirely different from those of silicate melts. Data on the physical properties of carbonatite liquids is limited (summarized in Treiman &

Schedl, 1983). Compared to polymerized silicate melts, carbonatite magmas have very low viscosities ($\simeq 5 \cdot 10^{-6}$ kg/m/s), low heats of fusion ($\simeq 50\text{-}150 \cdot 10^{3}$ J/kg) and very high thermal diffusivities ($\simeq 4 \cdot 10^{-5}$ J/m/s/K) (Treiman & Schedl, 1983). Heats of fusion for calcite calculated from liquidus relationships in binary systems vary between $15 \cdot 10^{3}$ and $30 \cdot 10^{3}$ J/mol (Flood et al, 1949; Bradly, 1962).

6.6 HYPOTHETICAL PROCESSES IN CARBONATITE MAGMA CHAMBERS

On the basis of many assumptions and on analogies with studies in systems with comparable geometries, Treiman & Schedl (1983) deduced characteristic parameters (Prandtl number, Rayleigh number, Reynolds number etc.) for a carbonatite magma chamber of cylindrical geometry and 1 km diameter. They arrive at the following conclusions: rapid crystal settling velocities are to be expected even for small grains (0.2-0.9 m/s for a grain of 1 mm diameter); convection driven by horizontal temperature gradients is expected to be turbulent because of the high Rayleigh numbers predicted (10^{17}-10^{20}); estimated growth rates onto the walls of the magma chamber are in the order of cm per year and allow considerable thickness of carbonatite growth in situ.

The likelihood of turbulent magma motion has some further important consequences:

- crystals may stay in suspension even if the net upward magma velocities are much smaller than calculated crystal settling velocities
- turbulence is characterized by high rates of heat, mass and momentum transfer that will enhance the reactivity of a carbonatite magma with silicate rocks
- although driven largely by temperature gradients, turbulence does not imply rapid equilibration of a magma chamber. The large range of scales at which turbulence operates will result in a large range of scale of transient heterogeneities within a magma chamber
- laterally persistent horizontal stratification due to crystal settling is not to be expected

- irregularities of the walls of a magma chamber will act as "back-eddies" and may cause irregularly shaped volumes of crystal accumulation.

7. CONCLUSIONS

1 Stable isotope data and initial strontium isotope ratios suggest a mantle origin for the rocks of the Aley carbonatite complex. The lack of knowledge of the parent magma composition makes it difficult to gain insight into processes in the mantle source region.

2 Similarly, available data do not yet allow discrimination between a process of progressive differentiation and a process of liquid immiscibility, both leading from an alkali carbonatite magma to a low temperature carbonatite melt.

3 Field observations suggest the following order of emplacement: syenite / dolomite carbonatite / calcite carbonatite / rare-earth carbonatite dikes.

4 The lamprophyric dikes and the Ospika diatreme appear to be closely related in time. Their petrogenetic relationship was not studied.

5 The petrogenetic relationship among the rocks of the complex is not established. The rare-earth dikes appear to be residual liquids (enriched in Sr, Ba, LREE, sulfide or sulfate) of a dolomite carbonatite-like parent magma.

6 The syenite is geochemically and texturally extremely heterogeneous but it clearly is an igneous rock as indicated by field relationships and relict micro-syenite textures. The primary alkali-rich phases are magnesio-arfvedsonite and possibly aegirine. The strong metasomatic overprint marked by metamorphic textures and the extensive growth of aegirine indicate interaction with large volumes of an alkali-rich fluid phase

7 The contact aureole is characterized by the presence of brownish alteration colours, locally elevated radioactivity and the absence of calc-silicates. It is possible that a highly mobile fluid phase penetrated the rocks of the contact aureole along bedding. The fluids that altered the syenite and those that altered the host rocks might be of the same parentage and the syenite may have acted as a "filter" or chemical trap for alkalies.

8 Temperatures in the wallrock probably did not exceed 400°C and are not consistent with temperatures predicted by a cooling model of a solidifying magma body.

9 The formation of an annular, cylindrical ductile shear zone around the complex and the fabrics within the carbonatite core suggest doming as the major mechanism of emplacment at the level exposed. Simple gravitational diapirism in the solid state is physically not possible because of the higher density of the carbonatite rocks compared to the host rocks. Solid syenite in a plastic condition intruded by carbonatite as a driving force may have been a possible mechanism for doming. Quartzite xenoliths from stratigraphic levels not much more than 1 km below the host rocks indicate intrusion of syenite into a high crustal level. Because a driving mechanism for extensive doming appears to be limited by physical properties of the rocks observed, the exposed level may be near the roof of the Aley complex. There is no indication whether the complex vented to the surface.

10 The formation of aegirine, amphiboles with high ferric-ferrous ratios and the presence of sulfate in some of the rare-earth dikes suggest high oxygen fugacities at least during the late stage of magma evolution.

BIBLIOGRAPHY

ABBEY (1980) Studies in "standard samples" fore use in the general analysis of silicate rocks and minerals, part 6:, 1979 edition of "usable values"

ANDERSON E.M. (1936) The dynamics of the formation of cone-sheets, ring-dykes, and cauldron-subsidences, Proc. Roy. Soc. Edinb., 56, 128-163.

BELL K., BLENKINSOP J., COLE T.J.S., and MENAGH D.P. (1982) Evidence from Sr isotopes for long-lived heterogeneities in the upper mantle, Nature, 298, 251-253.

BELL K., and POWELL J.L. (1970) Strontium isotopic studies of alkalic rocks: the alkalic complexes of Eastern Uganda, Bull. Geol. Soc. Amer., 81, 3481-3490.

BICKLE M.J., and POWELL R. (1977) Calcite-dolomite geothermometry for iron-bearing carbonates. The Glockner area of the Tauern window, Austria, Contrib. Mineral. Petrol., 59, 281-292.

BIGGAR G.M. (1969) Phase relationships in the join $Ca(OH)_2$-$CaCO_3$-$Ca_3(PO_4)_2$-H_2O at 1000 bars, Min. Mag., 37, 75-82.

BILLINGS M.P. (1945) Mechanics of igneous intrusion in New Hampshire, Am. J. Sci., 248-A, 40-68.

BOETTCHER A.L. (1984) The system SiO_2-H_2O-CO_2: Melting, solubility mechanisms of carbon, and liquid structure to high pressures, Am. Min., 69, 823-833.

BOGOCH R., and MAGARITZ M. (1983) Immiscible silicate-carbonate liquids as evidenced from ocellar diabase dykes, Southern Sinai, Contrib. Mineral. Petrol., 83, 227-230.

BOHNSTEDT-KUPLETSKAYA E.M., and BUROVA T.A. (1947) Fersmite, a new calcium niobate from the pegmatites of the Vishnevye Mts., the Central Urals, Am. Min., 32, 373.

BOWEN N.L. (1945) Phase equilibria bearing on the origin and differentiation of alkaline rocks, Am. J. Sci., 243A, 75-89.

BROWN R.L., JOURNEAY J.M., LANE L.S., MURPHY D.C., and REES C.J. (1986) Obduction, backfolding and piggyback thrusting in the metamorphic hinterland of the southeastern Canadian Cordillera, Jour. Struc. Geol., 8, 255-268.

BYRNES A.P., and WYLLIE P.J. (1981) Subsolidus and melting relation for the join $CaCO_3$-$MgCO_3$ at 10 kilobars, Geochim. Cosmochim. Acta, 45, 321-328.

CARSLAW H.S., and JAEGER J.C. (1959) Conduction of heat in solids, Oxford University Press

COOPER A.F., GITTINS J., and TUTTLE O.F. (1975) The system

Na_2CO_3-K_2CO_3-$CaCO_3$ at 1 kilobar and its significance in carbonatite petrogenesis, Am. J. Sci., 275, 534-560.

CURRIE J.B. (1956) Role of concurrent deposition and deformation of sediments in development of salt-dome graben structures, Bull. Am. Assoc. Petrol. Geol., 40, 1-16.

CURRIE K.L. (1975) The geology and petrology of the Ice River alkaline complex, British Columbia, Geol. Surv. Can., Bull., 245

CURRIE K.L. (1976) The alkaline rocks in Canada, Geol. Surv. Can. Bull., 239

D'ARCY G. (1949) Mineralogy of uranium and thorium bearing minerals, U.S. Atomic Energy Commission

ECKERMANN H. (1958) The alkaline and carbonatitic dykes of the Alnö formation on the mainland north-west of Alnö Island, Kungl. Sv. Vetenskapskad. Handl., 4, 7, Nr. 2

EGGLER D.H. (1978) The effect of CO_2 upon partial melting of peridotite in the system Na_2O-CaO-Al_2O_3-MgO-SiO_2-CO_2 to 35 kb, with an analysis of melting in a peridotite-H_2O-CO_2 system, Am. J. Sci., 278, 305-343.

EGGLER D.H. (1975) CO_2 as a volatile component of the mantle: the system Mg_2SiO_4-SiO_2-H_2O-CO_2, Phys. Chem. Earth., 9, 869-881.

EGGLER D.H., and ROSENHAUER M. (1978) Carbon dioxide in silicate melts: II. Solubilities of CO_2 and H_2O in $CaMgSi_2O_6$ (diopside) liquids and vapors at pressures to 40 kbar, Am. J. Sci., 278, 64-94.

ERICKSON R.L., and BLADE L.V. (1963) Geochemistry and petrology of the alkalic igneous complex at Magnet Cove, Arkansas, U.S. Geol. Survey Prof. Paper, 425

FANELLI M.F., CAVA N., and WYLLIE P.J. (1985) Calcite and dolomite without portlandite at a new eutectic in CaO -MgO - CO_2 - H_2O, with applications to carbonatites, Proc. 13th Gen. Mtg. Int. Mineral. Assoc., in press

FLEISCHER M. (1980) Glossary of mineral species, Mineralogical Record, Tucson, Arizona

FLEISCHER M. (1978) Relative proportions of the lanthanides in minerals of the bastnaesite Group, Can. Min., 16, 361-363.

FREESTONE I.C., and HAMILTON D.L. (1980) The role of liquid immiscibility in the genesis of carbonatites; an experimental study, Contrib. Mineral. Petrol., 73, 105-117.

GITTINS J., and TUTTLE O.F. (1964) The system CaF_2-$Ca(OH)_2$-$CaCO_3$, Am. J. Sci., 262, 66-75.

GITTINS J. (1979) Problems inherent in the application of calcite-dolomite geothrmometry to carbonatites, Contrib. Mineral. Petrol., 69, 1-4.

GOLD D.P., VALLEE M., and CHARETTE J.-P. (1967) Economic geology and geophysics of the Oka alkaline complex, Quebec, Canadian Mining and

Metallurgical Bulletin, Oct, 1131-1144.

GOLDSMITH J.R., and NEWTON R.C. (1969) P-T-X relations in the system $CaCO_3$-$MgCO_3$ at high temperatures and pressures, Am. J. Sci., 267-A, 160-190.

GRAF D.L., and GOLDSMITH J.R. (1955) Dolomite-magnesian calcite relations at elevated temperatures and CO_2 pressures, Geochim. Cosmochim. Acta, 10, 109-118.

GRAF D.L., and GOLDSMITH J.R. (1958) The solubility of $MgCO_2$ in $CaCO_3$: a rivision, Geochim. Cosmochim. Acta, 13, 218-219.

GREIG J.W. (1928) On the evidence which has been presented for liquid silicate immiscibility in the laboratory and in the rocks of Agate Point, Ontario, Am. J. Sci., 265, 373-402.

GRUENENFELDER M.H., and TILTON G.R. (1986) Lead and strontium isotope relationships in the Oka carbonatite complex, Quebec, Geochim. Cosmochim. Acta, 50, 461-468.

GUSSOW W.C. (1968) Salt diapirism: Importance of temperature, and energy source of emplacement, in: Diapirism and Diapires, Braunstain et al (eds.), Am. Assoc. Petrol. Geol.

HAMILTON D.L., FREESTONE I.C., DAWSON J.B., and DONALDSON C.H. (1979) Origin of carbonatites by liquid immiscibility, Nature, 279, 52-54.

HARKER R.J., and TUTTLE O.F. (1955) Studies in the system CaO-MgO-CO_2, part 2.: Limits of the solid solution along the binary join $CaCO_3$-$MgCO_3$, Am. J. Sci., 253, 274-282.

HAWTHORNE F.C. (1981) in: Rivews in mineralogy: Amphiboles and other hydrous pyriboles - mineralogy (Veblen, D.R., ed.), Min. Soc. Amer., 9A

HEINRICH E.W. (1967) Carbonatites: Nil-silicate igneous rocks, Earth-Sci. Rev., 3, 203-210.

HEINRICH E.W. (1966) The geology of carbonatites, John Wiley & Sons, New York

HELZ G.R., and WYLLIE P.J. (1979) Liquidus relationships in the system $CaCO_3$-$Ca(OH)_2$-CaS and the solubility of sulfur in carbonatite magmas, Geochim. Cosmochim. Acta, 43, 259-266.

HOGARTH D.D. (1977) Classification and nomenclature of the pyrochlore group, Am. Min., 62, 403-410.

HOGARTH D.D. (1961) A Study of pyrochlore and betafite, Can. Min., 6, 610-633.

INGERSOLL L.R., ZOBEL O.J., and INGERSOLL A.C. (1954) Heat conduction with engineering, geological and other applications, The University of Wisconsin Press

IRISH E.J.W. (1970) Halfway River map-area, British Columbia, Geol. Survey Can. Paper, 69-11

IRVING A.J., and WYLLIE P.J. (1975) Subsolidus and melting relationships for calcite, magnesite and the join $CaCO_3$-$MgCO_3$ to 36 kb, Geochim. Cosmochim. Acta, 39, 35-53.

JAEGER J.C. (1957) The temperature in the neighborhood of a cooling intrusive sheet, Am. J. Sci., 255, 306-318.

JONES A.P., and WYLLIE P.J. (1983) Low-temperature glass quenched from a synthetic, rare earth carbonatite. Implications for the origin of the mountain pass deposit, California, Economic Geology and the Bulletin of the Society of Economic Geologists, 78, 1721-1723.

JONES A.P., and WYLLIE P.J. (1986) Solubility of rare earth elements in carbonatite magmas, indicated by the liquidus surface in $CaCO_3$-$Ca(OH)_2$-$La(OH)_3$ at 1 kbar pressure, Applied Geochemistry, 1, 95-102.

KAPUSTIN Y.L. (1980) Mineralogy of carbonatites, Amerind Publishing Co., New Dehli

KOSTER VAN GROOS A.F. (1975) The distribution of strontium between coexisting silicate and carbonate Liquids at elevated pressures and temperatures, Geochim. Cosmochim. Acta, 39, 27-34.

KOSTER VAN GROOS A.F., and WYLLIE P.J. (1973) Liquid immiscibility in the join $NaAlSi_3O_8$ - $CaAl_2Si_2O_8$ - Na_2CO_3 - H_2O, Am. J. Sci., 273, 465-487.

KOSTER VAN GROOS A.F., and WYLLIE P.J. (1968) Liquid immiscibility in the Join $NaAlSi_3O_8$-Na_2CO_3-H_2O and its bearing on the genesis of carbonatites, Am. J. Sci., 266, 932-967.

KOSTER VAN GROOS A.F., and WYLLIE P.J. (1966) Liquid immiscibility in the system Na_2O-Al_{2-3}-SiO_2-CO_2 at pressures up to 1 kilobar, Am. J. Sci., 264, 234-255.

KRESTEN P. (1980) The Alnö complex: Tectonics of dike emplacement, Lithos, 13, 153-158.

KUELLMER F.J., VISOCKY A.P., and TUTTLE O.F. (1966) Preliminary survey in the system barite-calcite-fluorite at 500 bars, in: Carbonatites, Tuttle,O.F. and Gittins,J. (eds.), John Wiley and Sons, Inc.,

KUTTY T.R.N., VISWANATHIAH M.N., and TAREEN J.A.K. (1978) Hydrothermal equilibria in Nd2O3 - CO2 system, Proc. Indian Acad. Sci., 87A, 69-74.

LE BAS M.J. (1981) Carbonatite magmas, Min. Mag., 44, 133-140.

LE-BAS M.J. (1977) Carbonatite-nephelinite volcanism, John Wiley & Sons, New York

MAKSIMOVIC Z, and PANTO G. (1979) Synchysite-(Nd), Am. Min., 64, 658.

MYSEN B.O., EGGLER D.H., SEITZ M.G., and HOLLOWAY J.R. (1976) Carbon dioxide in silicate melts and crystals. part I. Solubility measurements, Am. J. Sci., 276, 455-479.

NESBITT B.E., and KELLY E.C. (1977) Magmatic and hydrothermal inclusions in carbonatite of the Magnet Cove complex, Arkansas, Contrib. Mineral. Petrol., 63, 271-294.

OZISIK M.N. (1980) Heat conduction, John Wiley & Sons, New York

PALACHE C., BERMAN H., and FRONDEL C. (1944) Dana's system of mineralogy, 7th ed., vol. I, John Wiley & Sons

PALACHE C., BERMAN H., and FRONDEL C. (1951) Dana's system of mineralogy, 7th ed., vol. II, John Wiley & Sons

PECORA W.T., and KERR J.H. (1953) Burbankite and calkinsite, two new carbonate minerals from Montana, Am. Min., 38, 1169-1183.

PELL J. (1985) Carbonatites and related rocks in British Columbia, B.C. Ministry of Energy, Mines & Pet. Res., Geological Fieldwork 1984, 84-94.

PELL J. (1986b) Carbonatites in British Columbia: the Aley property, B.C. Ministry of Energy, Mines & Pet. Res., Geological Fieldwork 1985,

PELL J. (1986a) Diatreme breccias in British Columbia, B.C. Ministry of Energy, Mines & Pet. Res., Geological Fieldwork 1985,

PINEAU F., JAVOY M., and ALLEGRE C.J. (1973) Etude systematique des isotopes de l'oxigene, du carbone et du strontium dans les carbonatites, Geochim. Cosmochim. Acta, 37, 2363-2377.

PRIDE K.R. (1983) Geological survey on the Aley claims, Omineca Mining Division, British Columbia, B.C. Ministry of Energy, Mines & Pet. Res., Assessment Report 12018,

RAMDOHR P. (1955) Die Erzmineralien und ihre Verwachsungen, Akademie-Verlag, Berlin

RANKIN A.H. (1975) Fluid inclusion studies in apatite from carbonatites of the Wasaki area of Western Kenya, Lithos, 8, 123-136.

RANKIN A.H., and LE BAS M.J. (1974) Mineral. Mag., 41, 155-64.

RICE J.M. (1977) Contact metamorphism of impure dolomitic limestone in the Boulder Aureole, Montana, Contrib. Mineral. Petrol., 59, 237-259.

ROESLER H.J. (1981) Lehrbuch der Mineralogie, VEB Deutschwer Verlag fuer Grundstoffindustrie

ROMANCHEV B.P. (1972) Inclusion thermometry and the formation conditions of some carbonatite complexes in East Africa, Geochem. Internat., 9, 115-120.

SAHMA TH.G. (1956) Optical anomalie in arfvedsonite from Greenland, Am. Min., 41, 509-512.

SEMENOV E.I., and CHANG P'EI-SHAN (1963) Huanghoite, Am. Min., 48, 1179.

TAYLOR G.C., and STOTT D.F. (1973) Tuchodi Lakes map area, British Columbia, Geol. Survey Can. Memoir, 373

TAYLOR G.C., and STOTT D.F. (1979) Geology, Monkman Pass map area, British Columbia (93I), Geol. Survey Can. Open File Report, 630

TAYLOR G.C. (1979) Trutch (94G) and Ware east half (94F,E1/2) map-areas, Northwestern British Columbia, Geol. Survey Can. Open File Report, 606

TAYLOR G.C. (1983) Pine Pass map area (93O), Geol. Survey Can., Open File Report, 925

TAYLOR H.P.JR., FRCHEN J., and DEGENS E. (1967) Oxygen and carbon isotope studies of carbonatites from the Laacher See district, West Germany and the Alnö district, Sweden, Geochim. Cosmochim. Acta, 31, 407-430.

THOMPSON R.I. (1978) Geological maps and cross sections of Halfway River map area, British Columbia (94B), Geol. Survey Can., Open File Report, 536

THOMPSON R.I. (1979) A structural interpretation across part of the Northern Rocky Mountains, British Columbia, Canada, Can. J. Earth. Sci., 16, 1228-1241.

THOMPSON R.I. (IN PREP.) 1985, Stratigraphy, sructural analysis, and tectonic evolution of the Halfway River map area (94B), Northern Rocky Mountains, British Columbia, Geol. Survey Can., Memoir, preprint

TREIMAN A.H., and SCHEDL A. (1983) Properties of carbonatite magma and processes in carbonatite magma chambers, Journal of Geology (USA), 91, 437-447.

TROEGER W.E. (1979) Optical determination of rock-forming minerals, part 1, E. Schweizerbart'sche Verlagsbuchhandlung, Stuttgart

TURCOTTE D.L., and SCHUBERT G. (1982) Geodynamics : Application of continuum physics to geological problems, John Wiley & Sons, New York

TUTTLE O.F., and GITTENS J. (1966) Carbonatites, John Wiley & Sons, New York,

VLASOV K.A. (1966) Mineralogy of rare elements, v.2, Israel Program for Scientific Translations, Jerusalem

WATKINSON D.H., and WYLLIE P.J. (1969) Phase equilibrium studies bearing on the limestone-assimilation hypothesis, Geol. Soc. Amer. Bull., 80, 1565-1576.

WENDLANDT R.F., and HARRISON W.J. (1979) Rare earth partitoning between immiscible carbonate and silicate liquids and CO_2 vapor: Results and implications for the formation of light rare earth-enriched rocks, Contrib. Mineral. Petrol., 69, 400-419.

WYLLIE P.J., and BOETTCHER A.L. (1969) Liquidus phase relationships in the system $CaO-CO_2-H_2O$ to 40 kilobars pressure with petrological applications, Amer. J. Sci., 267-A, 489-508.

WYLLIE P.J., and TUTTLE O.F. (1960) The system $CaO-CO_2-H_2O$ and the origin of carbonatites, Jour. Petrol., 1, 1-46.

WYLLIE P.J., and JONES A.P. (1985) Experimental data bearing on the origin of carbonatites, with particular reference to the Mountain Pass rare earth deposit, Applied Mineralogy, Conference Proceedings, Los Angeles, California, Feb.1984, 935-949.

WYLLIE P.J., and BIGGAR G.M. (1966) Fractional crystallization in the "carbonatite systemes" $CaO\text{-}MgO\text{-}CO_2\text{-}H_2O$ and $CaO\text{-}CaF_2\text{-}P_2O_5\text{-}CO_2\text{-}H_2O$, 4th Intl. Mineral. Assoc. Papers, 67-82.

WYLLIE P.J., and HUANG W.L. (1975) Peridotite, kimberlite, and carbonatite explained in the system $CaO\text{-}MgO\text{-}SiO_2\text{-}CO_2$, Geology, 3, 621-624.

WYLLIE P.J., and HUANG W.L. (1976) Carbonatite and melting reactions in the system $CaO\text{-}MgO\text{-}SiO_2\text{-}CO_2$ at mantle pressures with geophysical and petrological applications, Contrib. Mineral. Petrol., 54, 79-107.

APPENDIX A: MINERALOGY AND MINERAL CHEMISTRY

Appendix A contains electron microprobe analyses of minerals, back-scattered electron images (SEM-EDS), photo micrographs, autoradiographs, block diagrams with optical properties, composition diagrams and energy-dispersive patterns (SEM-EDS) for most minerals studied. The tables are listed in numerical order at the beginning of appendix A followed by the figures. The EDS-patterns are appended and structured in the same sequence as in chapter 3.

Electron Microprobe Analyses

All the electron microprobe analyses were done using the ARL-SEMQ in the Department of Geology at the University of Calgary. The instrument was run at 15 keV and 0.15 nA measured on brass. The electron beam was focused for silicate analyses. A split beam was used for carbonate analyses. Data reduction was done off-line using ZAF correction procedures.

Compositions of standards used are listed in table 11. The standard sets used for individual mineral groups are shown in table 12.

Mineral group analysed	Standard set used
Carbonates	283,94,113,86,267,120,119
Amphiboles / Pyroxenes	48,296,22,23
Feldspars	58,90,113,83,181,91

Table 11: Standard sets used for electron microprobe analysis. For number codes of standards see legend of table 12

Composition of Standards used for Electron Microprobe Analysis

No.	22	23	48	58	83	86	90	91	94	113	119	120	181	186	267	283	296
SiO2	55.74	49.01	40.45	55.60	49.42		64.39	53.94		68.80			42.14	56.88	39.68		40.30
TiO2		0.05	4.90					0.26					0.94				1.32
Al2O3	0.32		14.50	28.30	23.57		18.58	0.66		19.40			12.09	8.82	33.65		14.30
FeO	7.09	44.99	10.96		0.29	0.30	0.03	2.93		0.02		58.81	19.05				1.68
MnO	14.73	0.37	0.10			61.11		0.07				2.86	0.63				0.03
MgO	18.55	3.17	12.78			0.04		16.93		0.02	21.86	0.20	8.67	12.10			26.40
CaO	1.04	0.08	10.36	10.40				24.55	3.97	0.04	30.41		11.56	16.83	24.65	56.03	0.07
Na2O	0.08	0.04	2.56	5.70	1.67		1.14	0.24		11.80			1.63	5.37			0.43
K2O	0.02		2.04		6.23		14.92	0.01					0.93				10.10
BaO					18.43		0.82	0.01									
SrO									65.28								
Cr2O3								0.21									
H2O	0.32	0.86	2.04					0.03		0.02			2.36				3.10
F	0.28	1.00															
CO2					38.50				30.75		47.73	38.08			43.97		

22	Mn - Cummingtonite	86	Rhodochrosite	119	Dolomite	283	Iceland - Spar
23	Grunerite	90	Orthoclase	120	Siderite	296	Phlogopite
48	Hornblende	91	Clino - Pyroxene	181	Amphibole		
58	An(50) Glass	94	Strontianite	186	Diopside - Jadeite		
83	Hyalophane	113	Albite	267	Tanzanite		

Table 12: Composition of standards used for electron microprobe analysis given in weight percent. Standard numbers refer to the University of Calgary electron microprobe standard catalogue.

EMS ANALYSES OF DOLOMITE FROM CARBONATITE MR-85-5-I

WEIGHT PERCENT

No.	5-I-1	5-I-2	5-I-3	5-I-4	5-I-5	5-I-6	5-I-7	5-I-8	5-I-9	5-I-10	5-I-11	average
CaO	31.61	31.95	32.10	32.06	32.12	32.29	31.92	31.14	32.77	32.92	32.31	32.11
SrO	0.0	0.0	0.0	0.0	0.01	0.0	0.0	0.0	0.0	0.0	0.0	0.00
MnO	0.34	0.35	0.35	0.34	0.31	0.30	0.31	0.35	0.32	0.33	0.35	0.33
FeO	3.59	3.67	3.69	3.51	3.54	3.44	3.24	3.35	3.37	3.60	3.48	3.50
MgO	16.91	17.26	17.30	17.21	17.18	16.87	17.26	17.72	16.52	16.35	16.79	17.03
CO2 *)	45.68	46.38	46.56	46.31	46.34	46.04	46.07	46.04	46.01	46.09	46.04	46.14
total	98.12	99.61	100.00	99.42	99.51	98.93	98.79	98.59	98.99	99.29	98.97	99.11

MOLAR PROPORTIONS

CaCO3	54.30	54.06	54.10	54.33	54.40	55.03	54.37	53.07	55.90	56.04	55.08	54.61
SrCO3	0.0	0.0	0.0	0.0	0.01	0.0	0.0	0.0	0.0	0.0	0.0	0.00
MnCO3	0.46	0.46	0.47	0.45	0.41	0.40	0.42	0.47	0.43	0.44	0.46	0.44
FeCO3	4.81	4.85	4.85	4.64	4.68	4.58	4.31	4.45	4.49	4.78	4.63	4.64
MgCO3	40.43	40.62	40.58	40.58	40.49	39.99	40.90	42.01	39.19	38.74	39.82	40.31
total	100.00	100.00	100.00	100.00	100.00	100.00	100.00	100.00	100.00	100.00	100.00	100.00

Table 13: EMS-analyses of dolomite from dolomite carbonatite MR-85-5-I. *) = CO2 calculated

EMS ANALYSES OF ANKERITE FROM REE-DIKE MR-572A

WEIGHT PERCENT

No.	572A-1	572A-2	572A-3	572A-4	572A-5	572A-6	572A-7	572A-8	average
CaO	28.80	29.10	29.22	29.13	28.93	28.83	28.89	28.92	28.98
SrO	0.37	0.16	0.26	0.20	0.18	0.26	0.25	0.28	0.24
MnO	3.64	3.82	3.81	3.45	3.57	3.65	3.78	3.52	3.66
FeO	7.74	6.24	5.31	7.68	7.64	8.04	8.59	7.13	7.29
MgO	13.40	14.68	15.26	13.94	14.04	13.77	13.53	14.34	14.12
CO2 *)	44.39	45.12	45.31	45.00	45.00	44.96	45.16	45.02	45.00
total	98.33	99.11	99.17	99.40	99.36	99.52	100.21	99.21	99.29

MOLAR PROPORTIONS

CaCO3	50.92	50.61	50.61	50.79	50.45	50.33	50.21	50.41	50.54
SrCO3	0.35	0.15	0.24	0.19	0.17	0.24	0.24	0.27	0.23
MnCO3	5.08	5.25	5.22	4.76	4.93	5.04	5.19	4.86	5.04
FeCO3	10.68	8.47	7.18	10.45	10.40	10.95	11.65	9.70	9.93
MgCO3	32.96	35.52	36.76	33.81	34.05	33.44	32.72	34.77	34.26
total	100.00	100.00	100.00	100.00	100.00	100.00	100.00	100.00	100.00

Table 14: EMS-analyses of ankerite from rare-earth carbonatite dike MR-572A. *) = CO2 calculated

SEM ANALYSES OF CALCITE FROM CARBONATITE MR-85-2-J

WEIGHT PERCENT

No.	J-1	J-2	J-3	J-4	J-5	J-6	J-7	J-8	J-9	J-10	J-11	J-12	average
CaO	52.71	52.64	53.36	53.86	54.36	52.98	52.88	52.84	53.26	52.92	53.08	53.02	53.16
SrO	0.75	0.83	0.72	0.82	0.87	0.88	0.84	0.84	0.75	0.72	0.86	0.69	0.80
MnO	0.19	0.20	0.18	0.26	0.20	0.21	0.20	0.24	0.16	0.18	0.24	0.21	0.21
FeO	0.13	0.11	0.16	0.16	0.11	0.15	0.13	0.18	0.12	0.12	0.15	0.12	0.14
MgO	0.55	0.59	0.69	0.65	0.42	0.63	0.58	0.59	0.44	0.50	0.46	0.50	0.55
CO2 *)	42.48	42.51	43.15	43.59	43.67	42.86	42.70	42.72	42.77	42.58	42.76	42.65	42.87
total	96.81	96.89	98.27	99.34	99.63	97.71	97.33	97.40	97.49	97.02	97.55	97.19	97.72

MOLAR PROPORTIONS

CaCO3	97.37	97.18	97.05	96.97	97.68	97.01	97.20	97.06	97.73	97.55	97.42	97.57	97.32
SrCO3	0.74	0.83	0.71	0.80	0.85	0.87	0.84	0.83	0.74	0.72	0.86	0.69	0.79
MnCO3	0.28	0.30	0.26	0.37	0.28	0.31	0.29	0.35	0.23	0.26	0.35	0.31	0.30
FeCO3	0.19	0.16	0.23	0.23	0.16	0.21	0.18	0.26	0.18	0.17	0.21	0.17	0.20
MgCO3	1.41	1.53	1.75	1.63	1.04	1.60	1.49	1.50	1.12	1.29	1.17	1.27	1.40
total	100.00	100.00	100.00	100.00	100.00	100.00	100.00	100.00	100.00	100.00	100.00	100.00	100.00

Table 15: EMS-analyses of calcite from calcite carbonatite MR-85-2-J. *) = CO2 calculated

EMS ANALYSES OF ALBITE FROM SYENITE MR-533

WEIGHT PERCENT

No.	533-1	533-2	533-3	533-4	533-5	533-6	533-7	533-8	533-9	533-10	533-11	533-12	average
CaO	0.0	0.19	0.08	0.02	0.23	0.03	0.01	0.01	0.02	0.01	0.0	0.00	0.05
K2O	0.05	0.14	0.05	0.05	0.05	0.05	0.07	0.08	0.06	0.06	0.05	0.05	0.06
Na2O	11.67	11.28	11.28	11.63	11.83	11.60	11.58	10.80	11.61	11.65	11.54	11.66	11.51
BaO	0.06	0.09	0.03	0.0	0.02	0.0	0.02	0.0	0.0	0.0	0.0	0.0	0.02
SiO2	69.24	68.27	68.23	68.47	68.79	68.77	67.76	68.91	68.34	68.50	68.01	68.01	68.44
Al2O3	19.00	18.90	19.36	18.98	19.11	19.51	19.25	19.14	19.40	19.23	19.04	19.17	19.17
FeO	0.26	0.14	0.05	0.25	0.22	0.15	0.33	0.27	0.21	0.29	0.41	0.28	0.24
MgO	0.0	0.30	0.0	0.01	0.0	0.0	0.0	0.0	0.0	0.0	0.0	0.0	0.03
total	100.29	99.32	99.08	99.40	100.25	100.11	99.03	99.21	99.63	99.74	99.04	99.17	99.52

MOLAR PROPORTIONS NORMALIZED TO 8.0 OXYGENS

Ca	0.0	0.01	0.00	0.00	0.01	0.00	0.00	0.00	0.00	0.00	0.0	0.00	0.00
K	0.00	0.01	0.00	0.00	0.00	0.00	0.00	0.00	0.00	0.00	0.00	0.00	0.00
Na	0.99	0.96	0.96	0.99	1.00	0.98	0.99	0.92	0.99	0.99	0.99	1.00	0.98
Ba	0.00	0.00	0.00	0.0	0.00	0.0	0.00	0.0	0.0	0.0	0.0	0.0	0.00
Si	3.02	3.00	3.00	3.01	3.00	3.00	2.99	3.02	3.00	3.00	3.00	3.00	3.00
Al	0.98	0.98	1.00	0.98	0.98	1.00	1.00	0.99	1.00	0.99	0.99	1.00	0.99
Fe	0.01	0.01	0.00	0.01	0.01	0.01	0.01	0.01	0.01	0.01	0.01	0.01	0.01
Mg	0.0	0.02	0.0	0.00	0.0	0.0	0.0	0.0	0.0	0.0	0.0	0.0	0.00
O	8.00	8.00	8.00	8.00	8.00	8.00	8.00	8.00	8.00	8.00	8.00	8.00	8.00
total	100.00	100.00	100.00	100.00	100.00	100.00	100.00	100.00	100.00	100.00	100.00	100.00	100.00

Table 16: EMS-analyses of albite from syenite MR-533

EMS ANALYSES OF ARFVEDSONITE FROM SYENITE MR-551

WEIGHT PERCENT

No.	551-1	551-2	551-3	551-4	551-5	551-6	533-7	551-8	551-9	551-10	551-11	551-12	average
SiO2	54.78	55.01	54.73	54.82	54.62	55.14	54.42	54.60	54.43	54.39	54.37	54.66	54.66
TiO2	0.19	0.19	0.21	0.18	0.19	0.23	0.20	0.23	0.21	0.23	0.21	0.21	0.21
Al2O3	0.11	0.08	0.07	0.09	0.10	0.11	0.21	0.23	0.15	0.15	0.11	0.13	0.13
FeO	10.63	10.79	10.73	9.75	9.20	10.33	12.00	12.64	12.09	11.85	10.96	11.00	11.00
MnO	0.95	0.98	0.93	0.85	0.95	0.88	0.92	0.93	0.96	0.93	1.00	0.94	0.94
MgO	16.82	16.35	16.59	16.99	17.55	17.06	15.46	15.26	15.44	15.69	16.22	16.31	16.31
CaO	2.87	2.45	2.54	3.24	3.73	3.25	1.63	1.23	1.65	1.89	2.50	2.45	2.45
Na2O	8.22	8.39	8.33	7.91	7.86	7.81	8.78	8.77	8.79	8.59	8.29	8.34	8.34
K2O	1.76	1.90	1.84	1.74	1.70	1.66	1.80	1.94	1.87	1.73	1.69	1.78	1.78
BaO	0.0	0.01	0.0	0.0	0.01	0.01	0.05	0.0	0.00	0.0	0.03	0.01	0.01
F	2.55	2.59	2.41	2.42	2.45	2.19	2.36	2.45	2.36	2.41	2.74	2.45	2.45
H2O *)	0.70	0.70	0.70	0.70	0.70	0.70	0.70	0.70	0.70	0.70	0.70	0.74	0.70
total	99.57	99.44	99.08	98.70	99.07	99.38	98.54	98.98	98.67	98.58	98.81	99.02	98.99

MOLAR PROPORTIONS NORMALIZED TO 24.0 OXYGENS (O,OH,F)

Si	8.05	8.10	8.08	8.09	8.03	8.09	8.12	8.12	8.12	8.10	8.06	8.08	8.09
Ti	0.02	0.02	0.02	0.02	0.02	0.03	0.02	0.03	0.02	0.03	0.02	0.02	0.02
Al	0.02	0.01	0.01	0.02	0.02	0.02	0.04	0.04	0.03	0.03	0.02	0.02	0.02
Fe	1.31	1.33	1.32	1.20	1.13	1.27	1.50	1.57	1.51	1.48	1.36	1.36	1.36
Mn	0.12	0.12	0.12	0.11	0.12	0.11	0.12	0.12	0.12	0.12	0.13	0.12	0.12
Mg	3.68	3.59	3.65	3.74	3.85	3.73	3.44	3.38	3.43	3.48	3.58	3.59	3.60
Ca	0.45	0.39	0.40	0.51	0.59	0.51	0.26	0.20	0.26	0.30	0.40	0.39	0.39
Na	2.34	2.39	2.38	2.26	2.24	2.22	2.54	2.53	2.54	2.48	2.38	2.39	2.39
K	0.33	0.36	0.35	0.33	0.32	0.31	0.34	0.37	0.35	0.33	0.32	0.34	0.34
Ba	0.0	0.00	0.0	0.0	0.00	0.00	0.00	0.0	0.00	0.0	0.00	0.00	0.00
F	1.18	1.21	1.13	1.13	1.14	1.02	1.12	1.15	1.11	1.14	1.28	1.14	1.15
OH	0.69	0.69	0.69	0.69	0.69	0.69	0.70	0.69	0.70	0.70	0.69	0.73	0.69
O	22.13	22.11	22.18	22.18	22.17	22.30	22.19	22.15	22.19	22.17	22.02	22.13	22.16

Table 17: EMS-analyses of magnesio-arfvedsonite from syenite MR-551.
*) = estimated amount of water added for data reduction .

EMS ANALYSES OF ARFVEDSONITE FROM SYENITE MR-533

WEIGHT PERCENT

No.	533-1	533-2	533-3	533-4	533-5	533-6	533-7	533-8	average
SiO2	53.54	54.63	54.51	54.35	53.68	55.49	54.50	54.39	54.39
TiO2	1.28	0.75	1.52	0.77	0.76	1.09	1.54	1.10	1.10
Al2O3	1.60	0.43	0.56	0.72	1.53	1.59	0.22	0.95	0.95
FeO	9.57	12.04	11.79	11.50	10.19	11.25	12.87	11.32	11.32
MnO	0.54	0.65	0.76	0.37	0.75	0.64	0.75	0.64	0.64
MgO	16.68	14.90	15.07	15.44	16.32	14.38	14.13	15.27	15.27
CaO	2.84	0.69	0.77	0.72	3.76	0.57	0.40	1.39	1.39
Na2O	8.77	9.53	9.50	9.35	8.43	9.72	9.28	9.22	9.22
K2O	1.03	1.74	1.76	1.85	0.83	1.62	1.88	1.53	1.53
BaO	0.04	0.00	0.06	0.03	0.03	0.0	0.01	0.02	0.02
F	2.36	2.14	2.26	2.25	2.04	1.78	1.74	2.08	2.08
H2O *)	1.00	1.00	1.00	1.00	1.00	1.00	1.00	1.00	1.00
total	99.26	98.50	99.55	98.35	99.32	99.12	98.33	98.92	98.92

MOLAR PROPORTIONS NORMALIZED TO 24.0 OXYGENS (O,OH,F)

Si	7.81	8.10	8.01	8.05	7.86	8.12	8.13	8.01	8.01
Ti	0.14	0.08	0.17	0.09	0.08	0.12	0.17	0.12	0.12
Al	0.28	0.07	0.10	0.13	0.26	0.27	0.04	0.16	0.16
Fe	1.17	1.49	1.45	1.42	1.25	1.38	1.61	1.39	1.39
Mn	0.07	0.08	0.09	0.05	0.09	0.08	0.09	0.08	0.08
Mg	3.63	3.30	3.30	3.41	3.56	3.14	3.14	3.35	3.35
Ca	0.44	0.11	0.12	0.11	0.59	0.09	0.06	0.22	0.22
Na	2.48	2.74	2.71	2.68	2.39	2.76	2.68	2.63	2.63
K	0.19	0.33	0.33	0.35	0.16	0.30	0.36	0.29	0.29
Ba	0.00	0.00	0.00	0.00	0.00	0.0	0.00	0.00	0.00
F	1.09	1.00	1.05	1.06	0.94	0.82	0.82	0.97	0.97
OH	0.97	0.99	0.98	0.99	0.98	0.98	1.00	0.98	0.98
O	21.94	22.01	21.97	21.96	22.08	22.20	22.18	22.05	22.05

Table 18: EMS-analyses of magnesio-arfvedsonite from syenite MR-551.
*) = estimated amount of water added for data reduction

EMS ANALYSES OF AEGIRINE FROM SYENITE MR-533

WEIGHT PERCENT

No.	533-10	533-11	533-12	533-13	533-14	533-15	533-16	533-17	533-18	533-19	533-20	average
SiO2	53.00	52.64	53.04	52.68	52.77	52.49	51.83	52.51	52.65	52.92	53.34	52.71
TiO2	3.99	7.14	7.92	6.42	5.47	4.13	4.33	5.48	6.19	6.51	6.38	5.82
Al2O3	0.78	0.38	0.41	0.48	0.65	0.82	0.52	0.43	0.42	0.40	0.43	0.52
Fe2O3	24.71	21.75	20.67	22.73	24.30	25.05	23.76	23.92	23.24	22.82	22.69	23.24
MnO	0.42	0.42	0.60	0.42	0.19	0.22	0.40	0.21	0.39	0.42	0.39	0.37
MgO	2.45	2.84	2.80	2.50	2.23	2.31	2.52	2.35	2.58	2.73	2.73	2.55
CaO	2.62	1.05	0.90	1.26	1.77	2.00	1.70	0.50	0.69	0.64	0.61	1.25
Na2O	12.50	13.75	13.76	13.61	13.11	12.94	13.52	14.08	13.71	13.74	13.83	13.51
K2O	0.00	0.01	0.0	0.00	0.00	0.01	0.01	0.01	0.00	0.00	0.01	0.01
BaO	0.00	0.02	0.02	0.00	0.06	0.01	0.00	0.08	0.04	0.05	0.03	0.03
F	0.0	0.02	0.0	0.0	0.04	0.0	0.0	0.03	0.00	0.04	0.0	0.01
total	100.48	100.03	100.12	100.12	100.60	99.97	98.59	99.60	99.92	100.27	100.43	100.01

MOLAR PROPORTIONS NORMALIZED TO 6.0 OXYGENS

Si	1.98	1.97	1.98	1.97	1.97	1.98	1.98	1.98	1.98	1.98	1.99	1.98
Ti	0.11	0.20	0.22	0.18	0.15	0.12	0.12	0.16	0.17	0.18	0.18	0.16
Al	0.03	0.02	0.02	0.02	0.03	0.04	0.02	0.02.	0.02	0.02	0.02	0.02
Fe	0.70	0.61	0.58	0.64	0.68	0.71	0.68	0.68	0.66	0.64	0.64	0.66
Mn	0.01	0.01	0.02	0.01	0.01	0.01	0.01	0.01	0.01	0.01	0.01	0.01
Mg	0.14	0.16	0.16	0.14	0.12	0.13	0.14	0.13	0.14	0.15	0.15	0.14
Ca	0.11	0.04	0.04	0.05	0.07	0.08	0.07	0.02	0.03	0.03	0.02	0.05
Na	0.91	1.00	0.99	0.99	0.95	0.95	1.00	1.03	1.00	1.00	1.00	0.98
K	0.00	0.00	0.0	0.00	0.00	0.00	0.00	0.00	0.00	0.00	0.00	0.00
Ba	0.00	0.00	0.00	0.00	0.00	0.00	0.00	0.00	0.00	0.00	0.00	0.00
F	0.0	0.00	0.0	0.0	0.00	0.0	0.0	0.00	0.00	0.01	0.0	0.00
O	6.00	6.00	6.00	6.00	6.00	6.00	6.00	6.00	6.00	5.99	6.00	6.00

Table 19: EMS analyses of aegirine from syenite MR-533. All Fe treated as ferrous iron

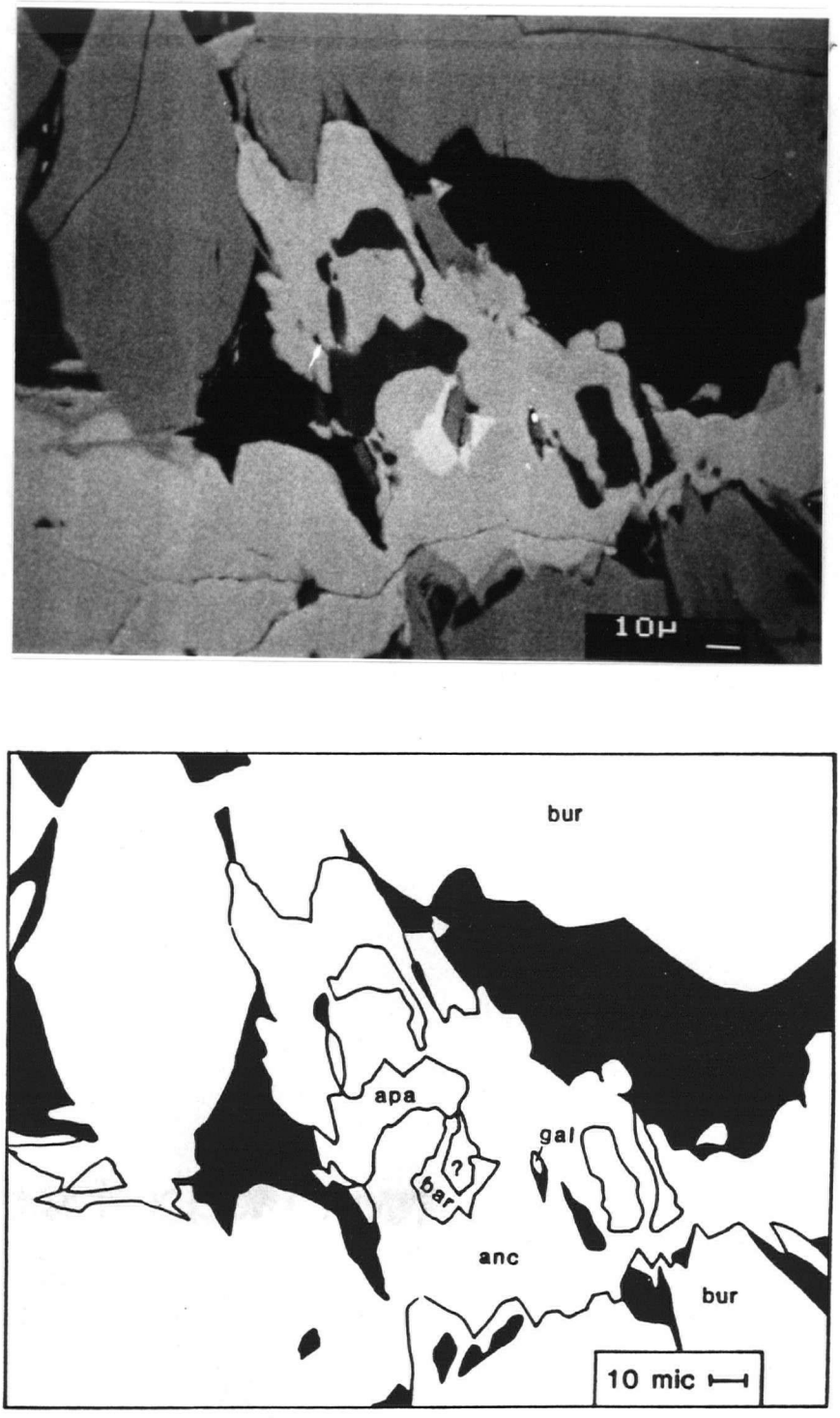

Figure 26: Back scattered electron image of REE-carbonate assemblage (MR-143B). anc = ancylite; apa = apatite; bar = barite; bur = burbankite; gal = galena; ? = Ca>>Sr>Ba,Ce,La; black areas = holes

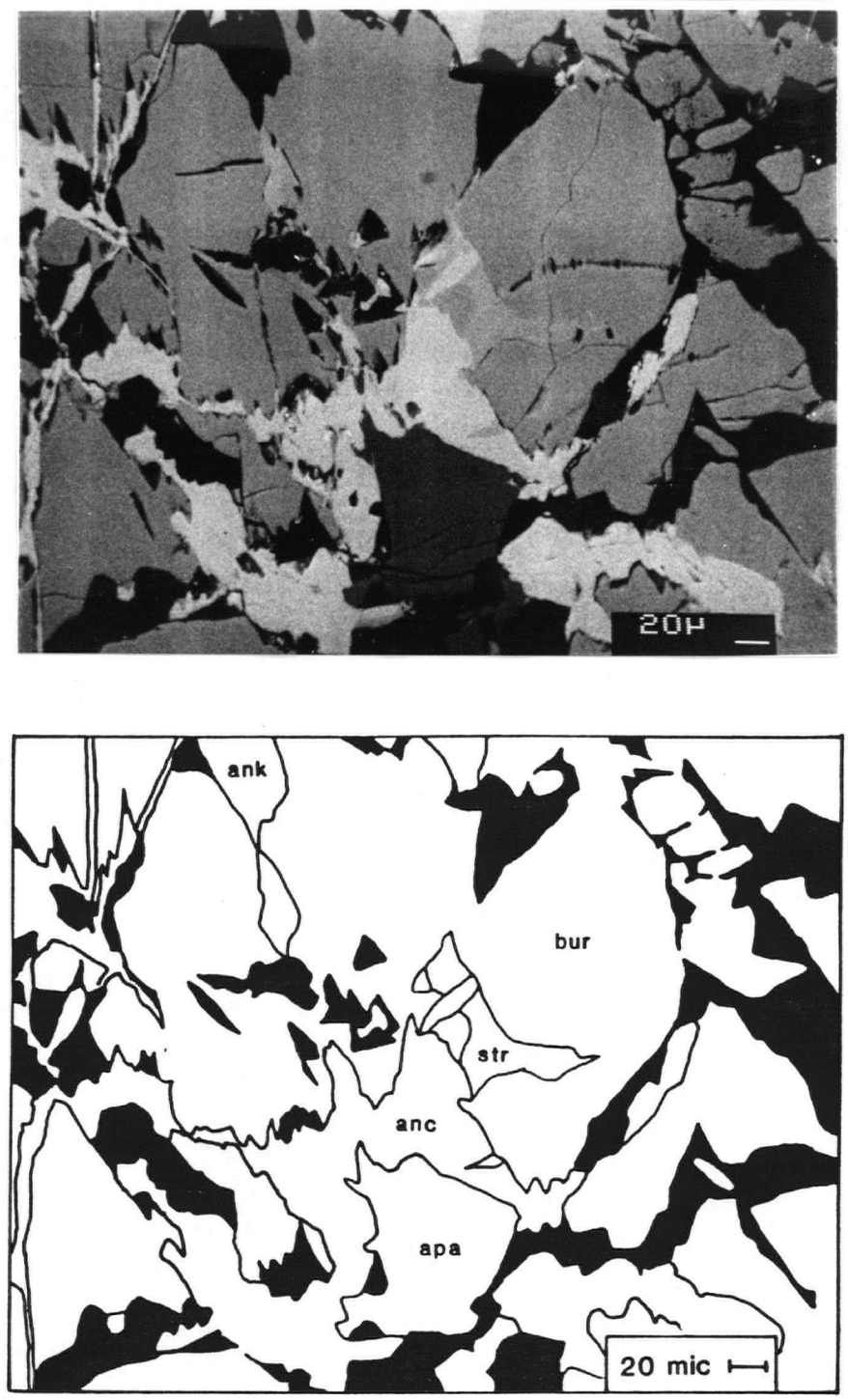

Figure 27: Back scattered electron image of REE-carbonate assemblage (MR-143B). anc = ancylite; apa = apatite; ank = ankerite; bur = burbankite; str = strontianite; black areas = holes

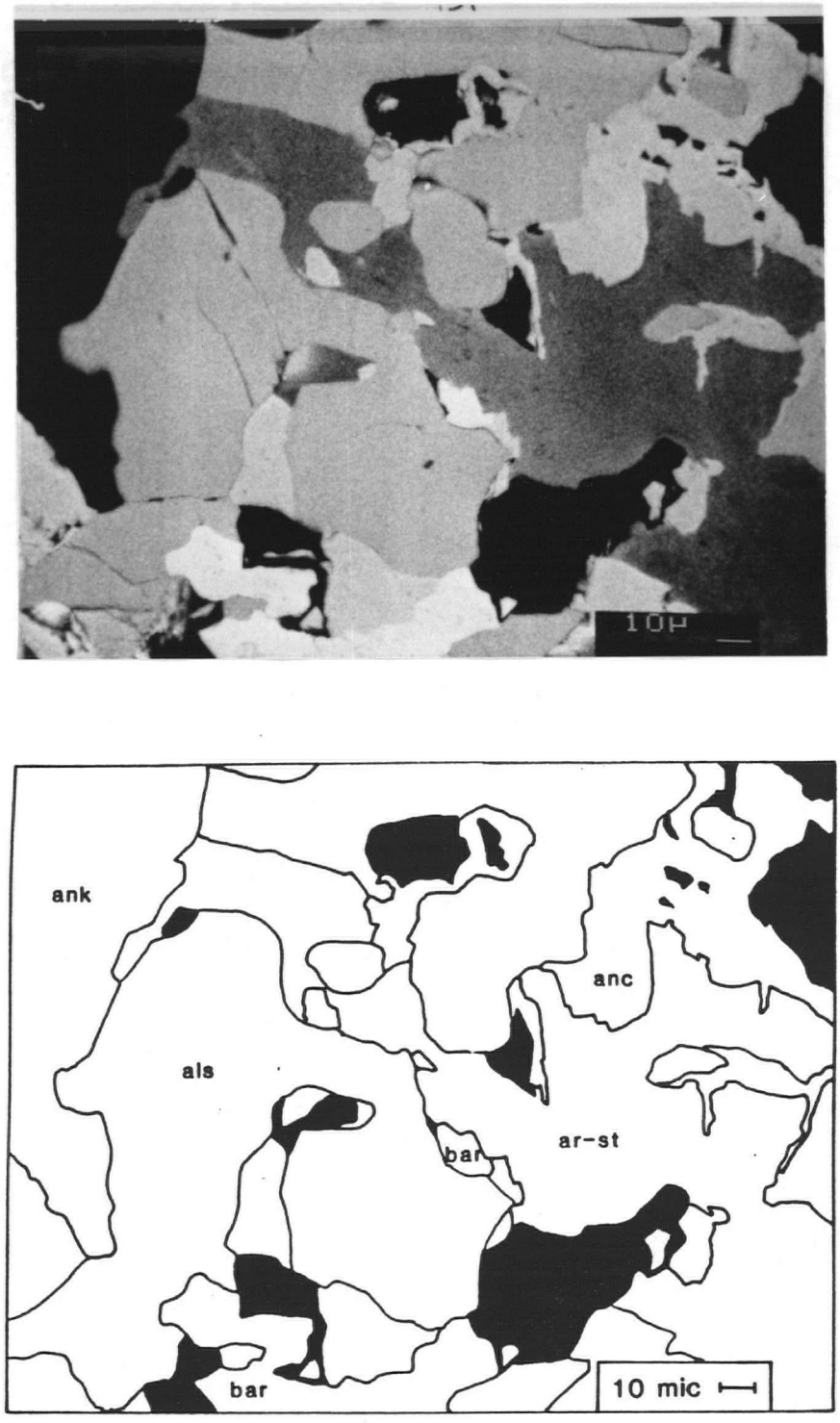

Figure 28: Back scattered electron image of REE-carbonate assemblage (MR-572A). anc = ancylite; als = alstonite; ank = ankerite; ar-st = aragonite - strontianite solid solution; bar = barite; black areas = holes

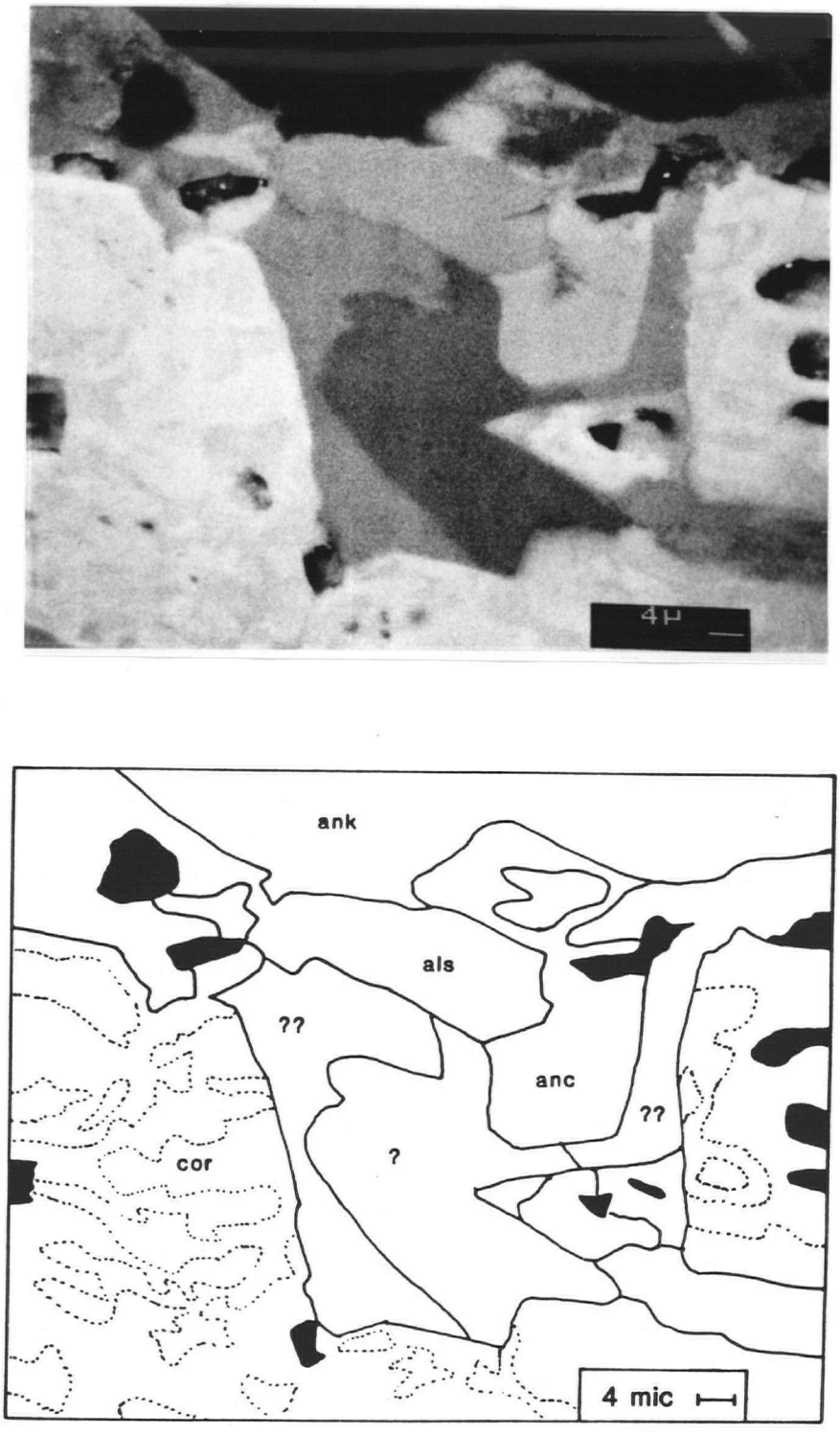

Figure 29: Back scattered electron image of REE-carbonate assemblage (MR-572A). anc = ancylite; als = alstonite; ank = ankerite; cor = cordylite; ? = Ca>>Sr>Ba,Ce,La; ?? = Sr,Ca,Ba; black areas = holes

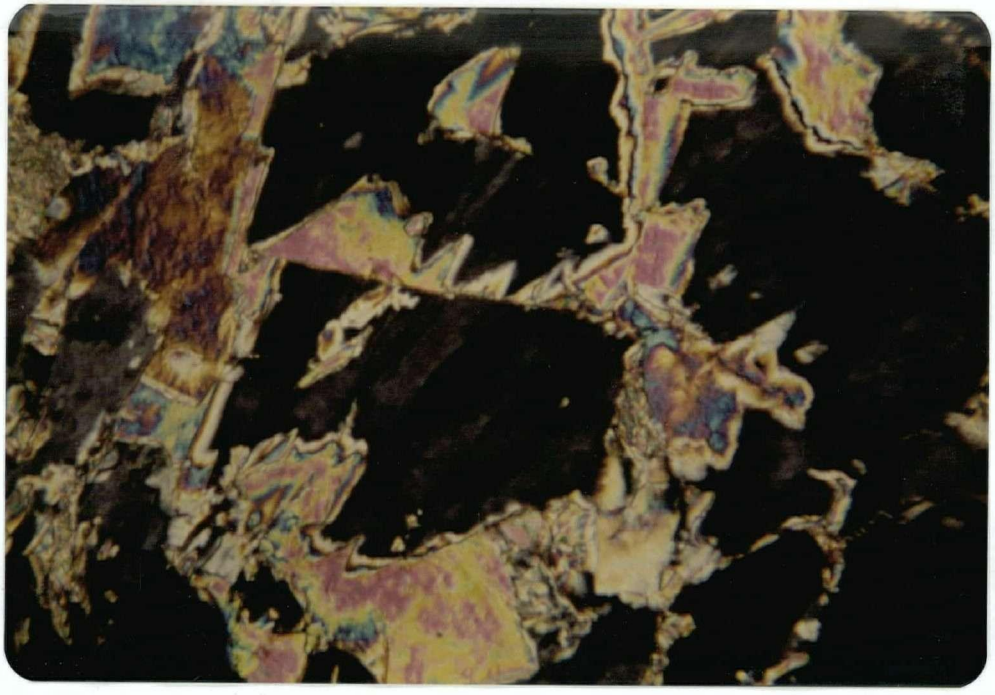

Figure 30: Photomicrograph of burbankite (grey) and alteration assemblage (MR-572A)

Figure 31: Photograph of rare-earth aggregates (predominantly burbankite) in rare-earth carbonatite dike of the north ridge.

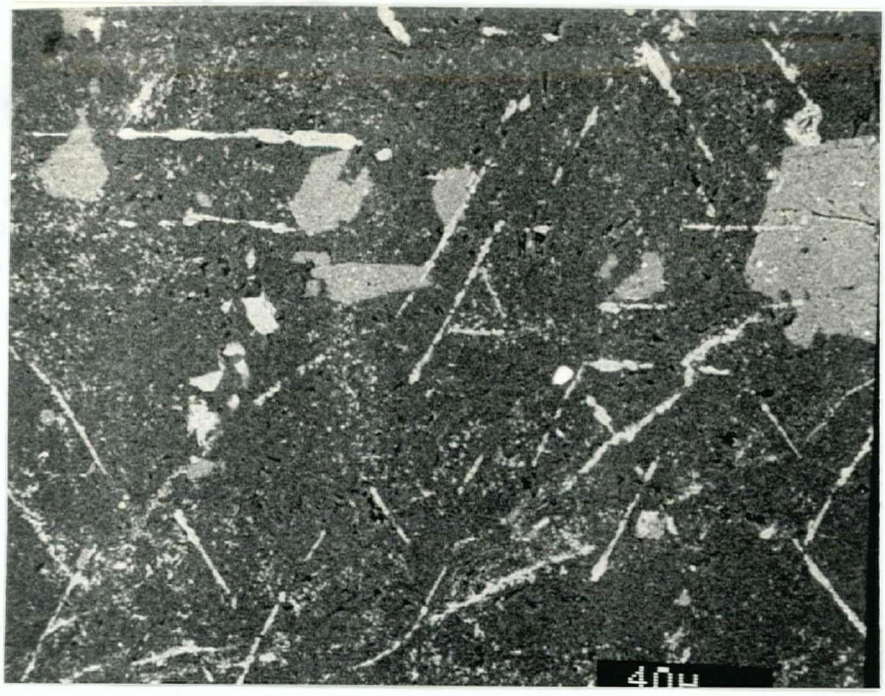

Figure 32: Back-scattered electron image of dolomite (dark) with rutile lamellae (bright needles). Medium grey phase is apatite. Very bright spots are monazite and thorianite (MR-710)

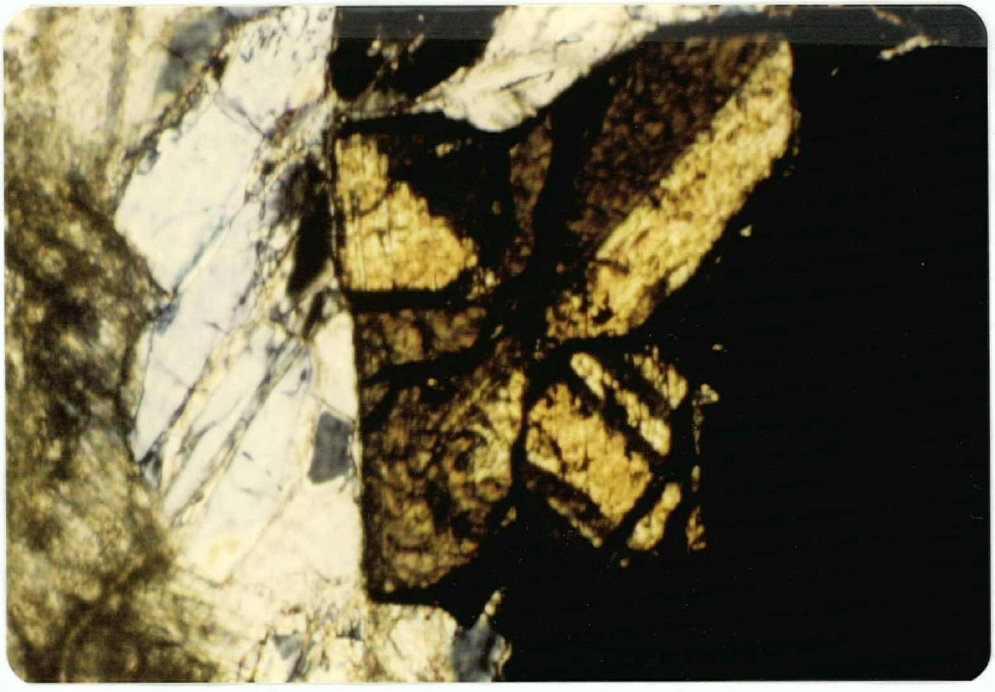

Figure 33: Photomicrograph of twinned baddeleyite

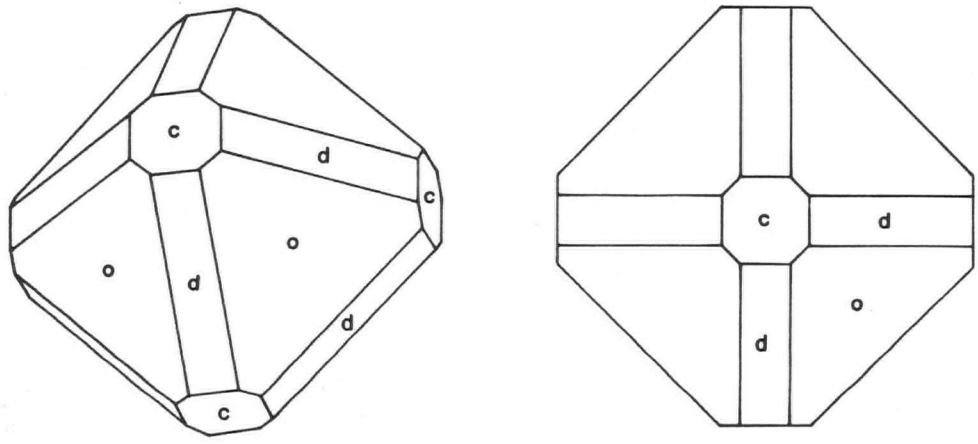

Figure 34: Common habit of small pyrochlore crystals. c = cube, o = octahedron, d = rhombic dodecahedron

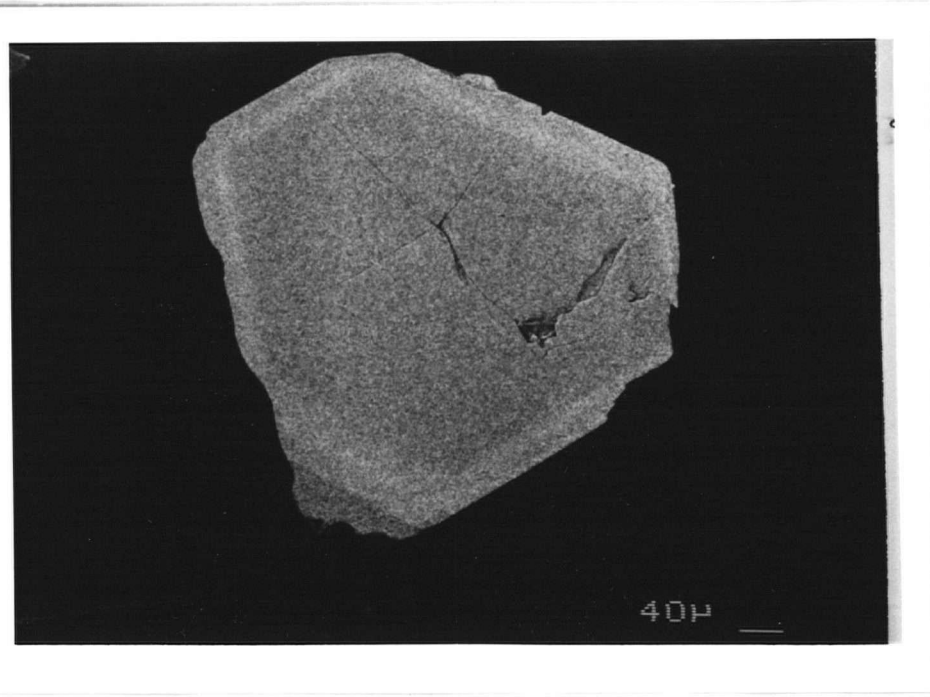

Figure 35: Back-scattered electron image of zoned pyrochlore grain (MR-85-5-D)

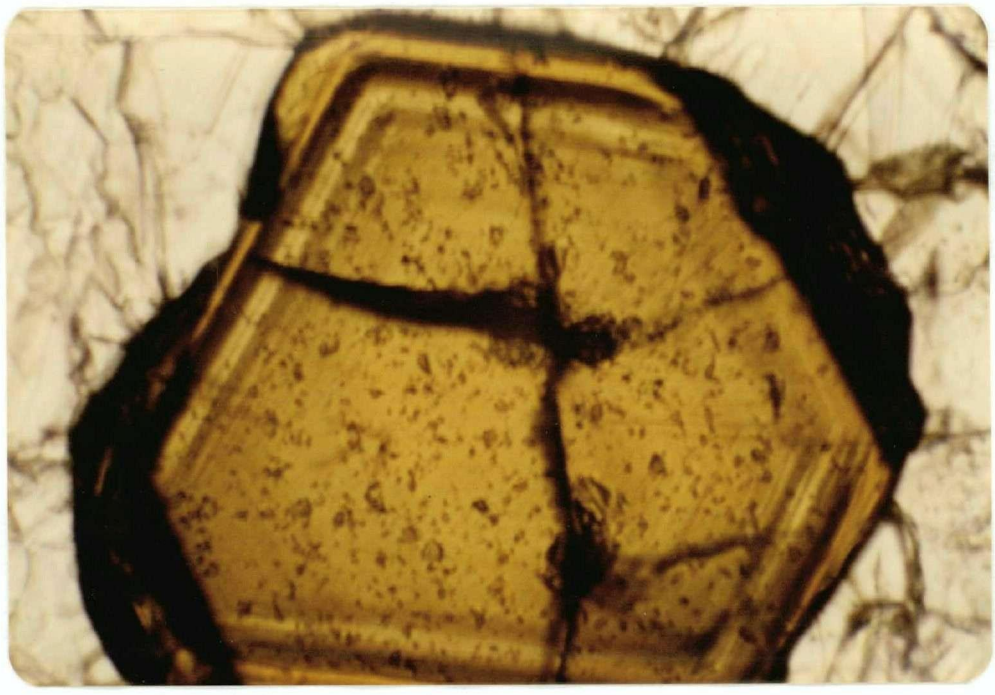

Figure 36: Photomicrograph of zoned pyrochlore under plane polarized light (MR-85-2-JI)

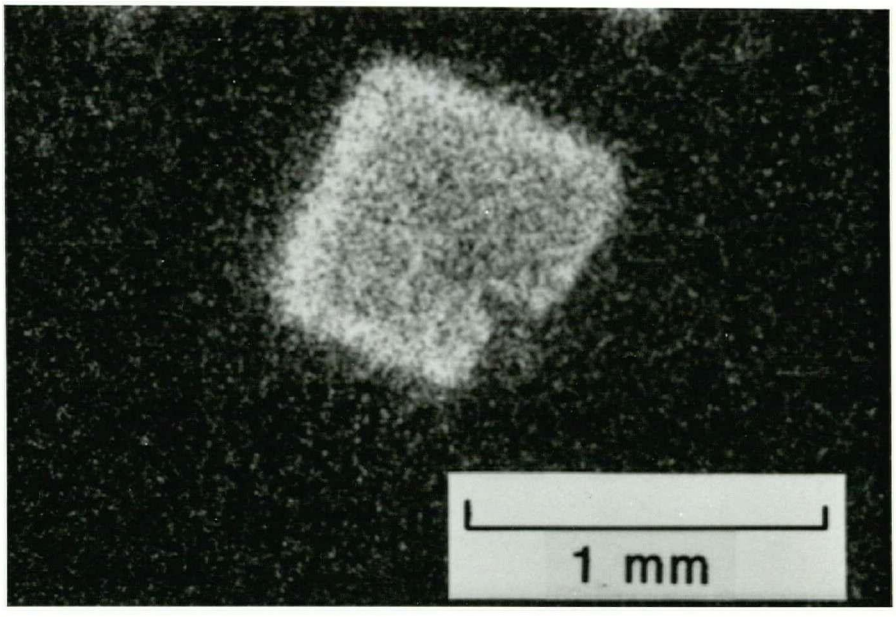

Figure 37: Autoradiograph of zoned pyrochlore.

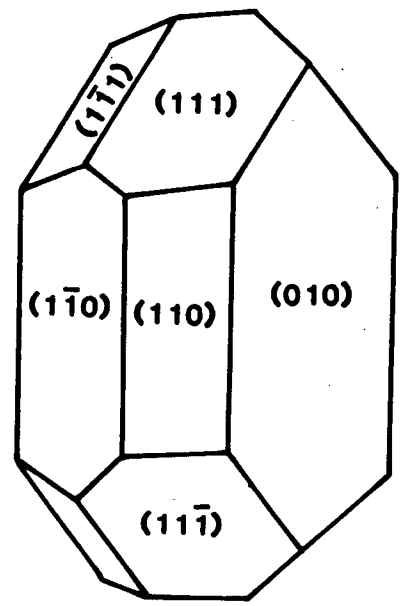

Figure 38: Habit of primary fersmite (after P.C. LeCouteur, Cominco Ltd.)

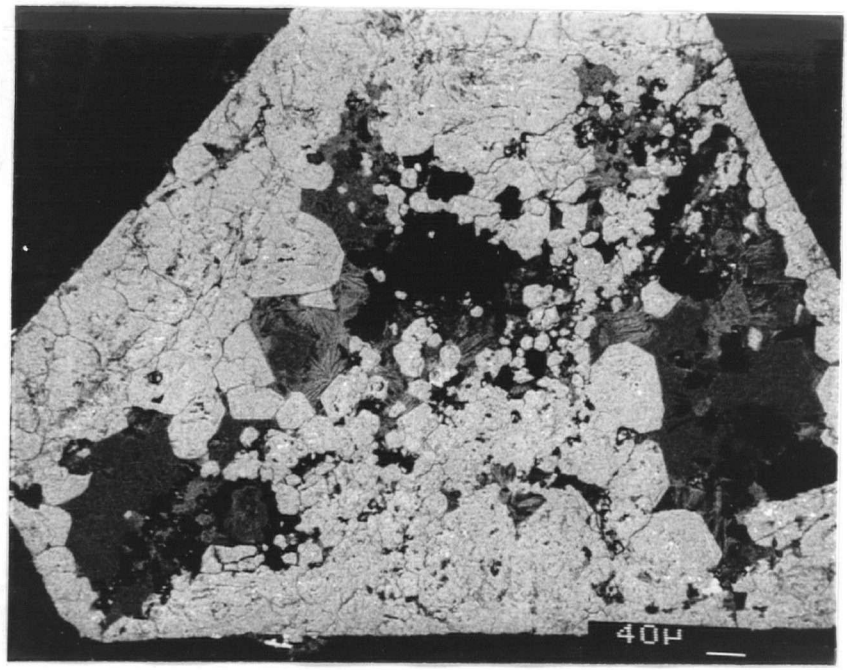

Figure 39: Back-scattered electron image of fersmite (bright phase) replacing euhedral pyrochlore

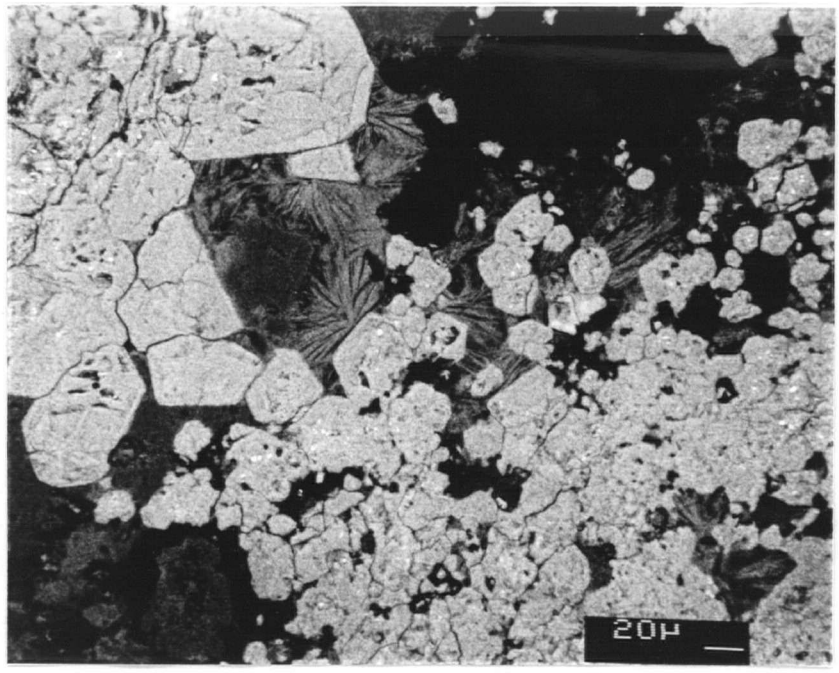

Figure 40: Detail of figure 39. Radiating textured phase is a Nb-oxide (possibly fersmite with a different composition)

Figure 41: Photomicrograph of micro-syenite xenolith with anomalous blue arfvedsonite (crossed nicols) (MR-301I)

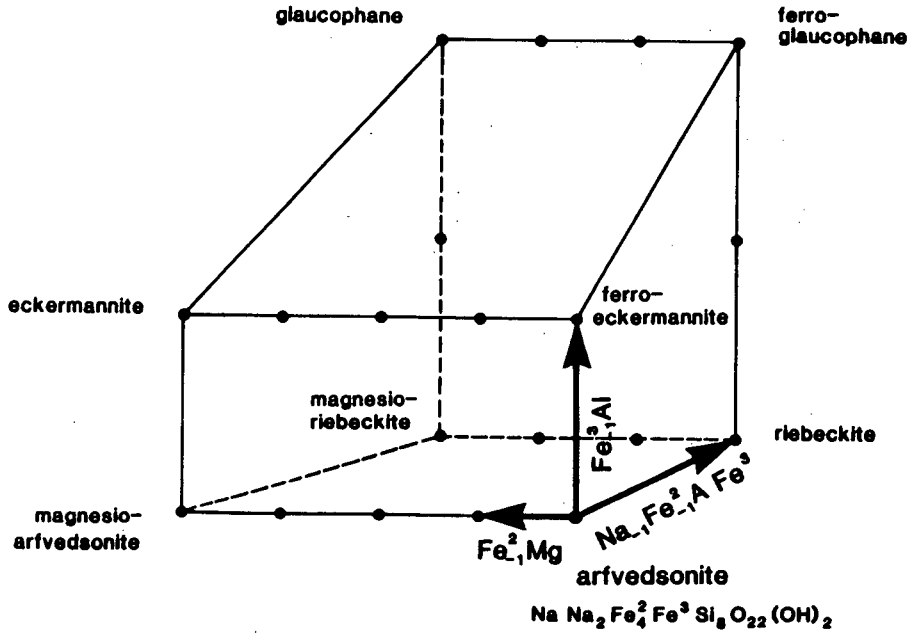

Figure 42: Composition space for sodic amphiboles (classification after Hawthorne (1981))

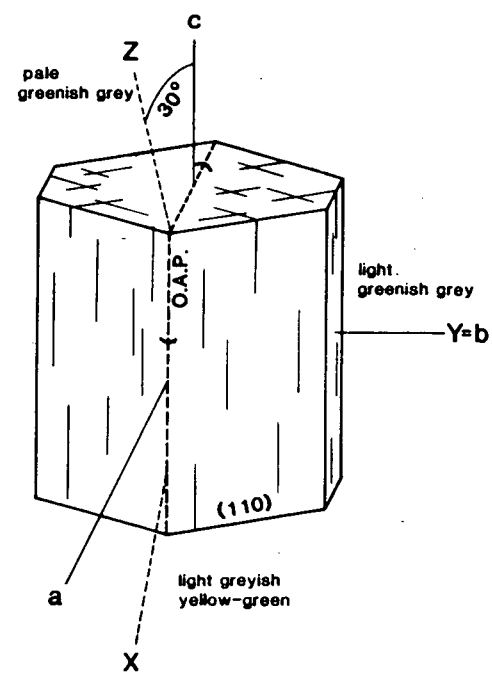

Figure 43: Block diagram with optical properties for magnesio - arfvedsonite (MR 533)

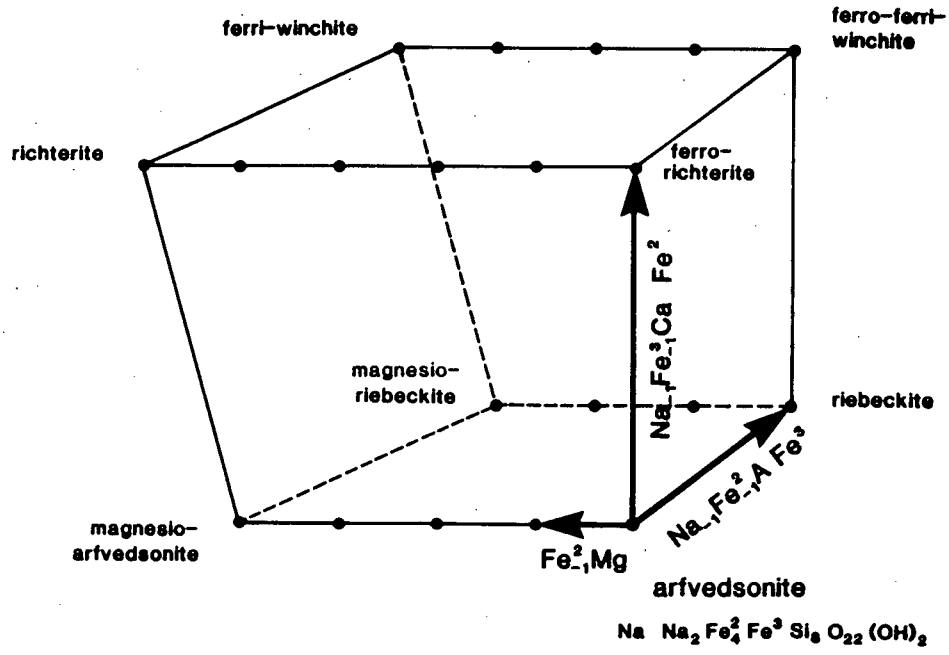

Figure 44: Composition space for sodic-calcic amphiboles (classification after Hawthorne (1981))

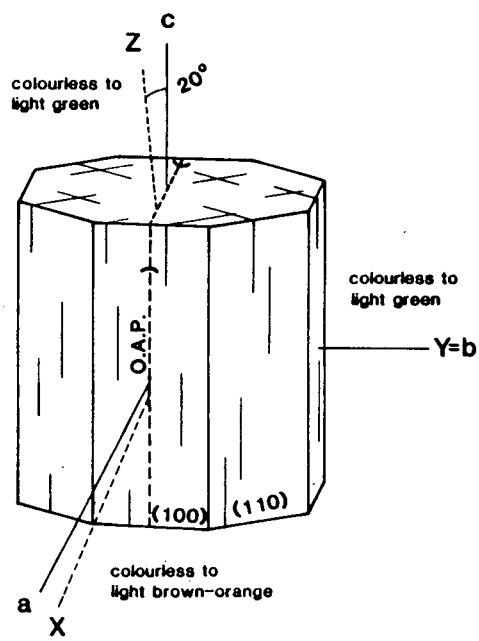

Figure 45: Block diagram with optical properties for richterite (MR-398)

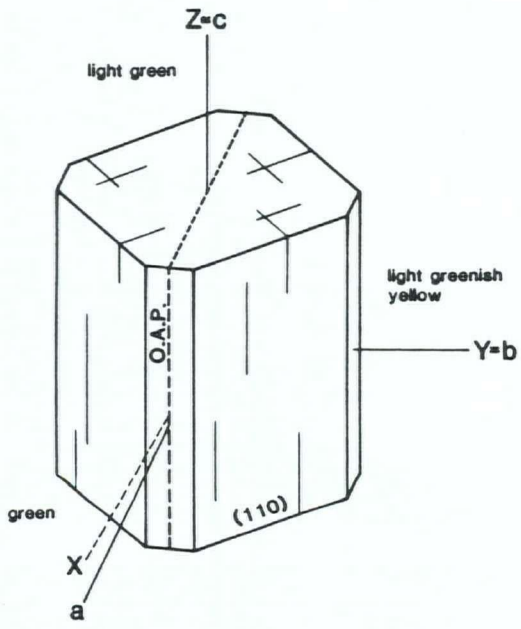

Figure 46: Block diagram with optical properties for aegirine (MR-533)

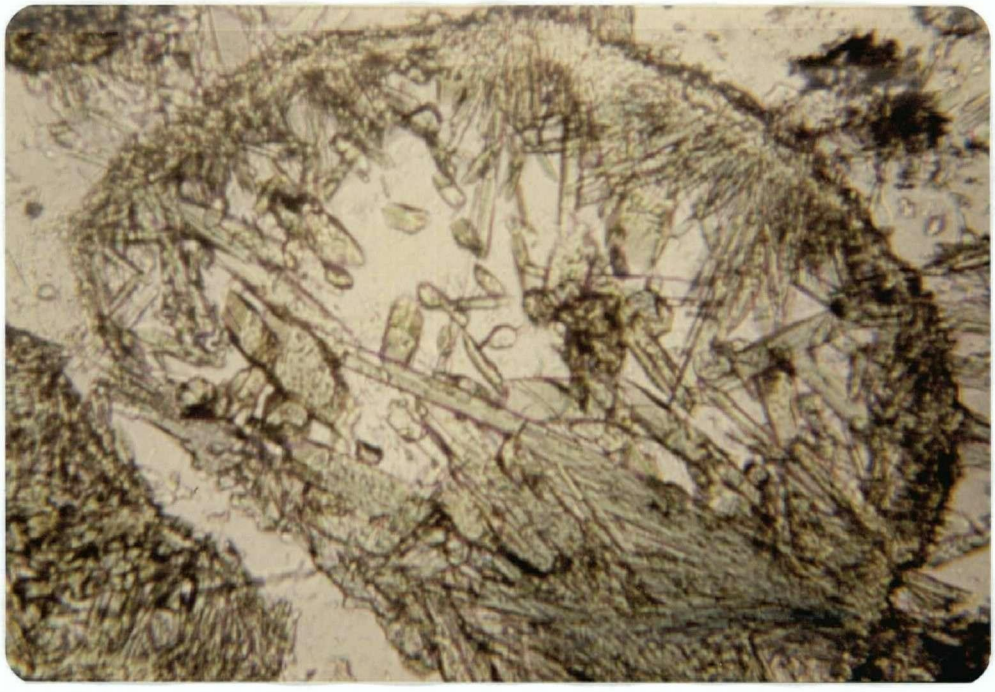

Figure 47: Photomicrograph (plane polarized light) of syenite with globular texture. Globule contains acicular aegirine (green), albite and calcite (high relief)

EDS-271 (MR-85-5-I) ***dolomite*** dolomite carbonatite

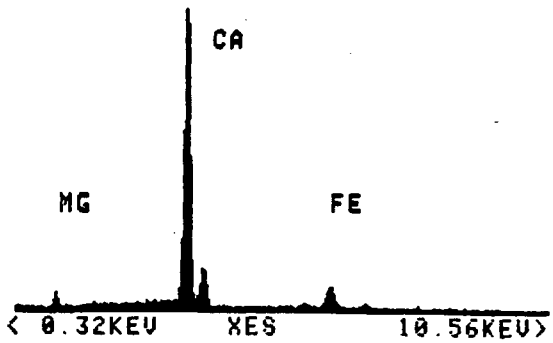

EDS-100 (MR-572A) ***dolomite*** rare-earth carb. dike

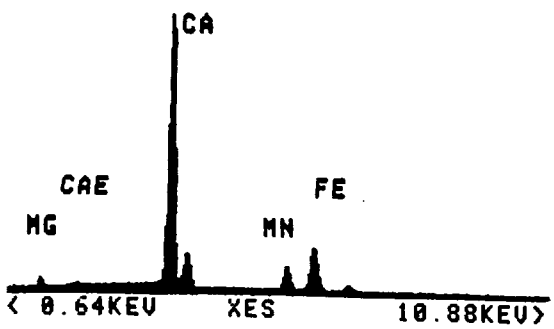

EDS-228 (MR-85-5-J) ***calcite*** calcite carbonatite

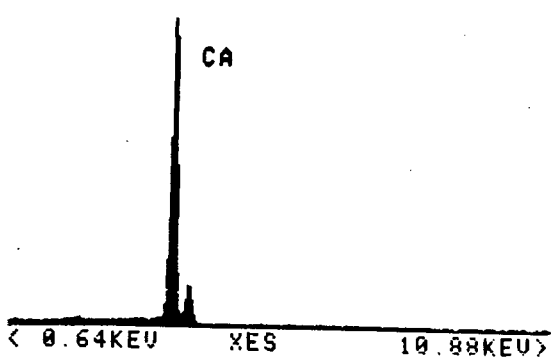

EDS-24 (MR-143B) ***strontianite*** rare-earth carb. dike

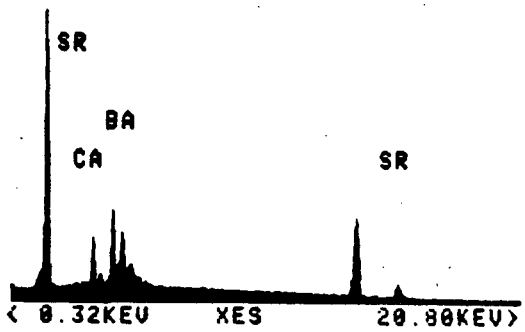

EDS-136 (MR-572A) ***alstonite*** rare-eart carb. dike

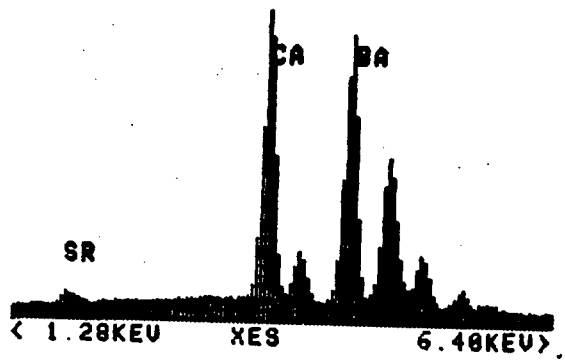

EDS-131 (MR-572A) ***aragonite-strontianite ss*** rare-earth carb. dike

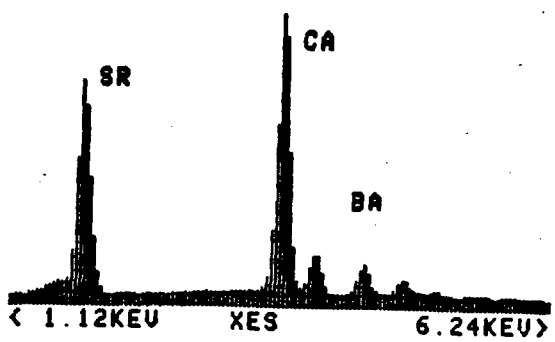

EDS-112 (MR-572A) ***Sr-Ca-Ba Carbonate*** rare-earth carb. dike

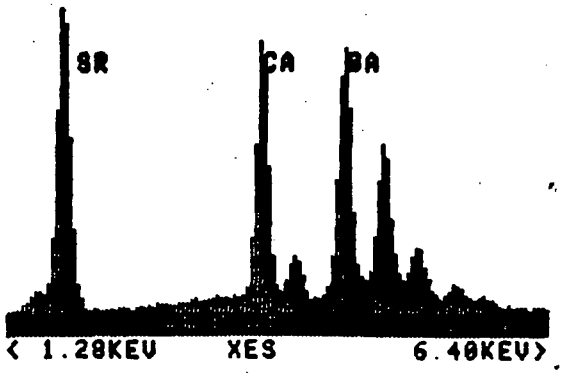

EDS-21 (MR-143B) ***burbankite*** rare-earth carb. dike

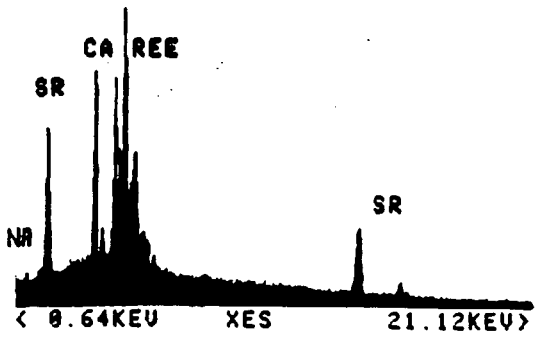

EDS-139 (MR-572A) ***ancylite*** rare-earth carb. dike

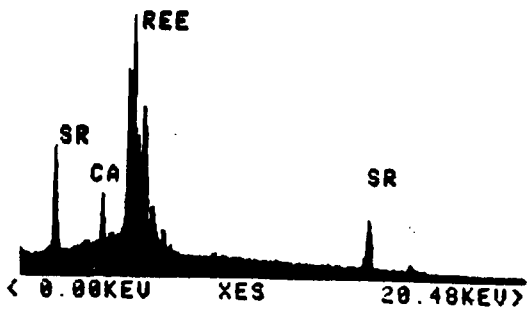

EDS-115 (MR-572A) ***cordylite*** rare-earth carb. dike

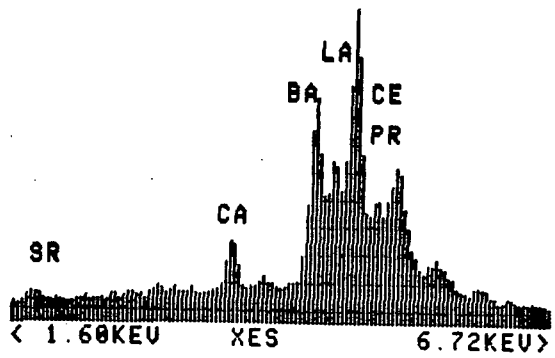

EDS-8 (MR-312) ***huanghoite*** rare-earth dolomite carb.

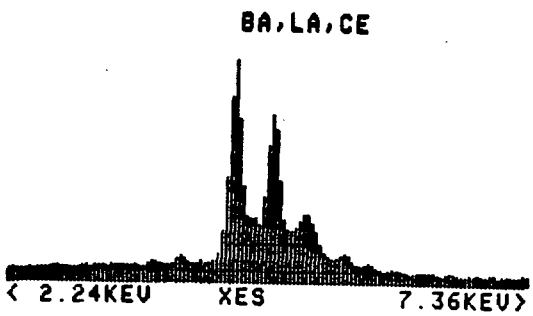

EDS-123 (MR-572A) ***Ce-Ba-La-Ca carbonate*** rare-earth carb. dike

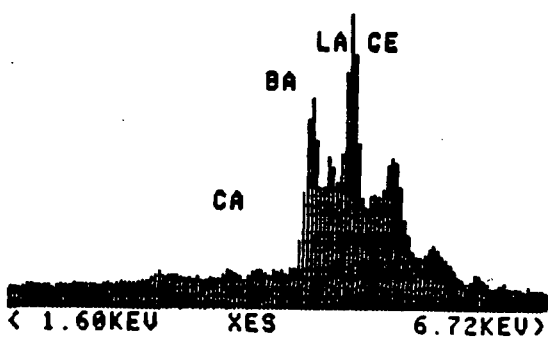

EDS-212 (MR-503) ***Ca-La-Nd carbonate*** rare-earth carb. dike

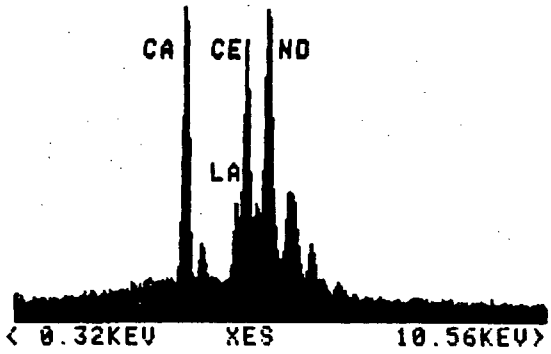

EDS-242 (MR-500) ***LREE carbonate*** contact aureole

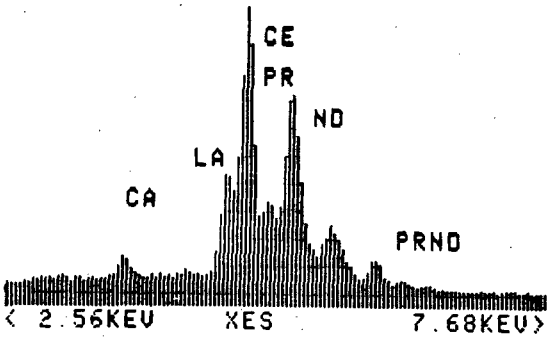

EDS-238 (MR-85-2-J) ***Ca-Sr-Ba-Ce carbonate*** calcite carbonatite

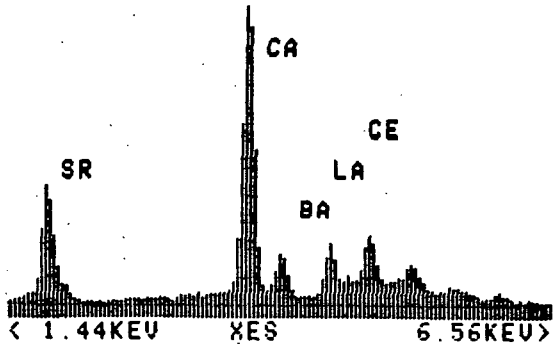

EDS-19 (MR-143B) ***apatite*** rare-earth carb. dike

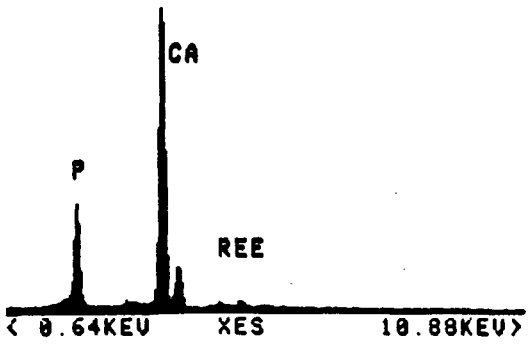

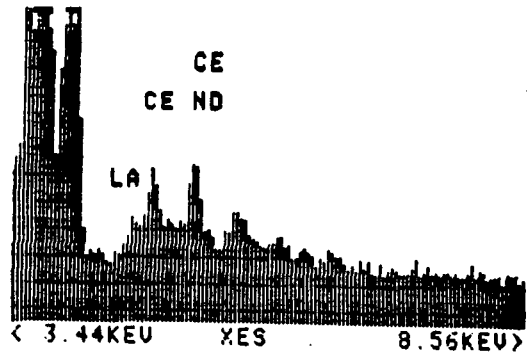

EDS-227 (MR-85-2-J) ***apatite*** calcite carbonatite

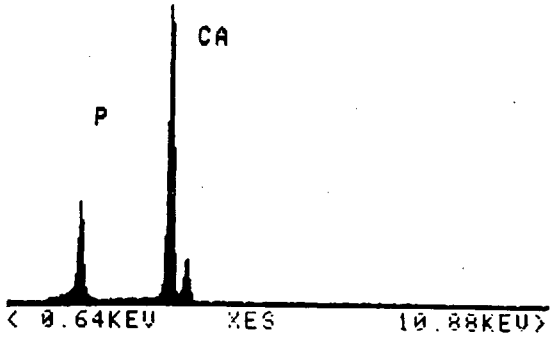

EDS-79 (MR-417) ***monazite*** dolomite carbonatite

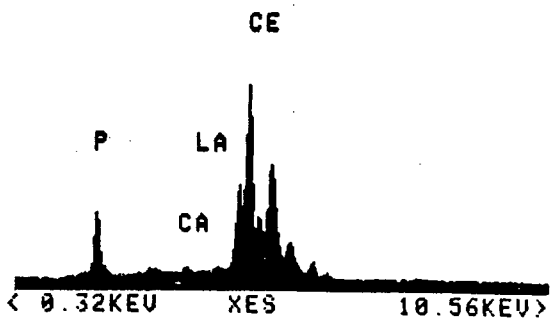

EDS-2 (MR-710) ***monazite*** dolomite carbonatite

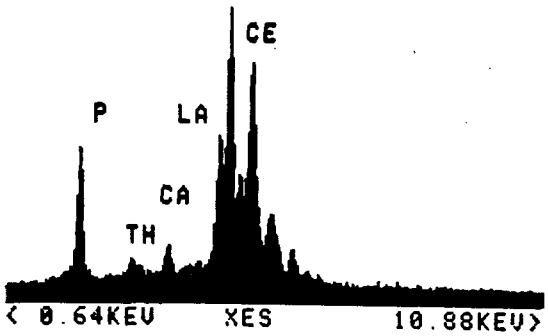

EDS-15 (MR-710) ***cheralite*** dolomite carbonatite

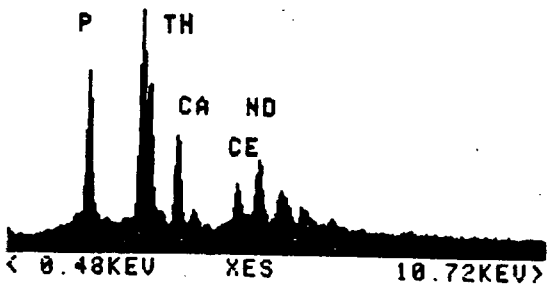

EDS-12 (MR-395II) ***rutile*** dolomite carbonatite

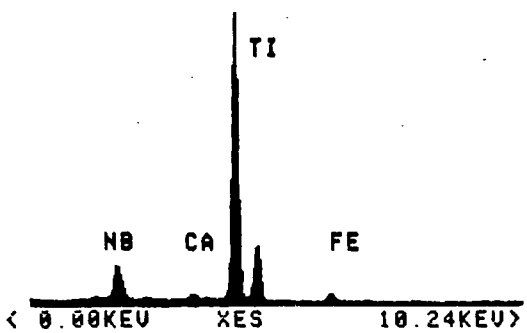

EDS-180 (MR-365) ***magnetite*** calcite carbonatite

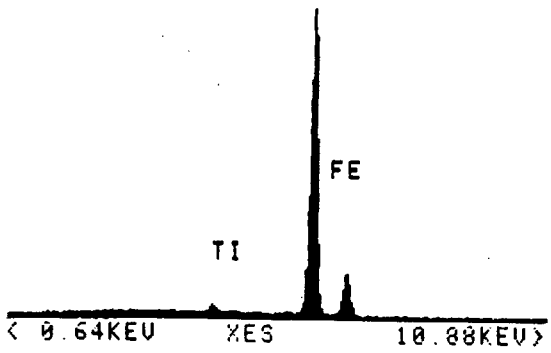

EDS-172 (MR-317) ***magnetite*** calcite carbonatite

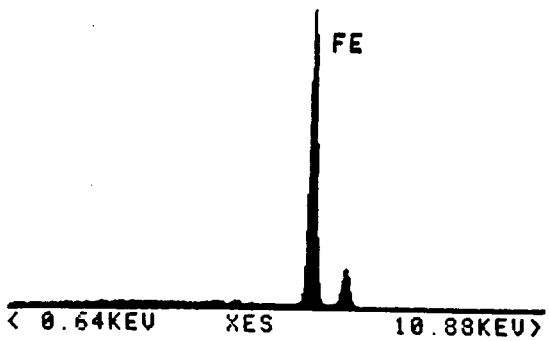

EDS-165 (MR-310) ***baddeleyite*** calcite carbonatite

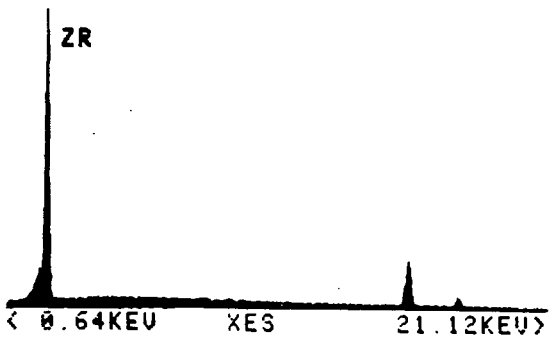

EDS-224 (MR-85-2-J) ***pyrochlore (rim)*** calcite carbonatite

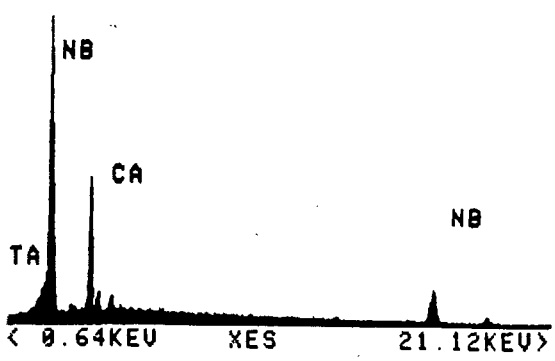

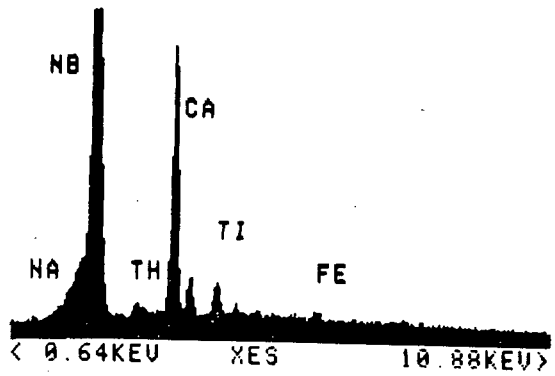

EDS-225 (MR-85-2-J) ***pyrochlore (core)*** calcite carbonatite

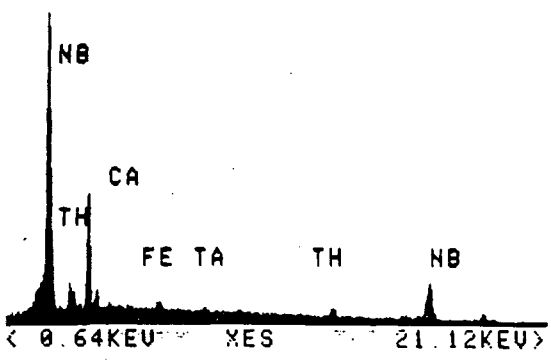

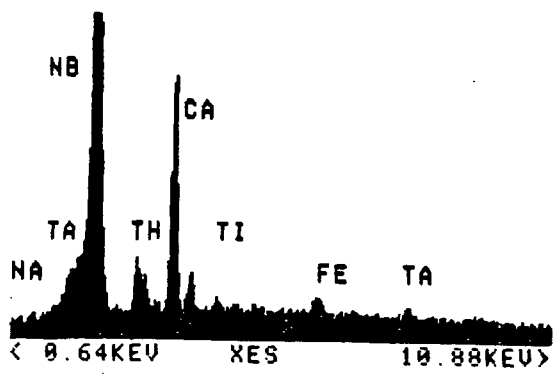

EDS-278 (MR-85-5-D) ***pyrochlore (rim)*** calcite carbonatite

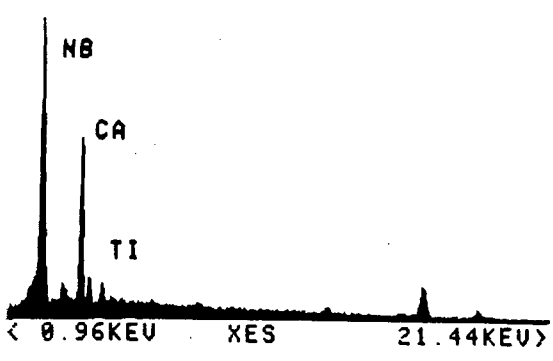

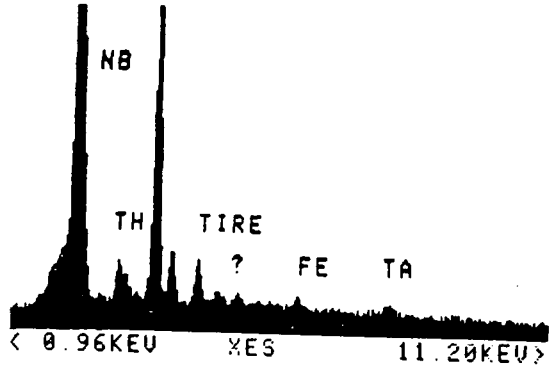

EDS-277 (MR-85-5-d) ***pyrochlore (core)*** calcite carbonatite

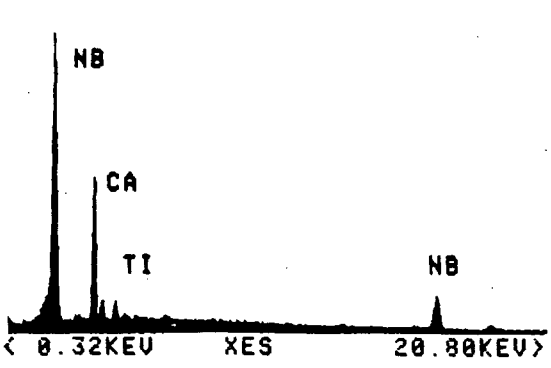

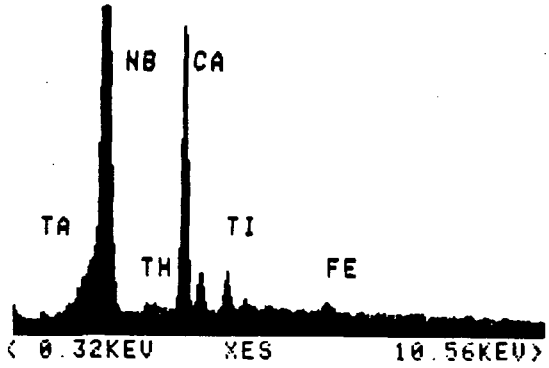

EDS-267 (MR-85-5-I) ***fersmite*** dolomite carbonatite

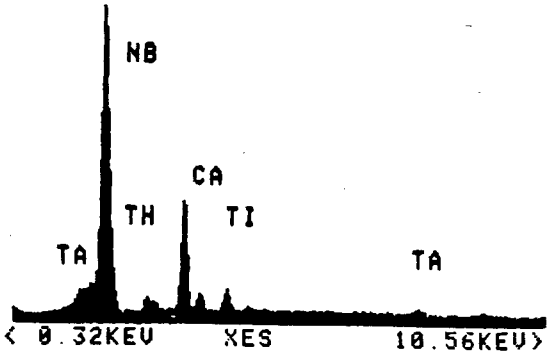

EDS-70 (MR-417) ***fersmite*** dolomite carbonatite

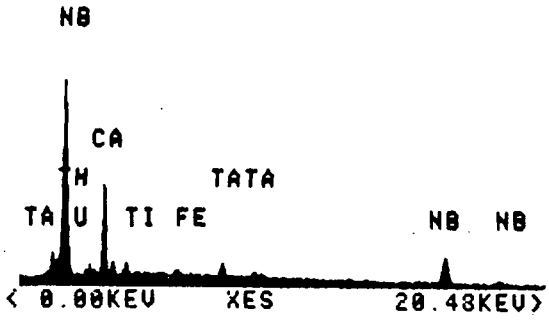

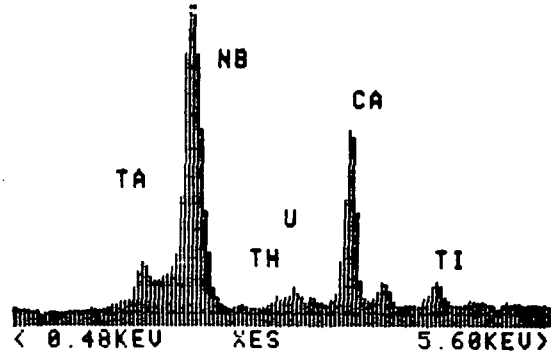

EDS-7 (MR-710) ***columbite*** dolomite carbonatite

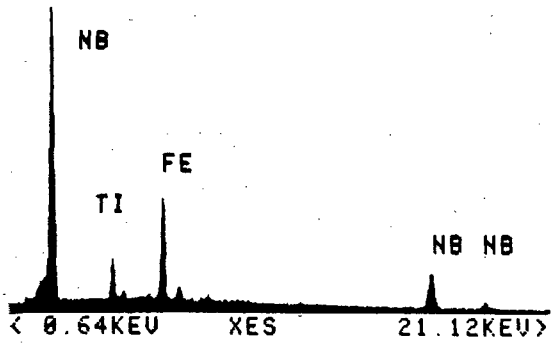

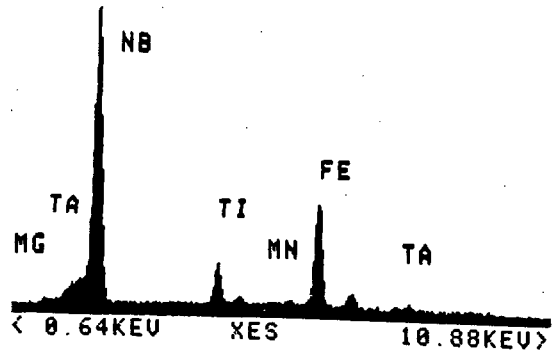

EDS-151 (MR-310) ***zirkelite*** calcite carbonatite

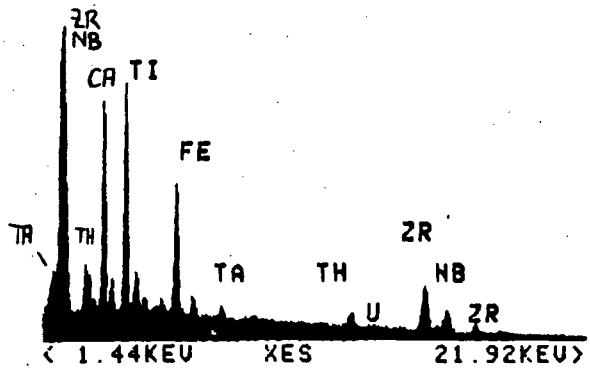

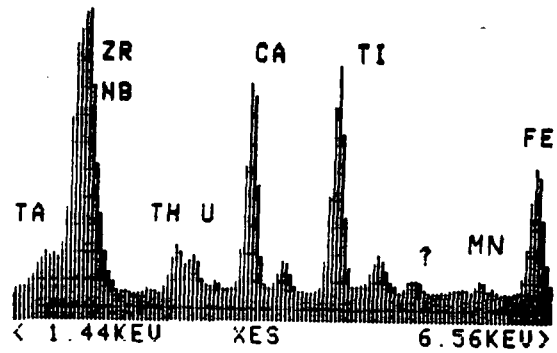

EDS-72 (MR-417) ***Ta-Ca zirconate-niobate*** dolomite carbonatite

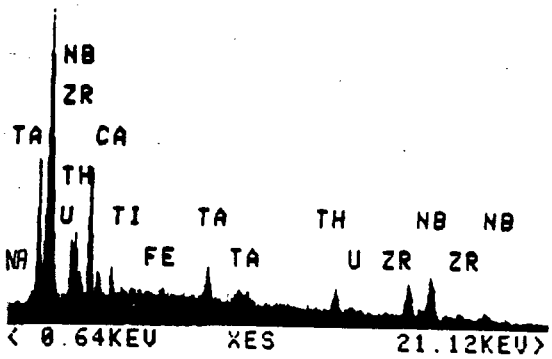

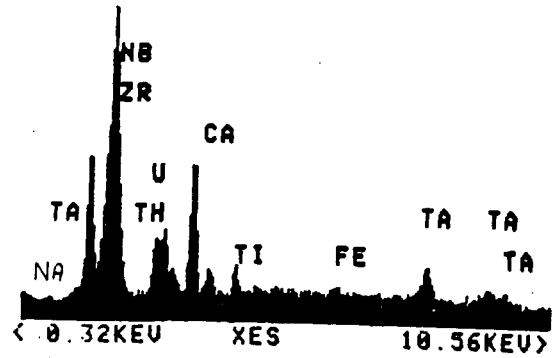

EDS-50 (MR-533I) ***albite*** syenite

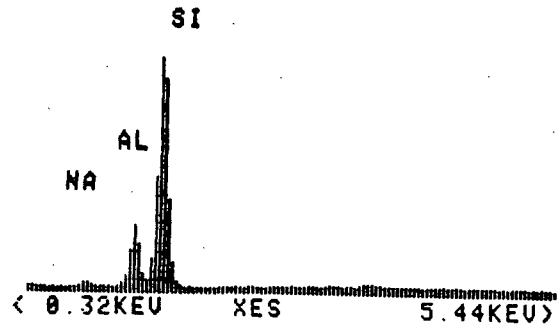

EDS-259 (MR-301I) ***alkali feldspar*** syenite

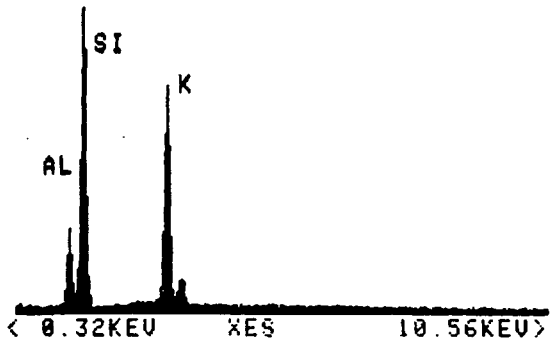

EDS-81 (MR-417) ***chlorite*** dolomite carbonatite

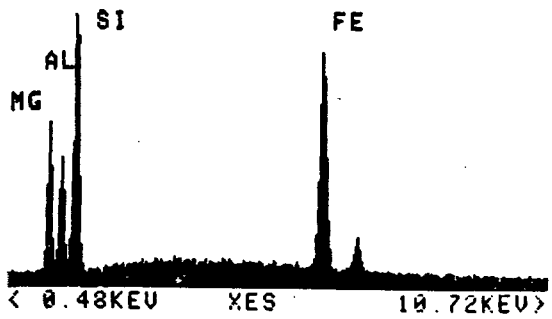

EDS-77 (MR-412E) ***biotite*** Ospika diatreme

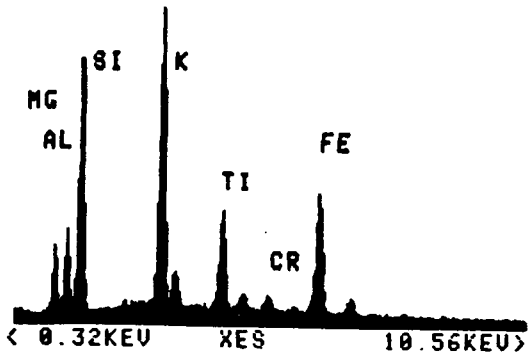

EDS-223 (MR-85-2-J) ***biotite (rim)*** calcite carbonatite

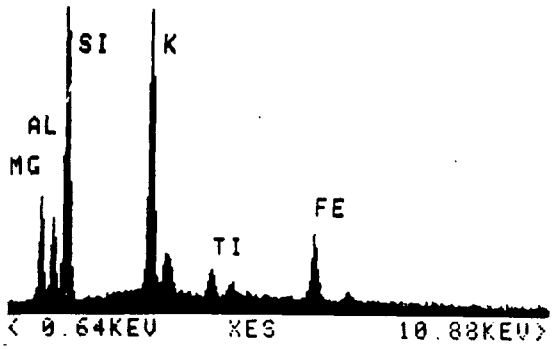

EDS-222 (MR-85-2-J) ***biotite*** calcite carbonatite

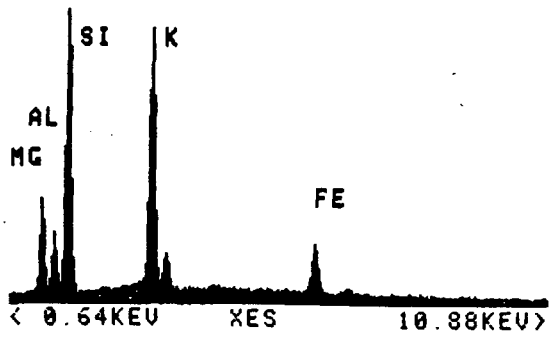

EDS-54 (MR-533) ***magnesio-arfvedsonite*** syenite

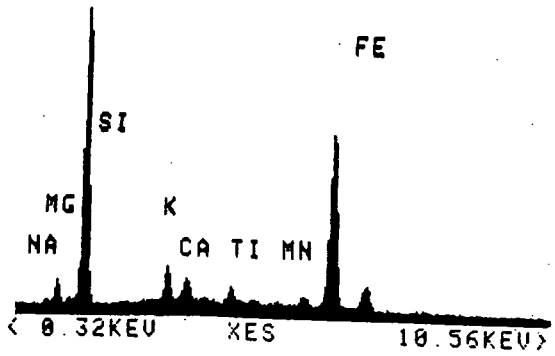

EDS-95 (MR-316) ***magnesio-arfvedsonite*** syenite

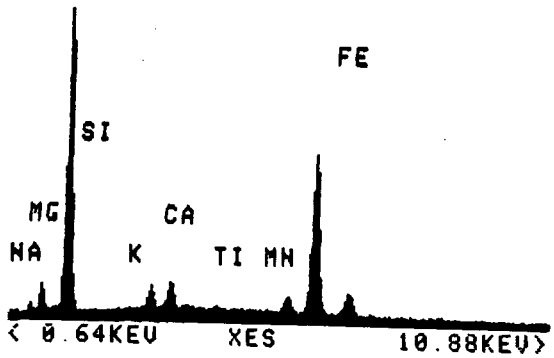

EDS-11 (MR-535) ***richterite*** calcite carbonatite

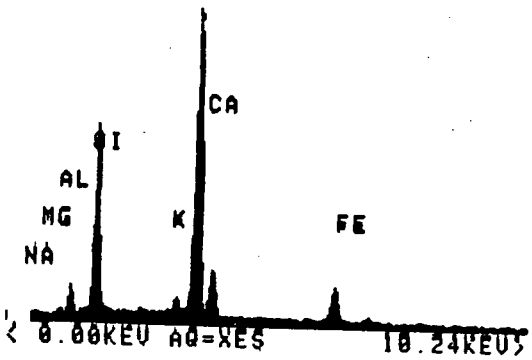

EDS-68 (MR-533) ***aegirine*** syenite

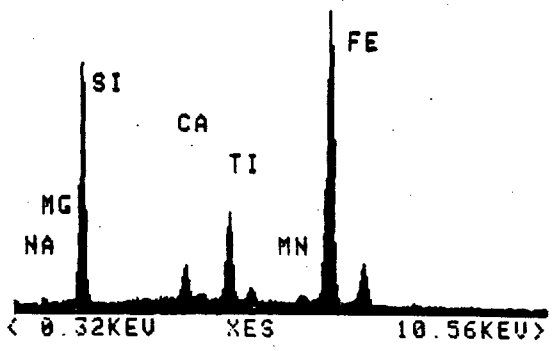

EDS-88 (MR-316) ***aegirine*** syenite

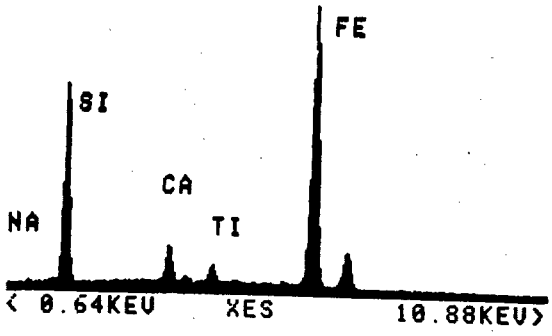

EDS-255 (MR-301I) ***lorenzenite*** syenite

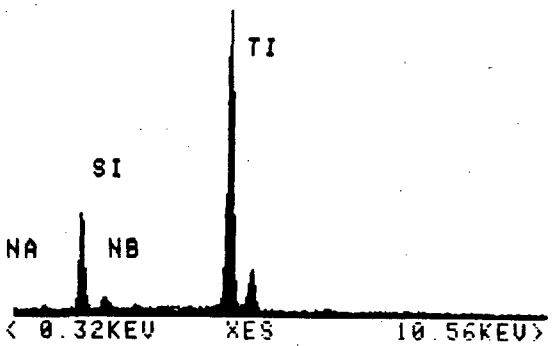

EDS-78 (MR-417) ***thorite*** dolomite carbonatite

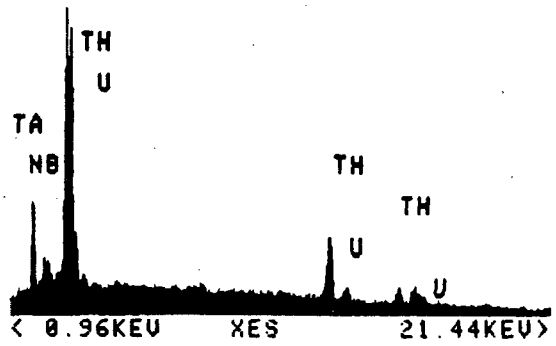

EDS-201 (MR-524) ***cerite*** contact aureole

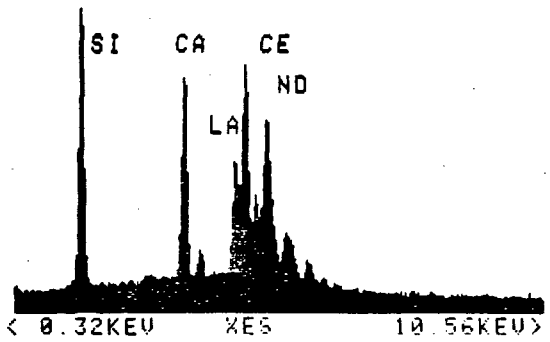

EDS-3 (MR-412H) ***Cr-diopside*** Ospika diatreme

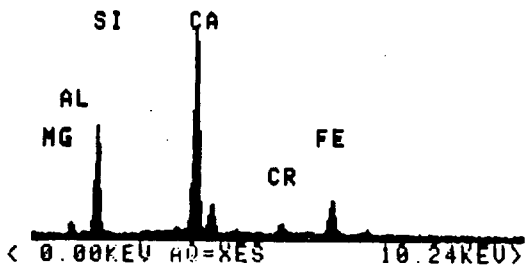

EDS-4 (MR-412B) ***augite*** Ospika diatreme

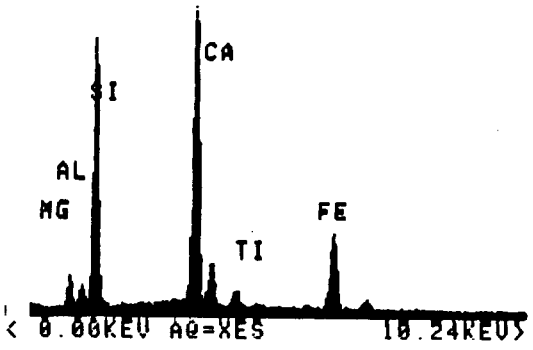

EDS-211 (MR-503) ***barite*** rare-earth carb. dike

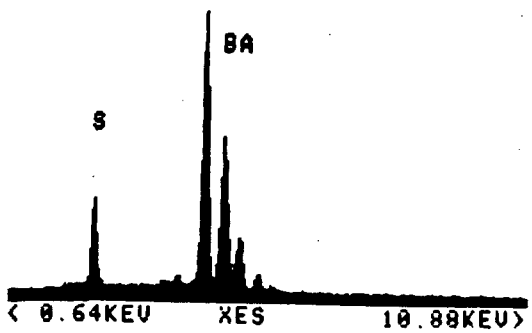

APPENDIX B: X-RAY FLUORESCENCE ANALYSES

CAUTIONARY NOTES

There are more pitfalls in the XRF-analyses of carbonatites than one might expect. The unusual chemical composition and physical properties of carbonatite samples produce a number of unavoidable problems which make X-ray analysis tedious:

Carbonatite samples are tough to mill, produce a large amount of dust and stick tenaciously to the walls of any mill.

One should start with plenty of sample to produce fused disks because the loss on ignition may be as high as 45 wt%.

The various metal oxides commonly present in carbonatites do not fuse easily and any slag may disturb the surface being analysed.

Non-silicate glasses tend to crack upon cooling.

Some "major" elements (Si, Al, K) may be minor elements in carbonatites and vice versa (P, Ba, Sr, REE) which can lead to unnoticed overlap of fluorescence peaks if "standard" procedures are followed.

Available standards are directed towards the analysis of silicate rocks and cover too small a range of concentrations (major elements and trace elements).

Existing data reduction programs may not be flexible enough to handle carbonatite compositions.

FLUORESCENCE PEAK OVERLAPS

Table 20 lists all the possible overlaps pertinent to carbonatite rock analysis. It is necessary to scan the 2Θ-range of interest in order to decide whether corrections must be performed. On automated equipment correction pellets should

be run in any case, or correction factors might be used during data reduction instead.

CONSIDERATIONS FOR CARBONATITE ROCK ANALYSIS

The following considerations must be included in setting up routine procedures for carbonatite rock analysis.

1. Spiked standards based on a carbonate matrix (Ca, Mg, Fe, P) must be prepared for a wide range of compositions.

2. Correction pellets are needed to resolve the possible peak overlaps (cf. table 20).

3. The major elements of low atomic number (Al and lighter) are best analyzed on fused disks.

4. Carbonatite samples need long fusion times in a furnace and disks must be cooled very slowly on a heated casting dish to avoid cracking.

5. Data reduction programs for major elements for calculation of mass attenuation coefficients must be flexible to handle different sets of major elements, ie. a subset of Si, Al, Ti, Fe, Mn, Mg, Ca, Na, K, P, S, Sr, Ba, REE, Nb, C, H, O.

6. Peak positions for background readings must be determined carefully.

7. Well-characterized standards of natural carbonatite would be desirable.

SAMPLE PREPARATION

In this study, samples were cleaned, crushed and split in the field camp using a standard jaw crusher to obtain grain sizes smaller than 10 mm in two subsequent runs. Splits were further processed at the University of British Columbia using a tungsten-carbide mill with grinding times betwen 40 and 200 seconds.

Element	Line	Order	Intensity	2θ	Comments
P	$K\alpha_{1,2}$	1	150	89.56°	
Ca	$K\beta_{1,3}$	2	15	89.96°	discrimination possible
Mg	$K\alpha_{1,2}$	1	150	45.17°	
Ca	$K\alpha_{1,2}$	3	3	46.08°	discrimination possible
Ti	$K\alpha_{1,2}$	1	150	86.14°	
Ba	$L\alpha_{1}$	1	100	87.17°	only if Ba high and Ti low
Pr	$L\alpha_{1}$	1	100	75.42°	
La	$L\beta_{1}$	1	50	75.28°	correction pellet
Ba	$L\alpha_{1}$	1	100	87.17°	
Pr	Ll	1	2	87.49°	only if Ba low and LREE high
Ti	$K\alpha_{1,2}$	1	150	86.14°	discrimination possible
V (Cr)	$K\alpha_{1,2}$	1	150	76.94°	
Ti	$K\beta_{1}$	1	20	77.27°	correction pellets
Ba	$L\beta_{3}$	1	6	77.36°	Cr-V not possible if Ba high
Nb	$K\alpha_{1,2}$	1	150	21.40°	
Y	$K\beta_{1}$	1	16	21.20°	only if Y high
U	$L\beta_{2}$	1	20	21.60°	only if U high
Zr	$K\alpha_{1,2}$	1	150	22.55°	
Sr	$K\beta_{1}$	1	16	22.42°	correction pellets
Sr	$K\beta_{3}$	1	8	22.44°	correction pellets
Th	$L\beta_{4}$	1	4	22.70°	only if Th high
Th	$L\beta_{4}$	1	20	22.73°	only if Th high
Y	$K\alpha_{1,2}$	1	150	23.80°	
Rb	$K\beta_{1}$	1	16	23.75°	only if Rb low
Rb	$K\alpha_{1,2}$	1	150	26.62°	
U	$L\alpha_{2}$	1	10	26.49°	only if U high and Rb present

Table 20: List of possible Peak overlaps. Elements to be analyzed are printed bold, interfering elements are in light print. Intensities are comparative within the same line series only.

Samples were split repeatedly to fill 50 ml glass vials. The final grinding was done in an automated agate mortar under acetone.

Powder pellets were prepared using 5 g of sample with polyvinyl alcohol as a binder mantled by boric acid. Boric acid might react with carbonate samples if they contain too much binding liquid.

Table 21 lists all the samples processed with the bulk sample mass and the masses of splits during grinding stages.

X-RAY FLUORESCENCE ANALYSIS

The analyses were done with a Phillips PW 1410 X-ray spectrometer. Warm up time was determined to be approximately 2 hours and samples were run in one batch for the individual groups of elements to be measured with a particular X-ray tube. Standards were run before and after the unknowns and sometimes in between. Standard sample "G-2" (Abbey, 1980) was run as a monitor with every group of four samples for major element analysis. Peak positions were checked periodically and adjusted. Systematically drifting conditions were always observed, probably due to temperature dependent changes in the geometry of the equipement and some analyzing crystals (ie. PDP crystal). Table 22 lists machine settings, peak and background positions of the elements measured.

DATA REDUCTION

Existing data reduction programs did not allow convenient changes to handle some carbonatite compositions. Therefore FORTRAN-77 routines were developed to calculate mass attenuation coefficients (MAC) and concentrations of unknowns. Counting and regression statistics were neglected (except detection limits) because regressions could often be based only on very few standards. The need for interpolation and extrapolation required a close and careful control of data handling. Regression lines defined by the standards were plotted and forced through the origin of the "corrected counts" and "concentration" axis. The slopes of these regression lines were used by the routines to calculate major and minor element concentrations. Mass attenuation coefficients for the unknowns were calculated iteratively with an average MAC as a starting value until convergence was achieved (4 to 5 iterations).

Sample No.	Rock type	Bulk sample [kg]	Crushed split	Ground split
MR-550	dol. carb.	10.3	1/16	1/4
MR-552	dol. carb.	4.5	1/8	1/4
MR-553	dol. carb.	12.1	1/16	1/4
MR-554	dol. carb.	5.4	1/16	1/2
MR-570	REE-dike	3.2	1/8	1/2
MR-503	REE-dike	4.5	1/8	1/4
MR-551	Syenite	6.0	1/16	1/2
MR-316	Syenite	10.6	1/8	1/8
MR-505	Sediment	3.7	1/8	1/4
MR-506	Sediment	4.5	1/8	1/4
MR-511	Sediment	2.6	1/8	1/2
MR-523	sedimrnt	2.4	1/4	1/4

Table 21: List of samples processed, dol. carb. = dolomite carbonatite.

Element measured	Target	2Θ peak position	2Θ background position	Counting time (peak / background)	Analysing crystal	Counters	Collimator	kV/mA
Nb	Mo	21.39°	−2.99°	20/20	LiF(200)	F+S	fine	50/40
Zr	Mo	22.54°		20/20	LiF(200)	F+S	fine	50/40
Y	Mo	23.79°	+0.61°	20/20	LiF(200)	F+S	fine	50/40
Sr	Mo	25.16°		20/20	LiF(200)	F+S	fine	50/40
U	Mo	26.17°		20/20	LiF(200)	F+S	fine	50/40
Rb	Mo	26.63°		20/20	LiF(200)	F+S	fine	50/40
Th	Mo	27.49°	+1.31°	20/20	LiF(200)	F+S	fine	50/40
Ce	Mo	71.66°	−0.73°	100/100	LiF(200)	F+S	fine	60/50
Nd	Mo	72.14°		100/100	LiF(200)	F+S	fine	60/50
Pr	Mo	75.37°	−1.17°	100/100	LiF(200)	F+S	fine	60/50
La	Mo	82.95°	+1.55°	100/100	LiF(200)	F+S	fine	60/50
Ba	Mo	87.22°	+5.00°	20/20	LiF(200)	F	fine	60/40
Ti	Mo	86.20°		20/20	LiF(200)	F	fine	60/40
Cr	Mo	69.43°	−0.98°	100/40	LiF(200)	F+S	fine	60/40

Table 22: List of machine settings for XRF analysis for minor and major elements.

MASS ATTENUATUIN COEFFICIENTS

	ABSORBER																				
	C	O	NA	MG	AL	SI	P	S	K	CA	TI	CR	MN	FE	SR	ZR	BA	CE	ND	LA	B
NA	1918.	4033.	539.	804.	1054.	1363.	1768.	2178.	3843.	4657.	6218.	7935.	8931.	9986.	3559.	4370.	5560.	6344.	6344.	6344.	1054.
MG	1153.	2424.	5520.	475.	625.	811.	1055.	1303.	2312.	2801.	3741.	4774.	5372.	6007.	2194.	2693.	5657.	5945.	5945.	5945.	600.
AL	724.	1522.	3466.	4340.	388.	504.	658.	814.	1453.	1760.	2351.	3000.	3376.	3775.	1409.	1730.	5867.	6562.	6562.	6562.	358.
SI	471.	990.	2255.	2824.	3473.	325.	425.	528.	946.	1146.	1531.	1953.	2198.	2458.	937.	1150.	3899.	4361.	4361.	4361.	222.
P	302.	663.	1510.	1890.	2325.	2815.	283.	352.	634.	768.	1025.	1308.	1472.	1647.	3685.	785.	2662.	2977.	2977.	2977.	143.
S	199.	458.	1042.	1305.	1604.	1943.	2322.	242.	438.	530.	708.	903.	1017.	1137.	3467.	3030.	1871.	2093.	2093.	2093.	94.6
K	65.0	157.	388.	486.	597.	723.	864.	1021.	163.	198.	264.	337.	379.	802.	1292.	1506.	731.	818.	818.	818.	31.6
CA	46.5	113.	289.	361.	444.	538.	643.	760.	1185.	147.	196.	251.	282.	316.	962.	1121.	552.	617.	617.	617.	22.8
TI	25.0	61.4	166.	209.	257.	311.	372.	439.	685.	782.	114.	145.	163.	183.	557.	649.	328.	367.	367.	367.	12.4
V	18.7	46.3	126.	162.	199.	241.	288.	340.	530.	606.	88.2	112.	127.	142.	432.	503.	257.	288.	288.	288.	9.36
CR	14.2	35.3	96.4	127.	156.	189.	226.	267.	416.	175.	607.	882.	99.2	111.	338.	394.	676.	228.	228.	228.	7.15
MN	10.9	27.2	74.7	100.	123.	150.	179.	211.	329.	376.	481.	69.8	78.6	87.9	268.	312.	718.	608.	608.	608.	5.51
FE	8.47	21.2	58.5	80.2	94.5	117.	143.	169.	263.	300.	384.	481.	62.8	70.2	214.	249.	632.	640.	640.	640.	4.30
RB	0.94	2.25	6.49	8.66	10.7	13.4	16.6	20.2	34.1	40.0	51.0	63.7	70.7	78.2	28.6	33.3	89.5	98.7	98.7	98.7	0.53
SR	0.83	1.90	5.49	7.34	9.09	11.4	14.1	17.2	29.1	34.1	43.5	54.3	60.3	66.7	24.6	28.6	77.2	85.1	85.1	85.1	0.46
Y	0.74	1.61	4.67	6.25	7.74	9.72	12.0	14.7	24.8	29.2	37.3	46.5	51.7	57.1	21.2	24.7	66.9	73.7	73.7	73.7	0.40
ZR	0.66	1.37	3.99	5.34	6.62	8.32	10.3	12.6	21.3	25.1	32.0	40.0	44.4	49.1	18.3	21.4	58.1	64.0	64.0	64.0	0.38
NB	0.59	1.17	3.42	4.58	5.68	7.14	8.84	10.8	18.4	21.7	27.6	34.5	38.3	42.3	112.	18.5	50.7	55.8	55.8	55.8	0.36
BA	25.7	63.2	171.	214.	263.	319.	381.	451.	702.	802.	117.	149.	167.	187.	571.	665.	336.	376.	376.	376.	12.8
LA	22.7	55.9	151.	192.	236.	286.	342.	403.	629.	718.	104.	133.	150.	168.	511.	596.	302.	338.	338.	338.	11.3
CE	20.1	50.0	134.	172.	212.	256.	306.	362.	564.	644.	93.7	120.	135.	150.	459.	535.	273.	305.	305.	305.	10.0
PR	17.8	43.9	120.	155.	190.	230.	275.	325.	507.	578.	740.	107.	121.	135.	412.	480.	246.	275.	275.	275.	8.89
ND	15.8	39.1	107.	139.	171.	207.	248.	293.	456.	521.	667.	96.8	109.	122.	371.	433.	223.	249.	249.	249.	7.92
TA	4.01	10.2	28.5	37.7	46.4	57.7	70.8	85.8	136.	155.	199.	249.	276.	306.	111.	129.	333.	367.	367.	367.	2.07
TH	0.95	2.47	7.11	9.50	11.7	14.7	18.2	22.1	37.3	43.5	55.7	69.6	77.2	85.4	31.1	36.3	97.2	107.	107.	107.	0.57
U	0.90	2.13	6.15	8.22	10.2	12.8	15.8	19.2	32.4	38.0	48.5	60.6	67.2	74.3	27.3	33.9	85.4	94.2	94.2	94.2	0.50

Table 23: Mass attenuation coefficients for various wavelengths and absorbing elements (Leroux & Tinh, 1977)

MAJOR ELEMENT CONCENTRATIONS OF STANDARDS (wt %)

	SIO2	TIO2	AL2O3	FE2O3	MNO	MGO	CAO	NA2O	K2O	H2O	CO2	P2O5	F	S	CR2O3	SRO	ZRO2	CE2O3
AGV1	59.61	1.06	17.19	6.78	0.10	1.52	4.94	4.32	2.92	0.78	0.02	0.51	0.04	0.01	0.	0.	0.	0.
G2	69.22	0.48	15.40	2.69	0.03	0.75	1.96	4.06	4.46	0.50	0.08	0.13	0.12	0.01	0.	0.	0.	0.
GSP1	67.32	0.66	15.28	4.30	0.04	0.97	2.03	2.81	5.41	0.58	0.12	0.28	0.37	0.03	0.	0.	0.	0.
BCR1	54.53	2.26	13.72	13.41	0.18	3.48	6.97	3.30	1.70	0.67	0.02	0.36	0.05	0.04	0.	0.	0.	0.
SY3	59.68	0.15	11.80	6.42	0.32	2.67	8.26	4.15	4.20	0.42	0.38	0.54	0.66	0.05	0.	0.	0.	1.0
W1	52.72	1.07	15.02	11.11	0.17	6.63	10.98	2.15	0.64	0.53	0.06	0.14	0.03	0.01	0.	0.	0.	0.
MIFE	34.55	2.51	19.58	25.76	0.35	4.57	0.43	0.30	8.79	2.92	0.19	0.45	1.59	0.	0.	0.	0.	0.
MIMG	38.42	1.64	15.25	9.49	0.26	20.46	0.08	0.12	10.03	2.10	0.15	0.01	2.86	0.	0.	0.	0.	0.
JB1	52.60	1.34	14.62	9.01	0.15	7.76	9.35	2.79	1.42	1.01	0.18	0.26	0.04	0.	0.	0.	0.	0.
JG1	72.36	0.27	14.20	2.16	0.06	0.76	2.17	3.39	3.96	0.54	0.08	0.09	0.05	0.	0.	0.	0.	0.
NIMD	38.96	0.02	0.30	16.96	0.22	43.51	0.28	0.04	0.01	0.30	0.40	0.02	0.01	0.02	0.	0.	0.	0.
NIMG	75.70	0.09	12.08	2.02	0.02	0.06	0.78	3.36	4.99	0.49	0.10	0.01	0.42	0.01	0.	0.	0.	0.
NIML	52.40	0.48	13.64	9.96	0.77	0.28	3.22	8.37	5.51	2.31	0.17	0.06	0.44	0.65	0.	0.5	1.5	0.
NIMN	52.64	0.20	16.50	8.91	0.18	7.50	11.50	2.46	0.25	0.33	0.10	0.03	0.03	0.01	0.	0.	0.	0.
NIMP	51.10	0.20	4.18	12.76	0.22	25.33	2.66	0.37	0.09	0.26	0.08	0.02	0.02	0.02	3.5	0.	0.	0.
NIMS	63.63	0.04	17.34	1.40	0.01	0.46	0.68	0.43	15.35	0.22	0.09	0.12	0.01	0.01	0.	0.	0.	0.
GA	69.96	0.38	14.51	2.77	0.09	0.95	2.45	3.55	4.03	0.87	0.11	0.12	0.05	0.	0.	0.	0.	0.
URS1	0.00	0.00	0.00	0.00	0.00	21.47	30.83	0.00	0.00	0.23	41.95	5.51	0.00	0.00	0.00	0.00	0.00	0.00

Table 24: Major element concentration of standards used (Abbey, 1980).

MASS ATTENUATION COEFFICIENTS FOR STANDARDS

	WAVELENGTH												
	NA	MG	AL	SI	P	S	K	CA	TI	V	CR	MN	FE
AGV1	3183.25	2077.35	1339.86	1164.55	1505.04	1043.69	400.20	308.46	201.14	155.16	113.91	98.23	77.04
G2	2922.16	1909.83	1215.55	1052.66	1546.24	1068.60	398.38	328.70	197.89	152.61	116.46	95.18	74.52
GSP1	3045.22	1935.37	1236.99	1063.81	1528.10	1057.47	398.69	334.06	201.33	155.30	119.03	97.34	76.29
BCR1	3601.51	2288.76	1520.14	1220.69	1475.02	1021.57	409.76	291.87	201.47	155.47	113.75	101.48	79.79
SY3	3215.09	2088.73	1374.69	1093.38	1451.76	1007.16	386.01	309.75	218.12	168.33	114.34	104.10	81.85
W1	3486.90	2175.19	1524.20	1243.93	1465.15	1012.71	400.00	279.88	214.08	165.27	109.22	104.54	82.25
MIFE	4279.43	2582.17	1730.01	1452.66	1384.18	959.66	418.21	335.98	194.72	150.28	124.39	98.85	77.91
MIMG	3318.14	1996.33	1747.16	1394.04	1395.89	963.79	377.52	348.40	200.10	154.42	125.70	99.25	78.29
JB1	3355.79	2121.40	1518.94	1235.52	1462.63	1012.09	394.29	286.45	210.17	162.21	111.01	103.32	81.28
JG1	2899.75	1870.16	1190.79	1015.54	1557.79	1076.20	399.63	326.17	197.43	152.26	115.07	94.45	73.93
NIMD	3411.64	2049.03	2335.98	1524.57	1488.87	1028.14	421.50	278.94	161.04	124.27	96.43	76.41	60.37
NIMG	2889.56	1862.82	1169.09	965.18	1564.23	1079.92	400.66	336.28	196.33	151.40	116.80	93.46	73.14
NIML	3376.81	2350.23	1481.78	1195.68	1448.34	1031.82	414.54	335.77	208.34	160.68	120.04	100.09	78.68
NIMN	3339.21	2098.59	1498.06	1253.51	1474.47	1018.13	396.38	277.94	215.85	166.63	106.26	103.17	81.12
NIMP	3475.98	2100.58	1930.69	1326.29	1503.51	1038.19	414.09	282.24	174.61	134.73	119.00	83.42	75.78
NIMS	2978.27	1803.76	1142.04	1038.34	1469.52	1015.57	375.55	410.75	239.06	184.54	142.95	114.00	89.66
GA	2941.36	1901.76	1215.38	1037.48	1545.50	1068.00	398.24	324.64	197.98	152.69	115.15	94.99	74.38

Table 25: Mass attenuation coefficients for standards used at wavelengths of interest.

MASS ATTENUATION COEFFICIENTS FOR STANDARDS (cont.)

	WAVELENGTH													
	FE	RB	SR	Y	ZR	NB	BA	LA	CE	PR	ND	TA	TH	U
AGV1	77.04	12.44	10.59	9.04	7.75	6.67	206.33	184.54	165.25	152.11	136.72	51.38	13.61	11.84
G2	74.52	10.01	8.52	7.26	6.22	5.35	203.02	181.57	162.58	147.42	132.46	42.12	10.96	9.53
GSP1	76.29	11.05	9.40	8.02	6.87	5.91	206.52	184.74	165.43	150.70	135.42	46.11	12.09	10.52
BCR1	79.79	16.09	13.70	11.70	10.04	8.64	206.63	184.84	165.51	157.03	141.20	65.36	17.58	15.30
SY3	81.85	13.03	11.09	9.47	8.12	6.99	223.75	200.14	179.24	161.10	144.82	53.54	14.25	12.40
W1	82.25	15.27	13.01	11.11	9.53	8.21	219.56	196.43	175.94	161.71	145.42	62.14	16.69	14.53
MIFE	77.91	21.79	18.57	15.87	13.63	11.73	199.58	178.64	159.98	152.99	137.58	87.45	23.82	20.71
MIMG	78.29	13.95	11.88	10.14	8.70	7.48	205.16	183.60	164.47	153.75	138.14	57.21	15.27	13.27
JB1	81.28	14.14	12.04	10.28	8.82	7.59	215.56	192.83	172.71	159.90	143.76	57.77	15.45	13.45
JG1	73.93	9.68	8.23	7.02	6.01	5.17	202.56	181.16	162.22	146.26	131.42	40.84	10.60	9.22
NIMD	60.37	15.06	12.82	10.95	9.39	8.08	165.09	147.76	132.24	118.59	106.48	61.47	16.47	14.31
NIMG	73.14	9.47	8.06	6.87	5.88	5.05	201.43	180.16	161.30	144.74	130.04	40.09	10.38	9.02
NIML	78.68	14.57	12.41	10.60	9.09	8.23	213.71	191.10	171.11	155.10	139.40	59.55	15.93	13.88
NIMN	81.12	14.08	11.99	10.24	8.78	7.56	221.39	198.06	177.40	159.64	143.54	57.53	15.39	13.39
NIMP	75.78	15.16	12.90	11.02	9.46	8.14	179.07	160.22	143.45	129.25	116.13	61.84	16.58	14.42
NIMS	89.66	11.40	9.71	8.27	7.09	6.10	245.17	219.42	196.58	176.29	158.44	47.60	12.49	10.85
GA	74.38	10.07	8.56	7.30	6.26	5.38	203.12	181.66	162.67	147.10	132.18	42.31	11.02	9.59

Table 26: Mass attenuation coefficients for standards used at wavelengths of interest.

MASS ATTENUATION COEFFICIENTS OF UNKNOWNS FOR WAVELENGTHS OF MAJOR ELEMENTS

	SI	AL	TI	FE	MG	CA	NA	K	P	S	SR	BA	ND	CE	MN
MR-503	1318.98	1999.15	233.10	129.06	2564.68	191.15	3907.10	258.29	978.13	678.73	16.09	239.15	154.77	191.86	154.88
MR-570	1174.75	1798.07	226.08	91.40	2369.36	149.42	3823.34	203.44	811.09	565.94	11.77	231.97	149.59	185.85	113.31
MR-550	1154.41	1767.47	238.77	90.71	2162.82	144.75	3556.49	197.49	778.40	552.21	9.93	244.96	157.97	196.25	113.82
MR-553	1165.65	1787.85	247.79	93.94	2158.45	148.58	3584.96	202.69	796.70	565.32	10.54	254.21	164.03	203.71	117.97
MR-552	1124.99	1724.69	259.26	98.83	2170.63	162.60	3607.15	221.35	771.54	614.92	11.04	265.96	171.74	213.15	123.93
MR-554	1162.49	1768.17	247.83	94.52	2132.34	150.98	3544.51	205.90	790.96	573.85	10.35	254.25	164.47	203.73	118.57
MR-316	953.12	1353.22	176.70	67.60	2051.80	274.28	2908.40	368.50	1451.94	1009.26	6.79	181.38	118.88	145.02	86.14
MR-551	914.86	1187.81	194.47	73.31	1858.78	320.14	2846.70	388.70	1536.54	1062.76	7.31	199.56	129.93	159.76	93.56
MR-511	1022.47	1505.92	299.14	113.64	2332.06	161.11	3692.46	214.22	858.73	594.87	12.49	306.91	198.51	245.96	143.01
MR-506	1033.99	1356.23	267.26	102.84	2122.10	217.92	3490.63	271.31	1082.34	748.05	11.21	274.18	178.68	219.77	129.75
MR-523	1022.47	1505.92	299.14	113.64	2332.06	161.11	3692.46	214.22	858.73	594.87	12.49	306.91	198.51	245.96	143.01
MR-505	1033.99	1356.23	267.26	102.84	2122.10	217.92	3490.63	271.31	1082.34	748.05	11.21	274.18	178.68	219.77	129.75

Table 27: Mass attenuation coefficients of unknowns calculated for wavelengths of major elements.

MASS ATTENUATION COEFFICIENTS OF UNKNOWNS FOR WAVELENGTHS OF MINOR ELEMENTS

	NB	ZR	Y	SR	U	RB	TH	TA	TI	BA	CE	ND	PR	LA	MN	S
MR-503	10.41	11.93	13.84	16.09	17.89	18.80	20.46	73.10	233.10	239.15	191.86	154.77	171.95	213.85	154.88	678.73
MR-570	8.03	8.67	10.09	11.77	13.12	13.81	15.03	54.59	226.08	231.97	185.85	149.59	166.33	207.31	113.31	565.94
MR-550	6.33	7.30	8.50	9.93	11.08	11.67	12.70	46.52	238.77	244.96	196.25	157.97	175.65	218.95	113.82	552.21
MR-553	7.14	7.74	9.02	10.54	11.75	12.37	13.47	49.26	247.79	254.21	203.71	164.03	182.37	227.25	117.97	565.32
MR-552	7.42	8.11	9.45	11.04	12.31	12.96	14.12	51.65	259.26	265.96	213.15	171.74	190.89	237.80	123.93	614.92
MR-554	6.60	7.60	8.85	10.35	11.54	12.15	13.23	48.44	247.83	254.25	203.73	164.47	182.84	227.29	118.57	573.85
MR-316	4.26	4.93	5.75	6.75	7.56	7.94	8.69	33.75	175.64	180.29	144.15	118.15	131.57	161.06	85.60	1003.98
MR-551	4.56	5.29	6.18	7.25	8.12	8.53	9.34	36.29	192.91	197.96	158.47	128.86	143.44	177.00	92.79	1055.38
MR-511	7.98	9.18	10.69	12.49	13.94	14.67	15.97	58.17	299.14	306.91	245.96	198.51	220.57	274.40	143.01	594.87
MR-506	7.12	8.22	9.58	11.21	12.51	13.16	14.35	52.94	267.26	274.18	219.77	178.68	198.60	245.20	129.75	748.05
MR-523	7.98	9.18	10.69	12.49	13.94	14.67	15.97	58.17	299.14	306.91	245.96	198.51	220.57	274.40	143.01	594.87
MR-505	7.12	8.22	9.58	11.21	12.51	13.16	14.35	52.94	267.26	274.18	219.77	178.68	198.60	245.20	129.75	748.05

Table 28: Mass attenuation coefficients of unknowns calculated for wavelengths of minor elements.

MAJOR ELEMENT CONCENTRATIONS OF UNKNOWNS (wt %)

	SIO2	AL2O	TIO2	FEO	MGO	CAO	NA2O	K2O	P2O5	S	SRO	BAO	ND2O	CE2O	MNO	LOI	TOTAL
MR-503	7.30	0.67	0.04	10.49	7.91	24.59	0.79	0.06	0.09	1.11	0.08	7.74	0.42	0.84	3.30	33.31	98.74
MR-570	0.65	0.21	0.01	8.41	11.29	28.14	1.13	0.04	0.14	0.06	0.66	0.69	0.12	0.56	4.11	42.55	98.77
MR-550	0.46	0.24	0.00	2.71	15.94	30.23	0.58	0.02	1.60	0.00	0.04	0.00	0.03	0.09	0.24	43.52	95.70
MR-553	0.25	0.12	0.00	0.95	16.44	30.65	0.07	0.01	1.20	0.01	0.52	0.01	0.01	0.03	0.77	42.	93.04
MR-552	0.52	0.16	0.01	1.92	15.03	34.43	0.0	0.02	8.73	0.01	0.53	0.01	0.04	0.11	0.77	40.16	100.25
MR-554	1.00	0.67	0.11	0.71	16.74	31.32	0.0	0.01	2.93	0.01	0.05	0.00	0.03	0.10	0.23	41.96	95.87
MR-316	65.60	4.23	0.67	11.86	2.52	4.00	7.70	0.24	0.69	0.02	0.04	0.15	0.01	0.02	0.27	0.84	98.86
MR-551	79.88	8.82	0.44	4.12	0.93	2.41	4.09	3.91	0.21	0.01	0.02	0.02	0.01	0.02	0.14	1.16	106.20
MR-511	15.06	2.64	0.08	0.73	1.74	44.05	3.05	0.46	0.27	0.0	0.07	0.06	0.00	0.01	0.08	37.15	105.45
MR-506	35.48	9.84	0.51	5.12	0.86	31.80	0.57	2.27	0.13	0.0	0.03	0.27	0.01	0.01	0.43	23.19	110.52

Table 29: XRF-analyses of major elements on powder pellets. Calculations are based on mass attenuation coefficients (table 23) and regression slopes determined from standards (table 24; Abbey, 1980).

MAJOR ELEMENT CONCENTRATIONS NORMALIZED TO 100 wt%

	SIO2	AL2O	TIO2	FEO	MGO	CAO	NA2O	K2O	P2O5	S	SRO	BAO	ND2O	CE2O	MNO	LOI	TOTAL
MR-503	7.44	0.68	0.04	10.67	8.06	25.06	0.81	0.06	0.09	1.13	0.08	7.83	0.43	0.86	3.36	33.31	100.00
MR-570	0.66	0.25	0.01	8.60	11.45	28.76	1.16	0.04	0.14	0.06	0.68	0.74	0.12	0.57	4.20	42.55	100.00
MR-550	0.50	0.26	0.0	2.95	17.34	32.89	0.63	0.02	1.74	0.0	0.04	0.0	0.03	0.10	0.26	43.52	100.00
MR-553	0.34	0.16	0.0	1.30	22.42	41.81	0.10	0.01	1.64	0.01	0.71	0.01	0.01	0.04	1.05	42.00	100.00
MR-552	0.52	0.16	0.01	1.92	14.79	34.29	0.0	0.02	8.69	0.01	0.53	0.01	0.04	0.11	0.77	40.16	100.00
MR-554	1.08	0.72	0.12	0.76	18.02	33.71	0.0	0.01	3.15	0.01	0.05	0.0	0.03	0.10	0.25	41.96	100.00
MR-316	66.36	4.28	0.68	12.00	2.55	4.05	7.79	0.24	0.70	0.02	0.04	0.15	0.01	0.02	0.27	0.84	100.00
MR-551	75.15	8.30	0.41	3.88	0.87	2.28	3.85	3.68	0.20	0.01	0.02	0.02	0.01	0.02	0.14	1.16	100.00
MR-511	13.86	2.43	0.07	0.67	1.60	40.53	2.81	0.42	0.25	0.0	0.06	0.06	0.0	0.01	0.07	37.15	100.00
MR-506	31.20	8.65	0.45	4.50	0.76	28.00	0.50	2.00	0.11	0.0	0.03	0.24	0.01	0.01	0.37	23.19	100.00

Table 30: Normalized major element concentrations from table 29.

TRACE ELEMENT CONCENTRATIONS OF UNKNOWNS (ppm)

	NB	ZR	Y	SR	U	RB	TH	TA	TIO2(%)	BA	CE	ND	PR	LA	MNO(%)	S
MR-503	29.	96.	96.	699.	0.	0.	839.	nd	0.01	69395.	7213.	3584.	nd	2291.	3.29	10868.
MR-570	3.	583.	13.	5546.	21.	3.	28.	nd	0.01	6169.	4757.	1020.	nd	2668.	4.11	nd
MR-550	490.	66.	41.	359.	4.	4.	128.	18.	0.00	39.	746.	237.	nd	307.	0.26	nd
MR-553	168.	465.	14.	4377.	223.	35.	1.	0.	0.00	1225.	224.	59.	nd	142.	0.77	59.
MR-552	1796.	499.	69.	4449.	19.	5.	21.	17.	0.01	85.	909.	310.	nd	322.	0.76	59.
MR-554	1384.	497.	122.	457.	74.	2.	184.	166.	0.11	33.	856.	297.	nd	355.	0.23	90.
MR-316	71.	267.	6.	302.	1.	2.	4.	nd	0.62	1343.	168.	56.	nd	63.	0.26	183.
MR-551	72.	887.	18.	141.	3.	35.	4.	nd	0.40	184.	143.	46.	nd	60.	0.14	62.
MR-511	19.	115.	29.	622.	5.	10.	6.	nd	0.08	503.	90.	34.	nd	64.	0.08	nd
MR-506	183.	70.	59.	257.	7.	43.	58.	nd	0.47	2422.	103.	64.	nd	38.	0.43	nd
MR-523	24.	41.	26.	292.	10.	8.	9.	nd	0.06	345.	0.	0.	nd	36.	0.04	nd
MR-505	144.	50.	60.	379.	0.	25.	109.	nd	0.29	41691.	73.	0.	nd	13.	0.55	nd

Table 31: XRF-analyses of trace elements. Calculations are based on mass attenuation coefficients (tab. 29) and regression slopes derived from concentrations of standards (Abbey, 1980).
nd = not determined.

APPENDIX C: TRANSIENT TEMPERATURE DISTRIBUTIONS CALCULATED FOR THE MARGIN OF A COOLING IGNEOUS BODY

The Model

The theory of heat conduction is well understood and a great number of exact solutions for various problems and geometries are described in the literature (Ingersoll et al,1954; Carslaw & Jaeger,1959; Ozisik,1980; Turcotte & Schubert,1982). Exact solutions to geological problems involving the heat of crystallization are restricted to simple geometries (Jaeger,1957; Carslaw & Jaeger,1959; Turcotte & Schubert,1982).

For models directed towards understanding the cooling of igneous bodies the heat of crystallization must be taken into account. To maintain a simple solution a more tractable geometry of the igneous body was chosen to be that of an infinite, parallel sheet. Compared with the more appropriate cylindrical geometry of the "Aley" complex the results will represent maximum temperature distributions. The differences are believed to be within the limits of the accuracy of the physical data set (Ingersoll et al,1954; Jaeger,1957).

Assumptions

An infinite slab of magma at the melting temperature (Tm) intrudes instantaneously into country rock initially at a uniform temperature (To). Solidification occurs at the melting temperature and proceeds parallel to the contact walls towards the center releasing the heat of crystallization (L). The solidified magma and the country rock are isotropic and have the same constant heat capacities (cp) and thermal diffusivities (κ). The model requires estimates of physical properies of the solid igneous rock (heat capacity, thermal diffusivity), the melting temperature and the heat of crystallization.

Symbols and units

Tm	Melting temperature	[K]
To	Temperature before intrusion	[K]
Tc	Temperature at contact	[K]
T	Temperature	[K]
κ	Thermal diffusivity	[s/m]
L	Heat of crystallization	[J/kg]
cp	Heat capacity	[J/kg/K]
ρ	Specific density of solid	[kg/m]
k	Thermal conductivity	[J/kg/m/s]
x	Distance from centre of coordinate system	[m]
xm	Position of solidification front	[m]
t	Time after intrusion	[s]
ts	Solidification time	[s]
b	Halfwidth of dike	[m]
λ	Model parameter	
erf	Error Function	
erfc	Complementary Error Function	
$2\sqrt{(\kappa t)}$	Characteristic thermal diffusion distance	[m]
$\eta = \frac{x}{2\sqrt{\kappa t}}$	Dimensionless similarity variable	
$\Theta = \frac{T-To}{Tm-To}$	Dimensionless time	

Coordinate System

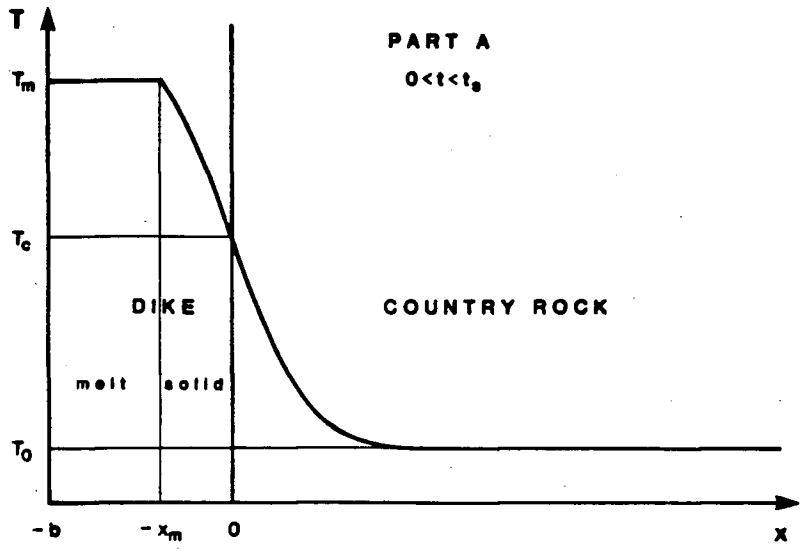

Figure 48: Coordinate system during solidification

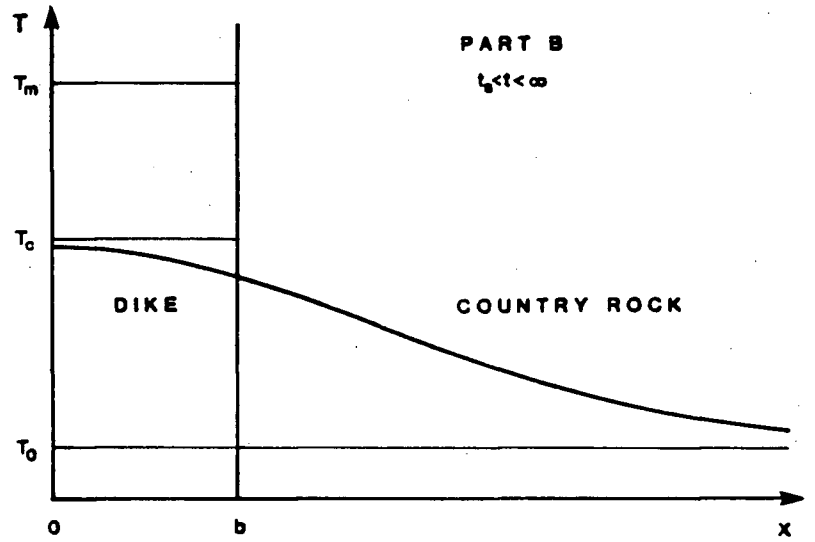

Figure 49: Coordinate system after solidification

Mathematics

Cooling during solidification

Equations:

I One dimensional transient heat conduction equation for a homogenious, isotropic solid:

$$(1)\quad \frac{\partial T}{\partial t} = \kappa \cdot \frac{\partial^2 T}{\partial x^2}$$

Boundary conditions:

$$T(xm,t)=Tm$$

$$T(\infty,t)=To$$

Initial condition:

$$T(x,0)=To$$

Note: There is no temperature gradient in the liquid phase and thus no heat will be conducted in the liquid.

II Heat balance equation at solidification front:

rate of heat liberated during solidification = heat flux in x-direction through the solid phase

$$(2)\quad \rho \cdot L \frac{d}{dt} xm(t) = -k\left[\frac{\partial T}{\partial x}\right]_{x=xm}$$

Heat conduction equation in dimensionless parameters (compare table on page 4 for parameter transformation):

$$(3)\quad -\eta \frac{d\Theta}{d\eta} = \frac{1}{2} \frac{d^2\Theta}{d\eta^2}$$

Boundary conditions:

$$\Theta(\infty)=0$$
$$\Theta(0)=1$$

Solution

Compare Carslaw & Jaeger,1959; Turcotte & Schubert,1982

$$(4)\quad \Theta(\eta) = \frac{\mathrm{erfc}(\eta)}{1+\mathrm{erf}(\lambda)}$$

$$\text{with}\quad (5)\quad \lambda = -\frac{xm(t)}{2\cdot\sqrt{(\kappa\cdot t)}}$$

$$\text{or}\quad (6)\quad T(x,t) = To+(Tm-To)\cdot\mathrm{erfc}\left[\frac{x}{2\cdot\sqrt{(\kappa\cdot t)}}\right]\cdot\frac{1}{1+\mathrm{erf}(\lambda)}$$

The parameter λ can be evaluated numerically from the transcendental function resulting from equation (2) after substitution of (5) into (2) and subsequent differentiation:

$$(7)\quad \frac{L\cdot\sqrt{(\pi)}}{cp\cdot(Tm-To)} = \frac{\exp(-\lambda^2)}{\lambda\cdot[1+\mathrm{erf}(\lambda)]}$$

The solidification time is calculated from (5)

$$(8)\quad ts = \frac{b^2}{4\cdot\kappa\cdot\lambda^2}$$

The contact temperature is a constant during solidification, depending on λ only:

$$(9)\quad Tc = To+(Tm-To)\ \frac{1}{1+\mathrm{erf}(\lambda)}$$

calculated from (4) with $\eta=0$

From equation (7) it is obvious that the parameter λ is dependent upon the ratio L/cp/(Tm-To), with L and Tm being the parameters with the strongest dependency on magma composition.

Cooling after Solidification

This is a cooling problem of an infinite solid with a given initial temperature distribution (Carslaw & Jaeger,1959; Ingersoll et al,1954; Ozisik,1982). A coordinate transformation, shifting the origin of the x-axis to -b is applied for symmetry reasons (compare figure 42).

Equations:

Heat conduction equation: $$\frac{\partial T}{\partial t} = \kappa \frac{\partial^2 T}{\partial x^2}$$

Initial Condition :

$$T(x,0) = f(x) = To+(Tm-To)\cdot erfc\left[\frac{x}{2\cdot\sqrt{(\kappa\cdot ts)}}\right]\cdot\frac{1}{1+erf(\lambda)}$$

Solution:

$$T(x,t) = \frac{1}{2\cdot\sqrt{(\pi\cdot\kappa\cdot t)}}\int_{-\infty}^{+\infty} f(u)\cdot exp\left[-\frac{(x-u)^2}{4\cdot\kappa\cdot t}\right]\cdot du$$

The integral has to be evaluated numerically.

General Applications

For this purpose three graphs are provided which enable a quick graphical evaluation of the solidification time (TS) and the contact temperature (TC) for any physical properties and any dimension. The following properties of the intrusive body have to be known:

- latent heat of fusion (L)
- heat capacity of solid (CP)
- diffusivity of solid (κ)
- halfwidth of intrusive body (B)
- melting temperature of intrusive body (TM)

- temperature of wallrock before intrusion (T0)

Note: The diffusivity can be calculated from the thermal conductivity (k), heat capacity (CP) and specific density (ρ) : $\kappa = k/(CP \cdot \rho)$

How to use the graphs:

- calculate $L^* \sqrt{\pi}/[CP \cdot (TM-T0)]$
- evaluate LAMBDA from figure 50
- evaluate TS/B^2 from figure 51 and calculate TS
- evaluate (TC-T0)/(TM-T0) from figure 52 and calculate TC

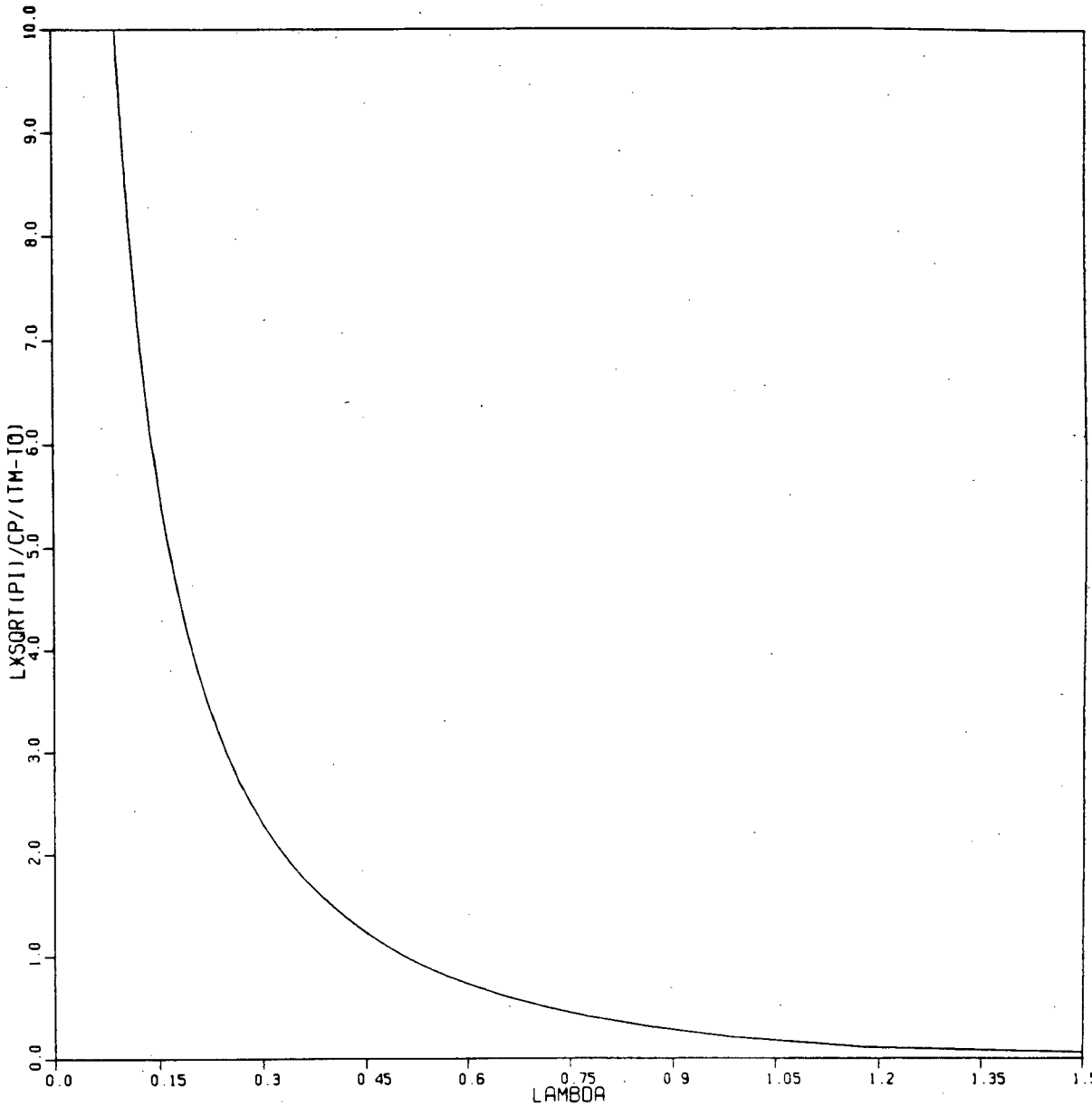

Figure 50: Model parameter λ

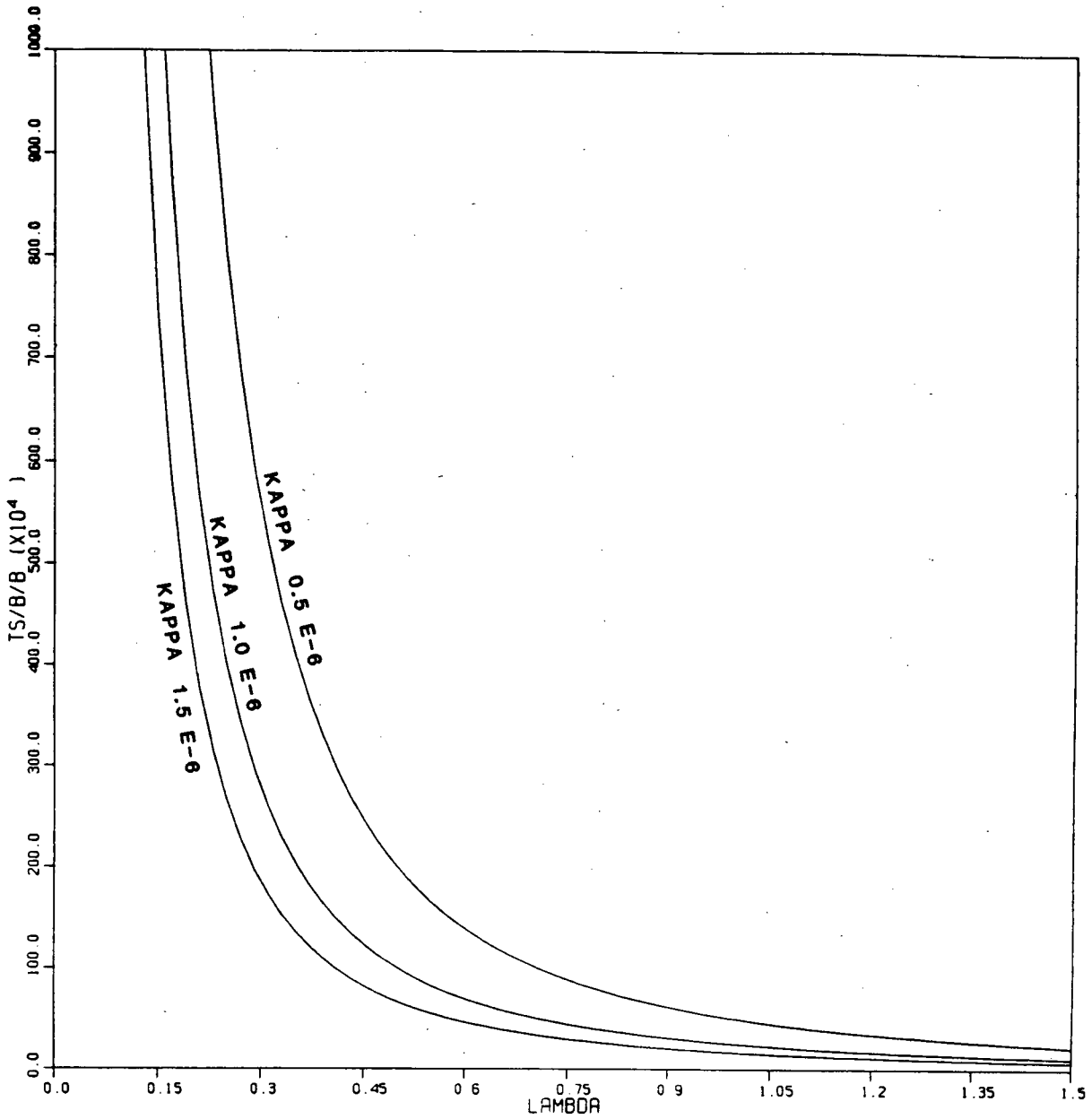

Figure 51: Solidification time as a function of λ

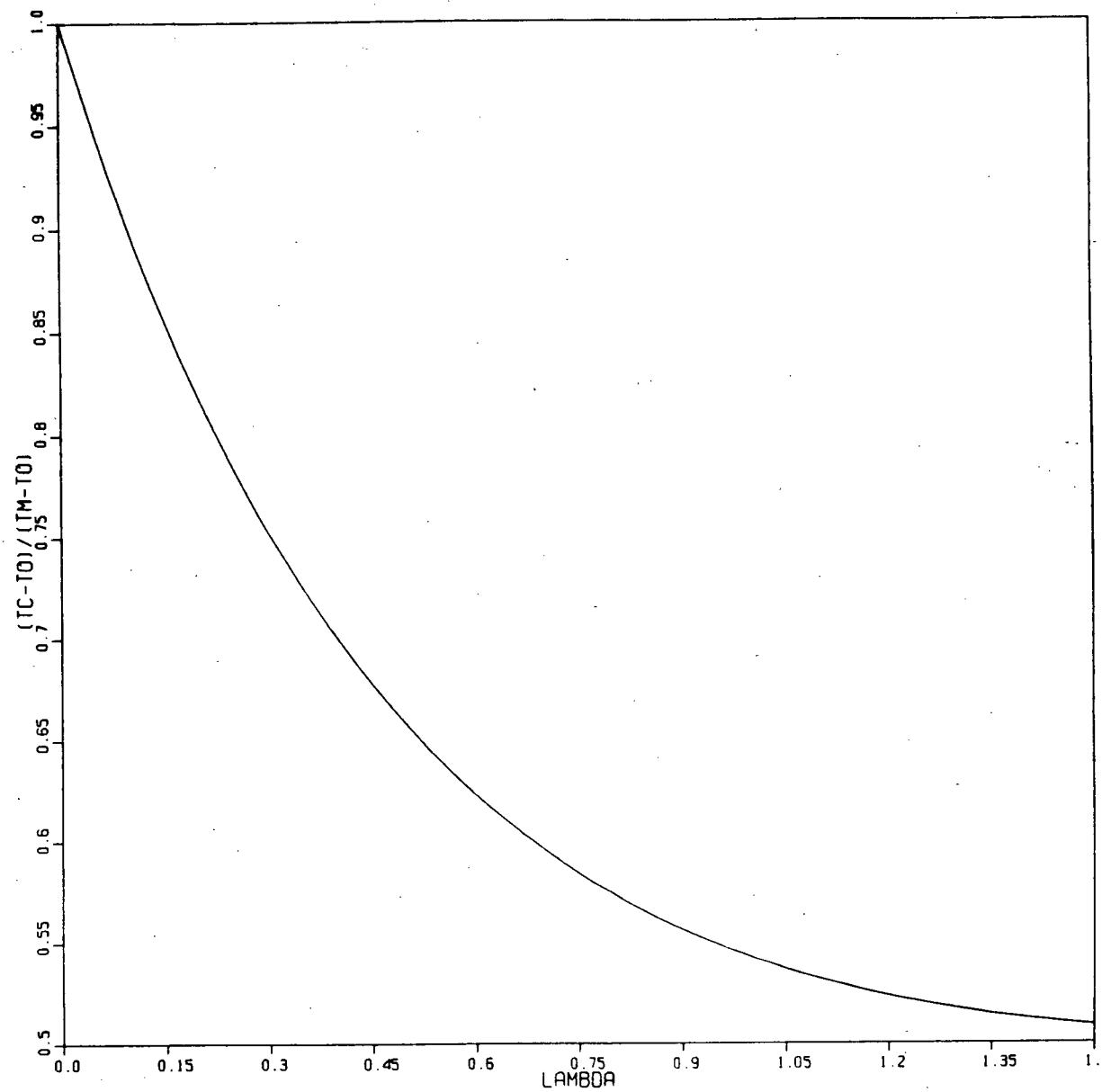

Figure 52: Dimensionless contact temperature as a function of λ

Sample calculations

Two time-temperature-distance (t-T-x) sections were calculated: one with syenite data (section 6.2: figure 25) and one for a carbonatite dike with a halfwidth of one meter (figure 53).

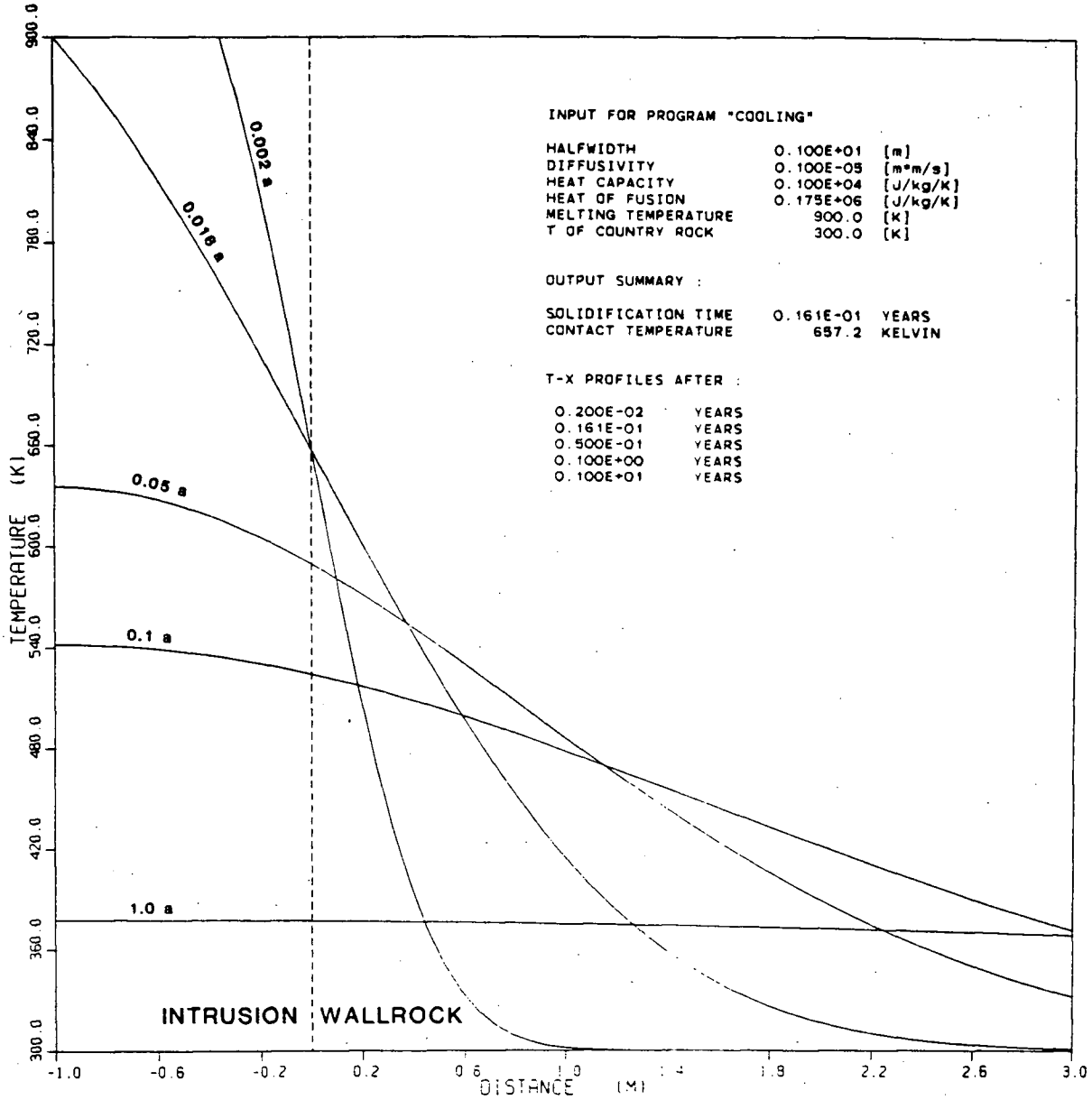

Figure 53: t-T-x diagram for a carbonatite dike

Program "COOLING"

A FORTRAN-77 program to calculate the transient temperature distribution around a cooling igneous body. The program is self explaining with an interactive input. All units are metric. The program may be called via the UBC-network (MTS) with the following command: $R URSM:COOLING.O . The plotroutine URSM:COOLPLOT.O will produce a t-T-x plot.

```
C     ****************************************************************
C     *                                                              *
C     *    PROGRAM COOLING : SOLIDIFICATION OF A DIKE OR SILL        *
C     *                                                              *
C     ****************************************************************
C
C     LIST OF VARIABLES:
C
C       B       HALFWIDTH OF DIKE  [m]
C       D       THERMAL DIFFUSIVITY OF COUNTRY ROCK  [m*m/s]
C       K       THERMAL CONDUCTIVITY OF COUNTRY ROCK  [J/s/m/K]
C       RO      DENSITY OF MAGMA [kg/m/m/m]
C       L       LATENT HEAT OF FUSION  [J/kg]
C       CP      HEAT CAPACITY OF COUNTRY ROCK  [J/kg/K]
C       T       TEMPERATURE  [K]
C       TM      MELTING TEMPERATURE OF MAGMA [K]
C       T0      TEMPERATURE OF COUNTRY ROCK  [K]
C       TC      TEMPERATURE AT THE CONTACT  [K]
C       TIME    COOLING TIME  [a]
C       TIMS    SOLIDIFICATION TIME  [s]
C       TIMSA   SOLIDIFICATION TIME  [a]
C
C     ****************************************************************
C
      IMPLICIT REAL*8 (A-L,O-Z)
      LOGICAL LO
      EXTERNAL FN,DF
      COMMON C1,C2,C3,C4,C6,Y,B,T0,TM
      CALL FTNCMD('ASSIGN 1=-INPUT;')
      CALL FTNCMD('ASSIGN 8=-PLOT;')
      NSTEP=50
      NLOOP=0
C
C     ****************** INTERACTIVE INPUT ************************
C
      WRITE(6,100)
  100 FORMAT(1X,'THIS PROGRAM CALCULATES THE TEMPERATURE PROFILE')
      WRITE(6,101)
  101 FORMAT(1X,'DURING SOLIDIFICATION OF A DIKE AS A FUNCTION OF')
      WRITE(6,102)
  102 FORMAT(1X,'TIME, DIMENSION AND PHYSICAL PROPERTIES')
C
      WRITE(6,103)
  103 FORMAT(1X,//,'INPUT DATA AND OUTPUT SUMMARY IN FILE "-INPUT"'
      WRITE(6,104)
  104 FORMAT(1X,'TO OBTAIN A PLOT RUN "COOLPLOT.O"',//)
C
      WRITE(6,110)
  110 FORMAT(/,1X,'ENTER HALFWIDTH OF DIKE [m] :')
      READ(5,111)B
  111 FORMAT(D20.10)
      WRITE(6,114)
  114 FORMAT(/,1X,'ENTER HEAT CAPACITY OF COUNTRY ROCK [J/kg/K] :')
      READ(5,111)CP
      WRITE(6,112)
  112 FORMAT(/,1X,'ENTER DIFFUSIVITY OF CONTRY ROCK [m*m/s]  :')
      READ(5,111)D
      WRITE(6,113)
```

```
      113   FORMAT(/,1X,'ENTER LATENT HEAT OF FUSION [J/kg] :')
            READ(5,111)L
            WRITE(6,115)
      115   FORMAT(/,1X,'ENTER MELTING TEMPERATURE OF MAGMA [K] :')
            READ(5,111)TM
            WRITE(6,116)
      116   FORMAT(/,1X,'ENTER TEMPERATURE OF CONTRY ROCK [K] :')
            READ(5,111)T0
            WRITE(6,117)
      117   FORMAT(/,1X,'ENTER PROFILE LENGTH (MULTIPLES OF HALFWIDTH) :')
            READ(5,111)BMULT
C
C
C
            WRITE(8,20)T0,TM,BMULT,B
       20   FORMAT(1X,4E15.5)
C
C     ******************** INPUT DATA SUMMARY **********************
C
            WRITE(1,50)
       50   FORMAT('INPUT FOR PROGRAM "COOLING"',/)
            WRITE(1,51)B
       51   FORMAT(1X,'HALFWIDTH              ',E10.3,'  [m]')
            WRITE(1,52)D
       52   FORMAT(1X,'DIFFUSIVITY            ',E10.3,'  [m*m/s]')
            WRITE(1,53)CP
       53   FORMAT(1X,'HEAT CAPACITY          ',E10.3,'  [J/kg/K]')
            WRITE(1,55)L
       55   FORMAT(1X,'HEAT OF FUSION         ',E10.3,'  [J/kg/K]')
            WRITE(1,56)TM
       56   FORMAT(1X,'MELTING TEMPERATURE    ',F10.1,'  [K]')
            WRITE(1,57)T0
       57   FORMAT(1X,'T OF COUNTRY ROCK      ',F10.1,'  [K]')
C
C     ******************** CALCULATION OF ts AND Tc ***************
C
            DPI=3.141592653589793D00
            X1=0.01D00
            X2=10.0D00
            EI=1.0D-12
            C1=L*DSQRT(DPI)/CP/(TM-T0)
C
            CALL ZERO1(X1,X2,FN,EI,LO)
C           WRITE(6,302)X1,X2
C302        FORMAT(1X,2E20.14)
C
C           IF(LO.EQ..FALSE.)GO TO 999
C
            TIMS=B*B/4.0/D/X1/X1
            TIMSA=TIMS/3.1536D07
            TIMSD=TIMSA*365.0
            TIMSH=TIMSD*24.0
C
            C4=1.0+DERF(X1)
            TC=T0+(TM-T0)/C4
C
            WRITE(6,200)TIMSA
      200   FORMAT(/,1X,'SOLIDIFICATION TIME :',E18.10,' YEARS')
```

```
117             WRITE(6,90)TIMSD
118          90 FORMAT(1X,'                        ',E18.10,' DAYS')
119             WRITE(6,91)TIMSH
120          91 FORMAT(1X,'                        ',E18.10,' HOURS')
121             WRITE(6,201)TC
122         201 FORMAT(/,1X,'CONTACT TEMPERATURE :',F8.2,' K')
123       C
124       C     ********************** OUTPUT DATA SUMMARY ******************
125       C
126             WRITE(1,60)
127          60 FORMAT(//,'OUTPUT SUMMARY :',/)
128             WRITE(1,61)TIMSA
129          61 FORMAT(1X,'SOLIDIFICATION TIME   ',E10.3,'  YEARS')
130             WRITE(1,62)TC
131          62 FORMAT(1X,'CONTACT TEMPERATURE   ',F10.1,'  KELVIN')
132             WRITE(1,63)
133          63 FORMAT(//,'T-X PROFILES AFTER :',/)
134       C
135       C     ****************** CALCULATION OF t-T-X PROFILES ***********
136       C
137         399 WRITE(6,118)
138         118 FORMAT(/,1X,'ENTER TIME AFTER INTRUSION [a] :')
139             READ(5,111)TIME
140       C
141             WRITE(1,70)TIME
142          70 FORMAT(1X,E10.3,'     YEARS')
143       C
144       C
145             NLOOP=NLOOP+1
146             CALL FTNCMD('ASSIGN 3=-3;')
147             WRITE(3,30)NLOOP
148          30 FORMAT(1X,I3)
149       C
150             TIMES=TIME*3.1536D07
151             C2=4.0*D*TIMES
152             C3=DSQRT(C2)
153             IF(TIMES.GT.TIMS)GO TO 400
154       C
155       C     ************* COOLING DURING SOLIDIFICATION ****************
156       C
157             YM=-X1*C3
158             WRITE(6,301)YM
159         301 FORMAT(1X,'SOLIDIFICATION FRONT AT  ',E12.3,' METERS')
160             YPLOT=YM+B
161             WRITE(8,300)YPLOT,TM
162         300 FORMAT(1X,2F12.4)
163       C
164             STEP=(BMULT*B-YM)/NSTEP
165             DO 310 N=1,NSTEP
166                YM=YM+STEP
167                C5=1.0-DERF(YM/C3)
168                T=T0+(TM-T0)*C5/C4
169                YPLOT=YM+B
170                WRITE(8,300)YPLOT,T
171         310 CONTINUE
172       C
173             GO TO 399
174       C
```

```
175     C       ***************** COOLING AFTER SOLIDIFICATION *************
176     C
177      400    TIMES=TIMES-TIMS
178             C2=4.0*D*TIMES
179             C3=DSQRT(C2)
180             C6=DSQRT(4.0*D*TIMS)
181             Y=0.0D00
182             STEP=(BMULT+1.00)*B/NSTEP
183             DU=1.0D00
184     C
185             DO 405 N=1,50
186                FDU=DF(DU)
187                IF(FDU.LT.1.0D-50)GO TO 406
188                DU=DU*5.0
189      405    CONTINUE
190     C
191      406    DST=DU/500.0D00
192     C
193             DO 410 N=1,NSTEP+1
194                AREA=0.0D00
195                X=-DU
196                F1=DF(X)
197     C
198                DO 420 M=1,1000
199                   X=X+DST
200                   F2=DF(X)
201                   DAREA=(F1+F2)/2.0*DST
202                   AREA=AREA+DAREA
203                   F1=F2
204      420       CONTINUE
205     C
206                T=1.0D00/C3/DSQRT(DPI)*AREA
207                WRITE(8,300)Y,T
208                Y=Y+STEP
209      410    CONTINUE
210     C
211             GO TO 399
212     C
213      998    STOP
214      999    WRITE(6,900)
215      900    FORMAT(/,1X,'ZERO1 FAILS')
216             STOP
217             END
218     C
219     C
220     C
221             FUNCTION FN(X1)
222               IMPLICIT REAL*8(A-L,O-Z)
223               COMMON C1,C2,C3,C4,C6,Y,B,T0,TM
224               FN=DEXP(-X1*X1)/X1/(1.0+DERF(X1))-C1
225               RETURN
226             END
227     C
228             FUNCTION DF(X)
229               IMPLICIT REAL*8(A-L,O-Z)
230               COMMON C1,C2,C3,C4,C6,Y,B,T0,TM
231               DF2=DEXP(-(Y-X)*(Y-X)/C2)
232               XPR=X
```

```
233               IF(X.LT.0.0D00)XPR=-X
234               DF1=T0+(TM-T0)*DERFC((XPR-B)/C6)/C4
235               DF=DF1*DF2
236               RETURN
237             END
```